AD-A158 606 INVESTIGATION OF CRYSTALLINE IRON-PLATINUM NICKEL AND AMORPHOUS RARE EART..(U) KOLLMORGEN CORP RADFORD VA G C HADJIPANAYIS ET AL. 15 MAR 83 0001AE 1/2

UNCLASSIFIED N00014-81-C-0752 F/G 20/3 NL

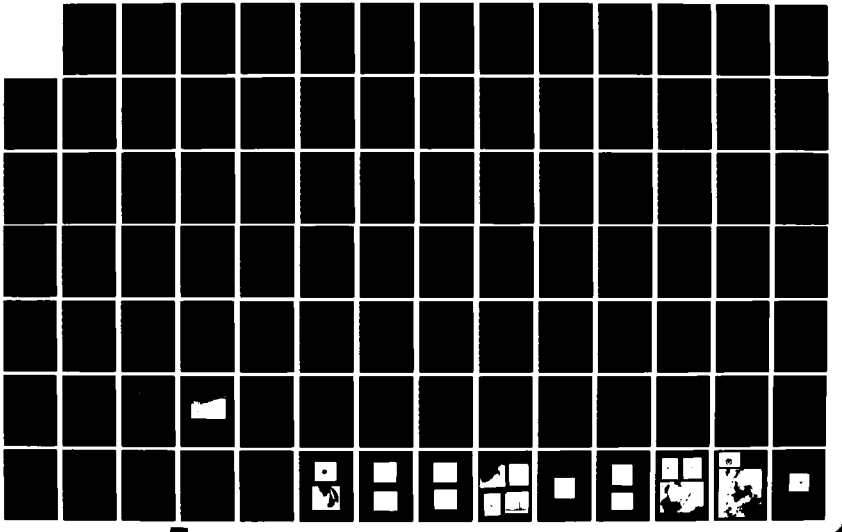

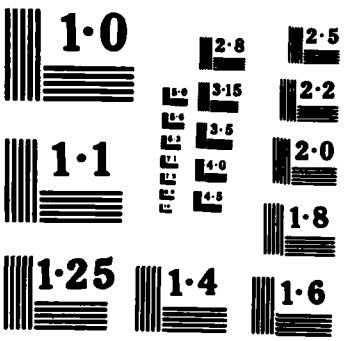

(1)

"INVESTIGATION OF CRYSTALLINE IRON-PLATINUM NICKEL AND AMORPHOUS RARE EARTH-IRON ALLOYS FOR PERMANENT MAGNETS"

By

George C. Hadjipanayis
Robert C. Hazelton
Industrial Drives Division,
Kollmorgen Corporation
201 Rock Road
Radford, Virginia 24141

and

Kenneth R. Lawless
Roseanne Prestipino
Materials Science Department
University of Virginia
Charlottesville, Virginia 22901

For

Office of Naval Research, Materials Division
Department of the Navy
800 N. Quincy Street
Arlington, Virginia 22217

Contract No. N00014-81-C-0752
Modification No. P00002

March 15, 1983

0001AE - Final Technial Report

CONTRACT NO.: N00014-81-C-0752
MODIFICATION NO.: P00002

REPORT PREPARED FOR: Materials Division, Code: 614A:DHP
Office of Naval Research
Department of the Navy
800 N. Quincy Street
Arlington, Virginia 22217

PREPARED BY: George C. Hadjipanayis
Robert C. Hazelton
Industrial Drives Division
Kollmorgen Corporation
201 Rock Road
Radford, Virginia 24141

and

Kenneth R. Lawless
Roseanne Prestipino
Materials Science Department
University of Virginia
Charlottesville, Virginia 22901

REPORT TITLE: "Investigation of Crystalline Iron-Platinum Nickel and Amorphous Rare Earth-Iron Alloys for Permanent Magnets"

REPORT DATE: March 15, 1983

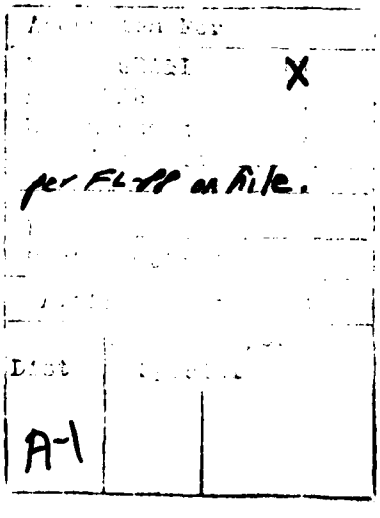

TABLE OF CONTENTS

I. INTRODUCTION

Samarium-cobalt magnets have large-energy products[1,2] but their cost is relatively high because of the use of expensive Sm and Co. A recent trend has been observed in industry to encourage conservation of cobalt and to find possible substitutes for this strategic material.

The purpose of this program was to develop a permanent magnet without the use of cobalt which could be substituted for the AlNiCo commercial magnets. A number of magnetic materials were identified with properties that could be exploited in permanent magnet development.

Splat-cooled PrGaFe amorphous alloys showed[3] relatively high coercive fields but small moments at room temperature. An attempt was made to enhance the magnetic properties of these materials by going to higher Fe concentrations and by crystallizing the original amorphous phase.

Rapid solidification techniques were used to improve the hard magnetic properties of RTbFe, RTbFeG and PrFeG alloys where R=Pr,Sm and MM(misch-metal) and G, a glass former ≡ B and Si. The use of rapid-quenching can lead to special microstructures and metastable phases which could not be produced otherwise. In addition, the crystalline Fe $Pt_{0.7}Ni_{0.3}$ alloys appeared to be very promising materials because of their good hard magnetic properties.[4] The successful substitution of nickel for platinum has encouraged the identification of other elements which could be further substituted for platinum to reduce the cost of the alloy while maintaining satisfactory magnetic properties.

The results of this investigation are very spectacular. Giant coercive fields beyond 40 kOe have been observed in PrTbFeCoB alloys. In $Fe_{75.5}Pr_{16.4}B_{4.8}Si_{3.3}$ the coercive field has reached the value of 67 kOe at cryogenic temperatures. Magnets with high energy products have been obtained for the first time in rapidly quenched PrFeB alloys over a wide range of compositions. In $Fe_{75.5}Pr_{16.4}B_{4.8}Si_{3.3}$ a 13 MGOe energy product has been achieved. This new fascinating material does not contain any of the expensive SM, Co and Tb materials but instead, it contains some Pr which is one of the most abundant light rare-earths. The new material has not yet been optimized either in chemical composition or in the heat treatment. Preliminary results indicate that higher Fe concentrations coupled with the appropriate heat treatment could lead to new hard magnetic materials with higher moments and therefore larger energy products.

II. BACKGROUND

In the last few years there has been considerable interest in the study of rare-earth amorphous and rapidly quenched alloys. This is because these materials show some important scientific and technological properties.[5,6,7,8] The amorphous rare-earth alloys show some kind of magnetic ordering at low temperatures. Below the ordering temperature the non-S-state rare-earth ion alloys develop a high magnetocrystalline anisotropy ($K \sim 10^8$ erg/cm^3) which restricts magnetic saturation and leads to very high coercive fields particularly at cryogenic temperatures.

The coercive fields decrease rapidly at higher temperatures and then disappear at temperatures much below the ordering temperature. This is in contrast to $Pr_{56}Ga_{14}Fe_{30}$ alloys[3] where a relatively high coercive field has been observed at room temperature. The moment of this material, however, is very small and this limits the energy product to very low values.

Crystallization has been observed[9] to enhance the hard magnetic properties of the amorphous rare-earth alloys. Savage et al[10] have observed an increase of the room temperature coercivity of $TbFe_2$ after crystallization leading to energy products of about 9 MGOe. The increase of coercivity has been attributed to the small, oriented crystallites of $TbFe_2$ laves phase which are formed during magnetic annealing around 525°C.

The idea of rapid solidification was used by Croat[11] to prepare partially crystallized rare-earth iron alloys with different quenching rates. The as-quenched alloys showed coercivities in the range

of 2-24 kOe and moments that were relatively low, limiting the energy product to only 2 MGOe. The high coercivities of these materials have been attributed to a fine metastable phase which forms over a specific interval of quench rate.

High coercive fields and energy products around 5 MGOe have been observed[12] after crystallization in the Metglas-type materials $Fe_{80}Tb_5La_5B_{10}$ where some B has been replaced by Tb and La. Koon et al[13] have attributed the high coercive fields to the presence of R_6Fe_{23} and Fe_3B phases.

Among the crystalline materials which do not contain any cobalt, the FePt system[14] appears to be a good candidate for permanent magnet development. Recent work has shown that 30% of the platinum in a FePt alloy can be replaced by nickel and still maintain coercivities of 2 kOe and potential energy products of up to 15 MGOe at room temperature. The high coercivities were explained[15] in terms of the highly anisotropic ordered tetragenal phase which is formed from the original disordered F.C.C. cubic phase after annealing around 700°C. Further substitution of Pt beyond 30% leads to alloys which do not exhibit the order-disorder transformation and have very low coercive fields. However, recent studies[16] have shown that partial substitution of Pt with In in $FePt_{0.7}Ni_{0.3}$ alloys increased the coercivity to above 1000 Oe after annealing in the temperature range of 600-700°C.

The results of all of these investigations are reported in the next sections.

III. EXPERIMENTAL TECHNIQUES

1. Sample Preparation

Alloys of nominal compositions were prepared in an arc furnace in 1 to 3 gram buttons. In the arc-melting process the buttons were turned over and melted at least three times to promote homogeneity. The buttons were then weighed to determine if any weight was lost.

For the crystalline FePtNi, the buttons were homogenized at 1050°C for 2 - 4 hours. In order to "freeze" the high temperature phases the samples were removed from the oven and rapidly quenched in water. The samples were then annealed between 600 - 700°C to develop the tetragonal phase with hard magnetic properties.

The amorphous samples were prepared in two ways. First of all, the PrGaFe samples were prepared at the University of Nebraska using an anvil and piston splat cooling apparatus. This method has a major disadvantage in that the quenching rate cannot be easily controlled. Since, in many cases, the magnetic properties of amorphous materials critically depend upon the quenching rate, a melt-spinning unit was constructed at Industrial Drives Division. By varying parameters such as wheel speed, crucible orifice size and gas pressure, the quenching rate can be well controlled and reproduced. All amorphous samples studied after the PrGaFe system were prepared using this technique.

2. Magnetic Properties

Measurements of magnetic properties and above room temperature (to 830°C) were made in a vibrating sample magnetometer (VSM) capable of applied fields up to 23 kOe. In general, the VSM was

used to measure hysterisis loops, measure magnet moments as a function of temperature (M vs T) and serve as an oven for magnetic annealing and "in-situ" magnetic measurements.

The VSM was interfaced with a Bascom-Turner data acquisition system allowing storage of all hysterisis loops and M vs T data on floppy discs.

Low temperature measurements (4.2 to 230 K) were carried out at the University of Nebraska in a VSM capable of fields up to 80 kOe. These measurements included hysterisis loops at selected temperatures and a.c. susceptibility measurements as a function of temperature.

The standard sample measurement sequence was as follows:

i. Samples were prepared for the VSM. In the case of the FePtNi solid pieces were cut to the proper size. For the amorphous materials, pieces were put into a tantalum pouch.

ii. An M vs T (thermomagnetic analysis) was then taken to determine whether any temperature dependent magnetic phase changes occurred. In general these data were taken at an applied field of $\sim$100 Oe.

iii. A room temperature hysterisis loop was taken to determine any changes in magnetic properties after the M vs T heat treatment.

iv. Various annealing procedures were carried out and room temperature loops taken to track the effects of annealing on magnetic properties.

3. Microstructure

In order to correlate the observed magnetic properties with the

physical properties of the samples a number of techniques were used. Transmission electron microscope studies were carried out at the University of Virginia using a Phillips 400 TEM with a resolution of 4Å. These include the imaging of sample microstructure and diffraction patterns.

Energy dispersive x-ray analysis was carried out at UVa in a JEOL SEM to determine the homogeneity of melt-spun samples. Both sides of the ribbons were examined to determine if there were any compositional differences between the side which contacted the wheel and the other side. The measurements are estimated to be $\pm$ 5% accurate using a semi-quantitative analysis.

X-ray diffraction spectra were generated at UVa and University of Nebraska using a Pickart x-ray diffractometer.

4. Differential Scanning Calorimetry

The crystallization of the samples was examined with differential scanning calorimetry using a DuPont 900 system with a maximum operating temperature of $600^{\circ}C$. The samples were heated and cooled at a rate of $10\text{-}20^{\circ}C$/min. Crystallization of the samples gives rise to strong exothermic peaks.

IV. PRASEODYMIUM-IRON-GALLIUM ALLOYS

The magnetic properties of splat-cooled $(Pr_{80}Ga_{20})_{100-x}$ Fe_x alloys[17] are listed in Table I. The $(Pr_{80}Ga_{20})_{70}Fe_{30}$ has the highest coercivity, H_c = 2400 Oe, but its magnetic moment is very weak, M_s = 22.5 emu/g. As the iron content is increased, the magnetic moment increases but the coercivity is substantially reduced to very small values (200 Oe). In $(Pr_{80}Ga_{20})_{70}Fe_{30}$ the room temperature coercivity decreases rather rapidly at higher temperatures and becomes negligible at around 420 K (Fig. 1a).

Thermomagnetic measurements [3,17] in $(Pr_{80}Ga_{20})_{70}$ Fe_{30} alloy indicate the presence of two peaks at 7 and 470 K. In $(Pr_{80}Ga_{20})_{20}Fe_{80}$ samples two peaks are observed at 780 and 1050 K respectively. This behavior indicates that these alloys are examples of a two magnetic phase system. This is further suggested by the constricted hysteresis loops which are observed at cryogenic temperatures (Fig. 1b).

Microstructure studies showed that the unannealed $(Pr_{80}Ga_{20})_{70}$ Fe_{30} sample is basically amorphous with very few scattered microcrystalline regions present. Energy dispersive analysis revealed some fluctuations in chemical composition of the amorphous phase. Regions rich in PrGa and PrFe have been observed on a 400Å scale indicating the existence of two amorphous phases corresponding to the high and low Curie temperature phases. The presence of the two magnetic phases might be responsible for the high coercivities which are observed in these materials.

The splat-cooled samples were heat-treated to higher temperatures

for crystallization. Differential scanning colorimetry measurements showed a number of exothermic and endothermic peaks in all samples. The exothermic peaks have been attributed to the crystallization of the amorphous material. Crystallization temperatures varied in the range of 620-780 K for the X=30 to X=80 samples (Table I).

The hard magnetic properties of all samples deteriorate rapidly after crystallization and the samples appear to be paramagnetic at room temperature. A.C. susceptibility measurements (Fig. 2) on a $(Pr_{80}Ga_{20})_{70}Fe_{30}$ sample showed a reduction in the magnitude of the higher temperature peak (470 K) and a drastic increase in the magnitude of the lower temperature peak ($\sim$8 K) indicating that the high T_c phase regions have transformed to the lower T_c phase after crystallization.

It thus appears that crystallization in these materials does not produce the metastable phases which are necessary for the high coercive fields observed in PrFe alloys[11]. It might be possible that the metastable phases in these materials can only be produced by the rapid solidification from the melt and not by annealing. An attempt was made to prepare partially crystallized PrGaFe alloys with different quenching rates by varying the pressure that drives the piston in the piston and anvil technique. A small variation of the coercivity with quenching rate has been observed but that was not reproducible since it was very difficult to control the quenching rate by this technique.

At this stage a decision was made to use the melt spinning technique in preparing the future alloys. The quenching rate with this method can be easily controlled by varying the speed of the

spinning wheel. Several PrGaFe samples were melt-spun with different quenching rates but their properties were very similar to those of splat-cooled samples. It was then decided to move on to the ternary RTbFe system which was proposed as an alternative system to PrGaFe alloys.

V. TERNARY RARE-EARTH SYSTEM

1. $SmTbFe_2$

Samples of $SmTbFe_2$ have been melt-spun at speeds of 900, 1900 and 3900 cm/s. The magnetic properties of these samples are listed in Table II and indicate some variations in the properties of the as-spun samples with the wheel speed. However, there is no clear trend in these measurements. Thermomagnetic data indicate that a structural change takes place upon heating the sample to 450°C (Fig. 3). This is accompanied by a change of magnetic properties as seen in Table II. In all cases, the saturation moment is increased by the described heat treatment and, in all but the slowest surface speed sample, the coercivity is increased.

2. Pr-Tb-Fe

i. $PrTbFe_2$

The results of similar measurements are shown in Table III for $PrTbFe_2$. In this case there appears to be a definite trend in coercivity and saturation moment with surface speed with M_s increasing with speed and H_{ci} decreasing with speed. Thermomagnetic analysis indicates the same structural transformation which is reflected in an increase in M_s and a decrease in H_{ci} (Fig. 4).

ii. $Pr_{0.5}Tb_{0.5}Fe_2$

A completely different behavior has been observed in the alloys with the RFe_2 composition. The as-quenched samples showed coercivities as high as 3 kOe, that are not changed with the heat treatment (Fig. 5). This is consistent with the thermomagnetic data which do not show any transformation upon heating to 520°C. The Curie temperature of the samples is around 380°C.

3. $MM_{20}Tb_{20}Fe_{60}$

The hysteresis loops of as-quenched and heat-treated samples are shown in Fig. 6. The coercivity and the moment of the as-spun samples change very little with the heat-treatment to 450°C. The Curie temperature of the samples is found to be 370°C.

In all of these alloys the shape of the as-quenched ribbons was very irregular. The samples appeared to be very brittle and crystalline. A decision was made to add a glass-forming material (B,Si) into the system in order to make the samples more glassy. Since, at that time the only material with a glass-former available was the 2605 Co Allied chemical Metglas-alloy$(Fe_{67}Co_{18}B_{14}Si_1)_X$ samples with $(RTbFe)_{1-X}$ $(Fe_{67}Co_{18}B_{14}Si_1)_X$ compositions were prepared and examined.

VI. PRASEODYMIUM (MISCH-METAL)-TERBIUM-IRON-COBALT-GLASS FORMER

1. $Pr_{11.1}Tb_{11.1}Fe_{66.8}Co_6B_{4.7}Si_{0.3}$

The shape and mechanical properties of the as-quenched ribbons were considerably improved after the addition of the glass former. The samples appear to be more ductile and shiny and they are magnetically soft in the as-quenched state(Fig. 7). The constricted shape of the loop suggests the presence of at least two magnetic phases, a soft phase and a hard phase. Thermomagnetic data (Fig. 8) up to 550°C indicate a structural transformation at around 260°C. The precipitated phase has a higher Curie temperature which is estimated to be around 475°C. The samples after the thermomagnetic analysis experiment develop very high coercive fields which could not be measured with the ordinary electromagnet (Fig. 9). The estimated room-temperature coercivity is higher than 40 kOe (Fig.9) and the maximum energy product, $(BH)_m$, is close to 2.5 MGOe.

Low temperature magnetic measurements show shifted hysterisis loops and field cooling effects. The coercivity was observed to increase with temperature (Fig. 10) rather than to decrease because of thermal activation of domain walls over the energy barriers. A similar behavior has been observed in splat-cooled PrGaFe alloys[3] and was explained in terms of a two-phase system. At higher temperatures the coercivity increases as the temperature is decreased. However, at a critical temperature (in this case, above room temperature) some of the domain become pinned so strongly in some orientation that the available field (80 kOe) cannot reorient them along the field direction. As the temperature is lowered, more and more domains

become "frozen" and do not participate in the reversible magnetization process. The loops, therefore, remain open and become narrower (smaller coercivity) as the temperature is decreased below the critical temperature.

The hysteresis loops of the as-quenched soft material are smooth and symmetric at cryogenic temperatures. A coercivity of 5 kOe has been observed at 4.2 K. At higher temperatures the coercivity decreases and becomes negligible around room temperature. However, the hysteresis loops change shape and become constricted at these temperatures (Fig. 7).

2. $Pr_{8.3}Tb_{8.3}Fe_{61.3}Co_{12}B_{9.3}Si_{0.8}$

The as-quenched samples are again magnetically soft. Thermomagnetic data indicate a Curie temperature around 450°C and a structural transformation at 220°C. A considerable hysteresis ($\sim$20°C) has been observed between the heating and cooling M vs T curves. After the M vs T heat treatment the samples become magnetically hard. However in this case, the coercivities are much lower, Hc$\sim$15 kOe, and the maximum energy product is estimated to be 1.2 MGOe.

3. $MM_{13.3}Tb_{13.3}Fe_{62.4}Co_{6}B_{4.7}Si_{0.3}$

When Pr is replaced by MM(misch-metal) the magnetic moment is slightly reduced but the coercivities of the heat treated samples are still so high that they cannot be measured with the electromagnet (H_c > 20 kOe). The maximum energy product of this sample was found to be 1.1 MGOe.

Thermomagnetic measurements show a Curie temperature of 400°C for the as-quenched sample. The Curie temperature of the precipitated phase is around 450°C.

4. Conclusion

The addition of glass-forming materials (B,Si) and Co into the PrTbFe system made it possible to achieve high-coercive fields through a simple heat treatment. This opened a new horizon for materials research and established these alloys as strong candidates for permanent magnet development. However, the new alloy contained some Co and Tb which are both expensive materials. It was also difficult at this point to determine the origin of the high coercive fields because of the multi-alloy system. An attempt was then made to take away sequentially, Co and Tb and the glass forming materials B and Si in order to find the effect of these elements on the final magnetic properties of the sample.

VII. PRASEODYMIUM-IRON(COBALT)-GLASS FORMER

1. Effect of Tb

It was believed at the time that the high coercive fields observed in PrTbFe-Metglas alloys were due to Tb. A similar effect has been observed by Koon et al[12,13] in FeBTbLa alloys. However, it was soon discovered that relatively high coercivities ($\sim$ 5-20 kOe) can be produced in alloys without Tb. These coercivities are much lower than those observed in the former alloys (Hc> 40 kOe). Therefore, one can assume that Tb has the tendency to increase the coercivity of these type of materials. That is probably why the coercivity of $Pr_{8.3}Tb_{8.3}Fe_{61.3}Co_{12}B_{9.3}$ is much lower than those observed with only 8.3% Tb (see Chapter VI) in $Pr_{11.1}Tb_{11.1}Fe_{66.8}Co_6B_{4.7}Si_{0.3}$ and $MM_{13.3}Tb_{13.3}Fe_{62.4}Co_6B_{4.7}Si_{0.3}$ alloys with 11.1 and 13.3 at % Tb respectively.

The magnetic properties of several alloys with Pr content varying in the range of 11.5 to 40 at % are shown in Figure 11. As the Pr/Fe ratio increases the coercivity of the sample is increased but the magnetic moment drops substantially. The best energy products have been obtained in alloys with 11.5 - 20 at % Pr.

The hard magnetic properties were first obtained by heating the as-quenched soft samples (Fig. 12) to 550°C and then cooling them quickly to room-temperature where the hysteresis loop was measured (Fig. 12). For the lower Pr-content alloys ($X \leq 20$ at %) this heat treatment was not sufficient to cause the structural transformation with the higher Curie temperature. It was soon found out, however, that a heat-treatment at higher temperatures (650 - 750°C) not only improved the squareness of the demagnetization curve (with a slight decrease of H_c) of the previous samples (Fig. 13) but also induced the structural transformation which is

required for the hard magnetic properties. Thermomagnetic data were taken during the described heat treatment and are shown in Fig. 14. The Curie temperature of the as-quenched phase is around 250°C. A structural transformation appears to take place around 300°C. The Curie temperature of the precipitated phase is estimated to be 430°C. Upon heating the sample to 550°C, a gradual increase of the magnetization has been observed in the M vs T curve up to 750°C. This is probably related to the precipitation of an α-Fe phase (see microstructure studies). The results of the thermomagnetic data for all the samples are listed in Table IV. As the Pr-content increases the Curie temperatures of the as-quenched and crystallized phase decrease.

2. Effect of Co

The amount of cobalt in the previous alloys was so small that it should not have any significant effect on the final magnetic properties of the sample. This was confirmed experimentally in PrFeBSi alloys which do not contain any cobalt. The coercivity is not affected by the absence of cobalt. However, the magnetic moment increases slightly and this leads to higher energy products which reach the value of 13 MGOe in $Pr_{16.4}Fe_{75.5}B_{4.8}Si_{3.3}$.

The magnetic properties of $Fe_{92-X}Pr_X(BSi)_8$ alloys are shown in Fig. 15. A behavior similar to that of FeCoPr(BSi) alloys has been observed in these samples. As the Pr content increases, the coercivity is increased but the magnetic moment is significantly reduced. The maximum energy products have been observed in alloys with Pr content around 15 at %. The magnetization of the low Pr content alloys reaches the value of 152 emu/g (Fig. 16) which translates to a value of $4\pi M_s$=13.9 kG. If a reasonably high coercivity could be induced in these samples, a high energy

product can be obtained with an upper limit of $(BH)m \simeq \frac{(4\pi MS)^2}{2} = 48$ MGOe. This value is certainly much higher than that predicted for the 1:5 and 2:17 rare-earth alloys.

The hard magnetic properties of these alloys are achieved through a simple heat treatment. The samples are heated relatively quickly to 750°C and then cooled to room temperature in a magnetic field. Thermomagnetic data show magnetic transitions at around 140, 330 and 750°C, and peaks around 280 and 700°C (Fig. 17). The first transition temperature (~140°C) has been associated with the Curie temperature of the as-quenched amorphous phase since it disappears after crystallization. The peak around 280°C is probably due to the precipitation of the crystalline phase (which takes place upon heating the sample to 250°C) with a Curie temperature of 330°C. At higher temperatures (~620°C) the intensity of magnetization increases due to the precipitation of a phase with Curie temperature around 750°C (maximum temperature reached). The precipitated high-temperature phase has been identified as α-Fe (see Section). The only difference between these samples and those containing cobalt is that in the Co samples the Curie temperatures of the amorphous and the precipitated main crystalline phase are higher by about 100°C. The as-quenched samples are highly inhomogenous and in some cases are not completely amorphous (Fig. 18, Fig. 19). In Fig. 18 the as-quenched sample contained some of the precipitated crystalline phase which is usually induced by heat treatment. Also, the sample shown in Fig. 19 contained some α-Fe in the as-quenched state. The Curie temperatures of the various $Fe_{92-x}Pr_x(BSi)_8$ alloys are listed in Table V.

3. Effect of Glas-Formers

It is concluded from the previous discussions that the glass-forming materials B and Si not only modify the mechanical properties of the as-quenched ribbons but they also influence significantly the final magnetic properties of the samples.

i. Effect of Silicon

When all boron is replaced by Si, the structural transformation which gives rise to the high H_c is not present and the materials appear to be magnetically very soft. This is shown in Fig. 20 for the $Pr_{24.7}Fe_{70.3}Si_5$ alloy. The magnetic moment of the heat-treated sample appears to be slightly larger than that of the as-quenched sample but its Curie temperature is much lower (Fig. 21). It is worth pointing out that the Curie temperature of the as-quenched phase is much higher than those of the other samples. When all Si is replaced by boron the usual structural transformation takes place upon heating the sample to 750°C and this gives rise to good hard magnetic properties. However the highest energy product has been obtained in the $Fe_{75.5}Pr_{16.4}B_{4.8}Si_{3.3}$ sample which contains a small amount of silicon.

ii. Effect of Boron

The effect of boron on the magnetic properties of $(Pr_6Fe_{23})_{100-x}B_x$ alloys is shown in Fig. 22. The coercivity and energy product have been observed to increase initially with the boron content and they peak around 10 at % boron. In $(PrFe_5)_{100-x}B_x$ alloys (Fig. 23) the optimum properties have been observed in samples with 5 at % boron. All of these samples do not show any sign of the α-Fe phase (Fig. 24) which usually is observed in the $M_H(T)$ data of Fe(Co)PrSi alloys (Fig. 17) after the high temperature heat treatment. The results of the thermomagnetic data in these samples are shown in Table VI. The Curie temperature of the crystallized phase is

around 310°C while the Curie temperature of the as-quenched phase increases from 140°C for X=5 to 170°C for X= 15 in $(Pr_6Fe_{23})_{100-x}B_x$ alloys and from 150°C for X=5 to 200°C for X=15 in $(PrFe_5)_{100-x}B$ alloys.

Having discussed, in general, the magnetic properties of Fe(Co)PrSiB alloys, we will now concentrate on the optimum alloy $Fe_{75.5}Pr_{16.4}B_{4.8}Si_{3.3}$ where the magnetic and structural properties will be discussed in more detail.

4. Optimum Alloy - $Fe_{75.5}Pr_{16.4}B_{4.8}Si_{3.3}$

A. As-quenched sample

The as-quenched sample shows a constricted hysteresis loop which is due to the coexistence of a soft phase and a hard phase with a coercivity of around 15 kOe (Fig. 25). The saturation magnetization of the sample is approximately 94 emu/g.

B. Heat treatments

The samples were heated in a magnetic field up to certain temperature and then cooled relatively quickly to room temperature. Thermomagnetic data were taken in the heating and cooling cycle to find out whether any magnetic transformation took place.

i. Heat treatment at 750°C

The thermomagnetic data up to 750°C are shown in Fig. 26. The Curie temperature of the as-quenched phase is found to be around 160°C. Upon heating the sample to 750°C, two broad peaks have been observed at around 270 and 650°C respectively. The lower peak may be associated with the onset of the precipitation of the main crystalline phase with Curie temperature around 340°C as shown in the cooling cycle (Fig. 26). The

higher temperature peak has been related to the precipitation of the α-Fe phase with a Curie temperature greater than 750°C (maximum temperature reached). The presence of α-Fe in the heat-treated sample has been confirmed with transmission electron microscopy studies (see Section VII, 4G).

The samples after the thermomagnetic experiment are magnetically hard and show high energy products which in some cases reach the value of 13 MGOe (Fig. 27). An additional heat treatment for 15 minutes at 750°C had very little effect on the magnetic properties of the samples. The coercivity was decreased to 14.5 kOe but the squareness of the demagnetization curve was slightly improved. Magnetizing the sample in a pulsed field of 63 kOe did not have any significant effect on the hysteresis loop.

Since the additional heat treatment did not change the magnetic properties significantly, it was assumed that the sample was probably in the overaged state after the thermomagnetic experiment. A heat treatment at a much lower temperature was then attempted.

ii. Heat treatment at 550°C

The sample was heated relatively quickly to 550°C and then cooled to room temperature. Thermomagnetic data were taken during the heat treatment and are shown in Fig. 28a. It appears that heating the sample to 550°C is not sufficient to transform completely the as-quenched phase to the higher Curie temperature ($\sim$ 330°C) phase. The hysteresis loop of the sample after the thermomagnetic experiment is almost identical to the as-quenched constricted loop (Fig. 29).

The sample then was subjected to a cumulative heat-treatment at 550°C and the results of this heat-treatment on the hysteresis loops are

shown in Fig. 29. After a long time of annealing at 550°C the harder phase grows at the expense of the softer phase and after five hours it occupies most of the volume of the sample. This is also shown in the thermomagnetic data (Fig. 28b) where the as-quenched low Curie temperature phase has been mostly transformed into the high Curie temperature phase after five hours of annealing at 550°C. However, the highest energy product achieved in this heat-treatment is only 7 MGOe (Fig. 30) because of the dip in the demagnetization curve due to the presence of a small amount of the soft phase (Fig. 29). To reduce the time of this heat-treatment and obtain a complete story of the magnetic properties versus annealing time, the intermediate temperature of 650°C was used.

iii. Heat-treatment at 650°C

The thermomagnetic data of the sample heated to 650°C are very similar to those of the 750°C heat-treatment (Fig. 26). The coercivity of the sample peaks after 15 minutes of annealing at 650°C while the highest energy products have been obtained after a 15 minutes heat-treatment(Fig. 31), the energy products are again considerably lower than those obtained in the 750°C heat-treatment.

iv. Heat-treatment at 250°C

Magnetic annealing in a field of 15 kOe has been attempted at 250°C which is the temperature where a local maximum has been observed in the heating cycle of the thermomagnetic data (Fig. 26). It was believed, at the time, that the maximum was due to the precipitation of the crystalline phase with a Curie temperature of 320°C which gave rise to the hard magnetic properties. However, the magnetic properties of the as-quenched soft sample did not change at all after six hours of heat treatment at 250°C. Thermomagnetic data on the heat-treated sample are similar to those of the as-quenched sample indicating that no major structural transformation takes place during this heat treatment.

C. Temperature dependence of magnetic properties

The temperature dependence of the magnetic properties of an $Fe_{75.5}Pr_{16.4}B_{4.8}Si_{3.3}$ sample is shown in Fig. 32. The coercivity increases at lower temperatures and reaches the value of 68 kOe at 4.2 K. This is the highest value reported for these materials at cryogenic temperatures. On the other hand, the remanence and the magnetization at the maximum applied field (H_a=80 kOe for $T \leq 260$ K, H_a=23 kOe for $T \geq 300$ K) increase with temperature and then peak at a temperature above room temperature. This might be due to the fact that at lower temperatures the applied field is not sufficient to saturate the sample (Fig. 33) because of the large coercive fields and therefore the magnetization is far away from saturation. At higher temperatures the coercive fields decrease drastically (Fig. 32) and the applied field is sufficient to roughly saturate the sample and therefore increase the magnetization.

D. Magnetic anisotropy

Hysteresis loops were measured in magnetic fields parallel and perpendicular to the plane of the ribbon in order to find out whether there is any macroscopic anisotropy in the sample. Pieces of the sample ribbon were wrapped in tantalum foil and stacked into a "plate" form where the loops were measured parallel and perpendicular to the plate. However, the sample pieces were too brittle and in some cases the plane of the ribbon might have been perpendicular to the plane of the "plate." In spite of the crude way of mounting the samples, there seems to be a considerable difference between the two loops (Fig. 34) indicating the presence of a magnetic anisotropy along the plane of the ribbon. More careful measurements are planned to be made in the future to estimate the magnitude of this anisotropy.

E. Differential scanning calorimetry measurements

Thermal analysis measurements in $Fe_{75.5}Pr_{16.4}B_{4.8}Si_{3.3}$ up to 500°C showed a large irreversible exothermic peak (Fig. 35) at around 425°C which has been associated with the crystallization of the amorphous part of the sample. The crystallization temperature is much lower than the temperature of the heat-treatment indicating that the crystallized phase in its early stage is not very effective for magnetic hardening. It is probable that at higher temperatures this phase grows faster to the right size for magnetic hardening or, it transforms into more stable phases which lead to the observed high coercive fields. Thermal analysis measurements are planned to be made up to 1200°C to investigate the structural transformations which occur during the heat-treatment of the sample.

F. X-ray diffraction studies

The x-ray diffraction measurements of the as-quenched and heat treated samples are shown in Fig. 35. In addition to the crystalline peaks the as-quenched diffraction pattern shows the two broad peaks which are characteristic of an amorphous structure. Thus one can say that the as-quenched sample is a mixture of amorphous and crystalline phases.

An attempt was made to match the d-spacings derived from these patterns with the d-spacings of known compounds of the iron - praseodymium -boron - silicon system. However, this is a difficult task since the only two stable phases reported in the PrFe system are the Pr_2Fe_{17} and $PrFe_7$[18] phases and none of these match the peaks of the diffraction patterns consistently. (A $PrFe_2$ phase has also been reported but this is produced only under high pressure[18].) In addition, the crystal structures

of the various rare-earth compounds are related to each other and this leads to superimposed peaks which make the analysis even more difficult. It might be possible that the crystalline structures observed are metastable phases which are produced only by the rapid solidification from the melt and have not yet been studied. Some of the peaks of the heat-treated sample have been attributed to the α-Fe phase.

It appears from these studies that more X-ray diffraction data are required to determine the crystalline structure of the as-quenched and precipitated phases. X-ray diffraction measurements will be obtained for all the different heat treatments and compared with each other and with the microstructure studies which will be made on the same samples.

G. Microstructure studies

The preparation of specimens for the transmission electron microscope studies was time consuming. At the beginning most of the time was spent to find a solution to electropolish these materials. A cooled methanol perchloric acid solution has been found to give us satisfactory results. The samples were further thinned by ion-milling. In addition to the electropolishing difficulties, the samples were very brittle and they tend to oxidize quickly so that they had to be examined right after their preparation.

The transmission electron microscope studies reveal three different type of microstructures in the as-quenched and heat-treated samples;

a) An amorphous microstructure has been observed mostly in the as-quenched samples and is easily characterized by the two halos in the electron diffraction patterns.

b) A very fine precipitate structure (Fig. 37) has been observed mostly in the heat-treated samples. The size of the precipitates is below 100 $\mathring{A}$ and this makes their characterization very difficult.

c) A coarse precipitate structure (up to 1μm) has been observed mostly in the heat-treated samples. The large precipitates have been identified as α-Fe and they are consistent with the thermomagnetic data (Fig. 25) which show the existence of a small amount of a phase with a Curie temperature around 750°C (the Curie temperature of iron is 780°C).

The surface of the samples was also examined with a scanning electron microscope equipped with an energy dispersive x-ray analysis unit. The $Fe_{75.5}Pr_{16.4}B_{4.8}Si_{3.3}$ sample appears to be fairly homogenous (up to the resolution of SEM $\sim$ 100Å) with very few scattered inclusions of a different phase. X-ray analysis studies show a chemical composition of 81.5 wt% Fe, 18.5% Pr and 2.5% Si (B is not detected by this technique) for the matrix and a 61 wt% Fe and 39% Pr for the inclusions.

The samples studied are not very homogenous so that the specimens have to be examined in many different areas before a conclusion about their microstructure can be made. The size of the precipitated phase is also very fine and that will require the use of more sophisticated electron microscopy techniques in order to determine their crystalline structure and chemical composition.

VIII. IRON-PLATINUM BASED ALLOYS

As has been mentioned in the Introduction, the FePt(Pd) alloys show good hard magnetic properties which can be exploited if Pt(Pd) is replaced by another inexpensive element. Several $FeNiPt(Pd)_{1-x}Ax$ alloys were prepared and studied.

i. Old Heat Treatment

The samples were heat-treated in a tube-type furnace equipped with a vacuum-tight retort. The samples, wrapped in tantalum foil, were placed in an Inconnel "boat", homogenized at 1100°C and then quenched to room temperature by removing the "boat" from the furnace to a water-cooled copper hearth. This quenching is needed to retain the high temperature cubic phase. The quenched samples were subjected to the usual heat treatment[15] between 600 and 700°C in order to precipitate the tetragonal phase[15] which would lead to hard magnetic properties.

The results of these measurements are presented in Table VII. All the FePtNi group samples exhibited a saturation magnetization M_s between 70 and 77 emu/g in the as-quenched state except for the Mo-sample which measured 63 emu/g. The FePdNi samples show a higher M_s in the range of 100-120$\frac{emu}{g}$. In $FePt_{0.6}Ni_{0.3}Mn_{0.1}$, the saturation magnetization was examined as a function of heat treatment (Table VII). M_s remained constant (69 - 72 emu/g) through the first six heat treatments but increased to 86 emu/g when subjected to a 4-hour heat treatment at 600°C. Only three samples developed a marginally significant coercivity after the described heat treatment. A coercivity of 450 Oe has been observed in $Fe_{0.9}Pt_{0.6}Ni_{0.4}Sn_{0.1}$ while the $FePt_{0.6}Ni_{0.3}Mn_{0.1}$ and $Fe_9Pt_{0.6}Ni_{0.4}Lu_{0.1}$ samples showed maximum coercivities of 260 and 1150 Oe, respectively.

These results definitely show no significant magnetic hardening after the aging heat treatment. It was suspected at the time that the lack of success was due to the low quenching rate from the homogenizing temperature to room temperature. If the quenching is not fast enough, the high temperature disordered phase-centered cubic phase, will not be retained. As a result, the samples will be overaged after any form of heat treatment and therefore, the volume fraction of the ordered phase will not be controlled.

ii. New Heat-treatment

To improve the quenching rate, the samples were first sealed under vacuum in a quartz tube, homogenized at 1100^{o}C and rapidly cooled to room temperature by breaking the quartz tube under tap water. This type of quenching was first tested on the known FePtNi and CoPt magnets. Thermomagnetic data were used to check whether the usual structural transformation takes place upon heating the samples to high "in-situ" in a vibrating sample magnetometer at various fixed temperatures (600 - 700^{o}C) for different times at the end of which, they were quenched to room temperature with Argon gas.

The results of the new heat treatment for the CoPt and FePtNi samples are shown in Fig. 38 and 39. The quenched samples are magnetically soft and saturate easily at relatively low fields, indicating the presence of the disordered f.c. cubic phase. When the quenched samples are heated to 600 or 700^{o}C for a certain period of time, they undergo a cubic-tetragonal transformation and they become magnetically hard. In CoPt the induced hard tetragonal phase has a lower Curie temperature than the soft cubic phase and it is harder to magnetize. (Fig. 38) An opposite behavior has been observed in FePtNi (Fig. 39) where the Curie temperature of the

precipitated tetragonal phase is higher than that of the original cubic phase. These results indicate strongly that the new quenching rate is fast enough for the cubic-tetragonal transformation to take place and produce the good hard magnetic properties.

The new heat treatment was subsequently used on the program samples and the results are shown in Fig. 40 - 43). Almost all of the new alloys showed a behavior similar to that of FeNiPtCu (Fig. 40) where no phase transformation has been observed in the temperature range covered. However, in $FePt_{0.5}Ni_{0.4}Sn_{0.1}$ the transformation occurred (Fig. 41) and produced a coercivity of 600 Oe after the thermomagnetic experiment heat-treatment. No optimization heat treatment has been attempted yet on this sample. A completely different behavior has been observed (Fig. 42) in a FeNiIn sample which does not contain any Pt. In this case several peaks have been observed in the thermomagnetic data (Fig. 42 - 43) and these indicate the presence of some kind of phase transformation. This alloy and that of $FePt_{0.5}Ni_{0.4}Sn_{0.1}$ look very promising and they need to be further investigated. Transmission electron microscope studies are required to examine the nature of the phase transformations which take place in these alloys upon heating to 700°C. This would certainly help us to understand the origin of the coercive fields observed in these two materials and therefore try to optimize them by the appropriate heat treatment.

IX. CONCLUSIONS

The FePr(B,Si) alloys appear to be outstanding materials for permanent magnet development. So far, the optimum properties have been obtained on a $Fe_{75.5}Pr_{16.4}B_{4.8}Si_{3.3}$ alloy which showed a saturation magnetization of .3 kG, a coercivity of 15 kOe and a maximum energy product around 13 MGOe. However, the higher Fe-content alloys look more promising since their saturation magnetization is much higher (13.9 KG). If a higher coercivity could be developed in these materials the energy product could be increased as high as 48 MGOe (upper limit). Presently, their coercivity is in the range of 3-5 kOe and this limits the energy product to 6 MGOe.

In addition, these alloys do not contain any cobalt and they consist of materials which are abundant and very cheap. In their present form they are much better than the commercial AlNiCo ($(BH)_m$ 10 MGOe, H_c 1.8 kOe), MnAlC ($(BH)_m$ 5 MGOe, H_c 3 kOe) and ferrite magnets ($(BH)_m$ 4 MGOe, H_c 4 kOe) and with some improvement will compete strongly with the rare-earth cobalt magnets.

The remanence of these alloys and therefore, their energy products can be slightly increased by magnetizing the samples to higher fields (since they are not fully saturated at 23 kOe) or, by measuring the hysteresis loops on aligned powdered samples along the direction of alignment. Higher energy products can also be achieved by optimizing the properties of the best alloy composition. Slight variations in chemical composition, heat treatment and the original quenching conditions can possibly lead to even higher energy products. In addition, one could substitute another rare-earth metal for Pr and find out the effect on the final magnetic properties of the sample. In particular, the substitution of

Nd for Pr appears to be very promising since it has been observed that the NdFe alloys have slightly higher moments than the PrFe alloys.

Very few experiments have been made to investigate the origin of magnetic hardening in these materials. Magnetic and microstructure studies show a structural transformation which takes place upon heating the samples to 750°C. The precipitated phase appears to be highly anisotropic. Transmission electron microscope studies showed a very fine precipitate structure with a size below 100A. However, it was extremely difficult to identify the crystalline structure and chemical composition of the precipitate phase with the existing data. The crystalline structures of the rare-earth systems are related to each other and this leads to overlapping peaks in the x-ray diffraction pattern which makes the interpretation more difficult. In addition, the as-quenched samples are not homogenous and therefore one has to examine several different areas of the sample in the electron microscope studies before a conclusion about the microstructure can be made.

REFERENCES

1. A. Menth, H. Nagel and R. S. Perkins, Ann. Rev. Mater. Sci. 8, 21 (1978).

2. R. W. Lee, J. Appl. Phys. 52, 2549 (1981).

3. S. G. Cornelison, D. J. Sellmyer and G. Hadjipanayis, J. Appl. Phys. 52, 1823 (1981).

4. G. Hadjipanayis, M. Sc. Thesis, University of Manitoba, Canada (1974).

5. R. W. Cochrane, R. Harris and M. J. Zuckermann, Phys. Rep. 48, 1 (1978).

6. J. J. Rhyne, Handbook on the Physics and Chemistry of Rare-Earths, edited K. A. Gschneider, Jr. and L. Eyrin (North Holland, Amsterdam, 1979) p.259.

7. G. Hadjipanayis, S. G. Cornelison, J. M. Gerber and D. J. Sellmyer, J. Mag. Magn. Mat. 21, 101 (1980).

8. G. Hadjipanayis, D.J. Sellmyer and B. Brandt, Phys. Rev. B 23, 3349 (1981).

9. A. E. Clark, Appl. Phys. Lett. 23, 642 (1973).

10. H. T. Savage, A. E. Clark, S. J. Pickart, J. J. Rhyne and H. A. Alperin, IEEE Trans. Magn. MAG-10, 807 (1974).

11. J.J. Croat, IEEE Trans. Magn. MAG-18, 1442 (1982).

12. N. C. Koon and B. N. Das, Appl. Phys. Lett. 39, 840 (1981).

13. N. C. Koon, B. N. Das and J. A. Geohegan, IEEE Trans. Magn. MAG - 18, 1448 (1982).

14. N. Vlasova and Z. Vintaykin, Fiz. Metalloved 27, 631 (1968).

15. G. Hadjipanayis and P. Gaunt, IEEE Trans. Magn. MAG-12, 393 (1976).

16. G. Hadjipanayis, unpublished work.

17. G. Hadjipanayis, S. H. Wollins, R. C. Hazelton, K. R. Lawless, R. Prestipino and D. J. Sellmyer, J. Appl. Phys. 53, 7780 (1982).

18. JCPDS X-ray diffraction data file.

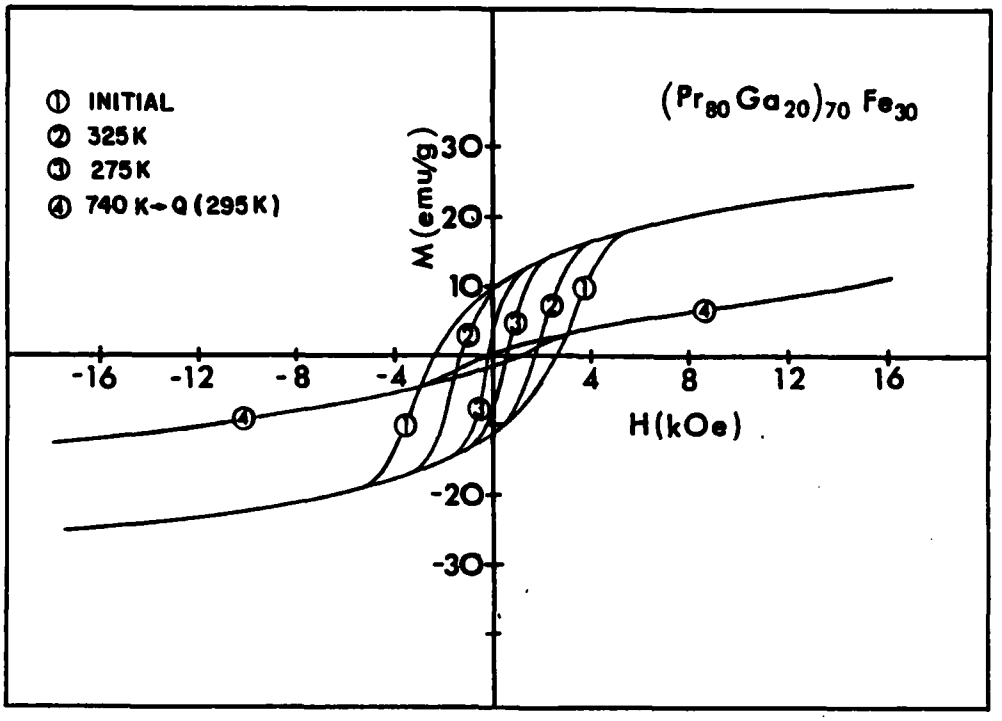

1-a.

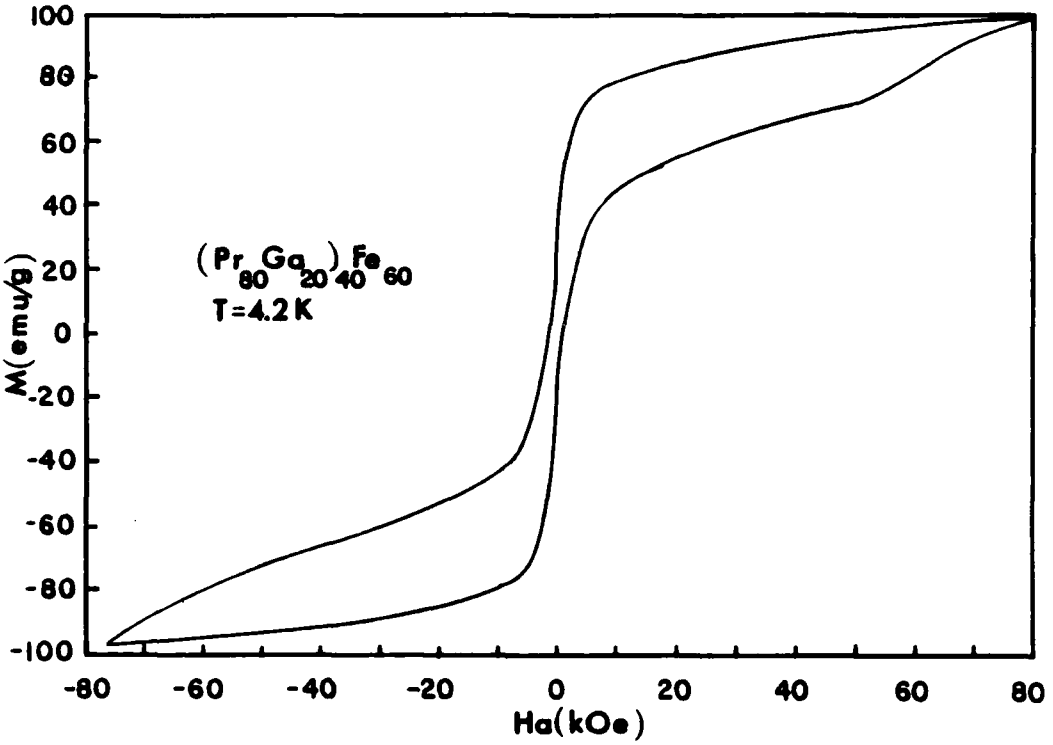

1-b.

FIG. 1-a. Temperature dependence of hysteresis loops for $(Pr_{80}\ Ga_{20})_{70}Fe_{30}$;

1-b. Low temperature hysteresis loop for $(Pr_{80}\ Ga_{20})_{40}Fe_{60}$.

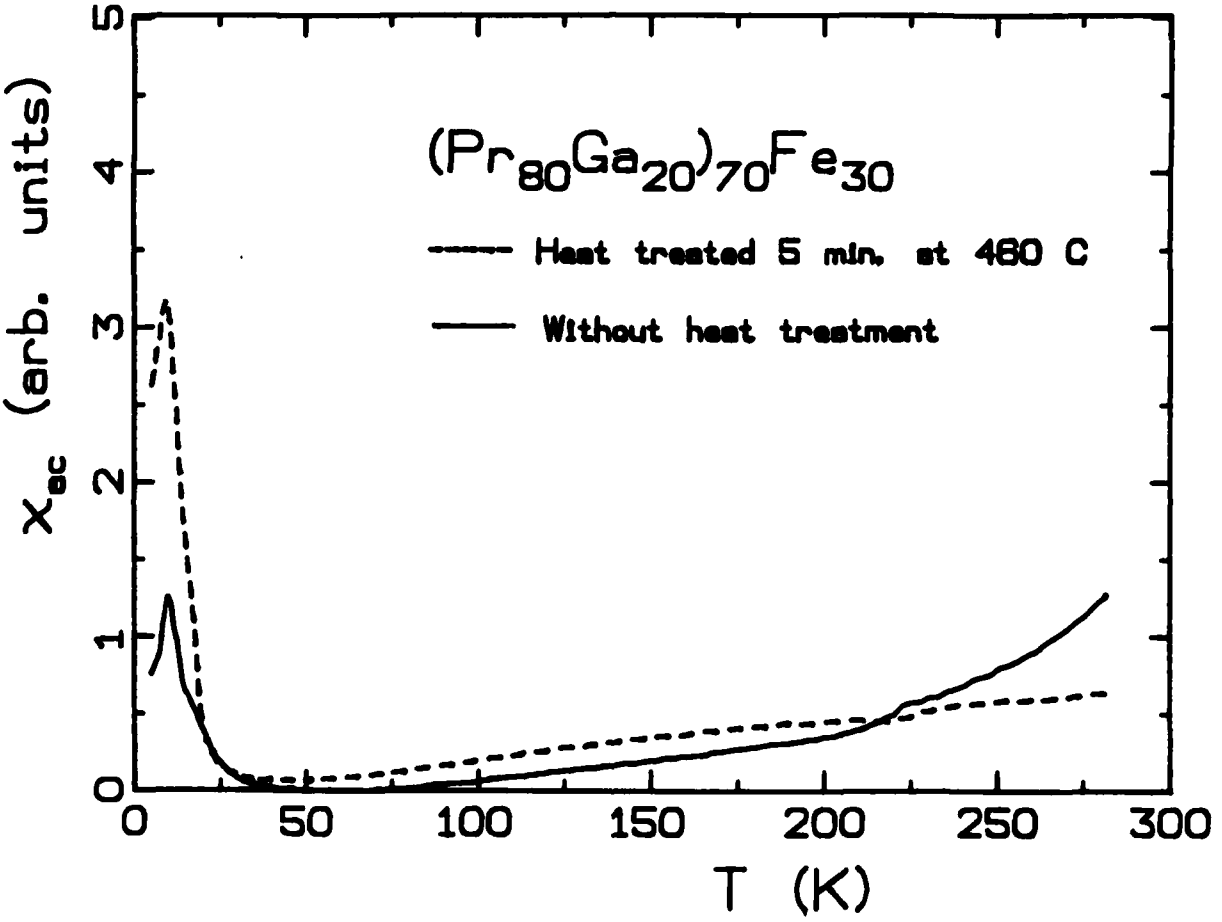

FIG. 2 A.C. susceptibility of an amorphous and a partially crystallized $(Pr_{80}\ Ga_{20})_{70}\ Fe_{30}$ sample.

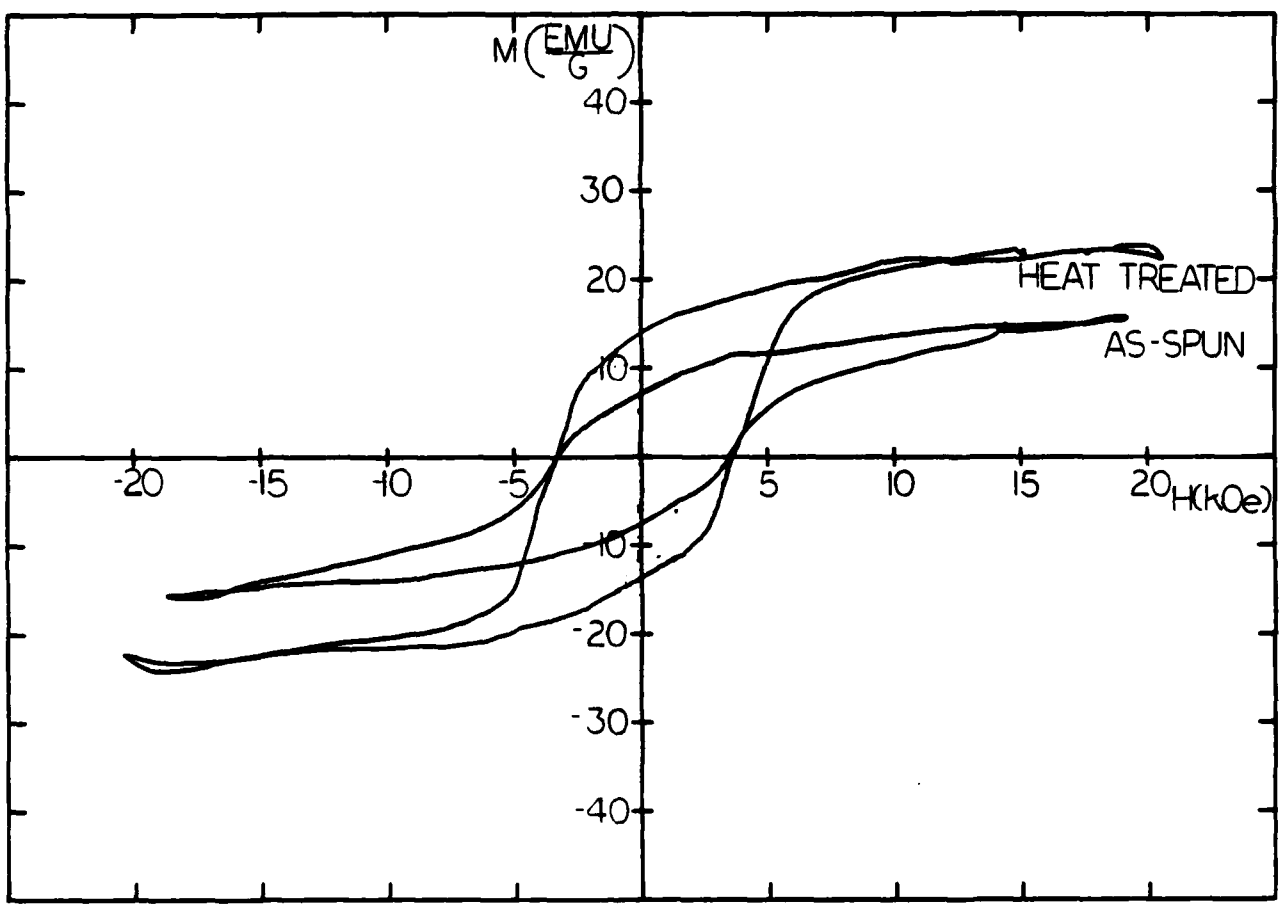

FIG. 3. Hysteresis loops of melt-spun Sm Tb Fe_2 before and after heat treatment at 450°C for 30 minutes.

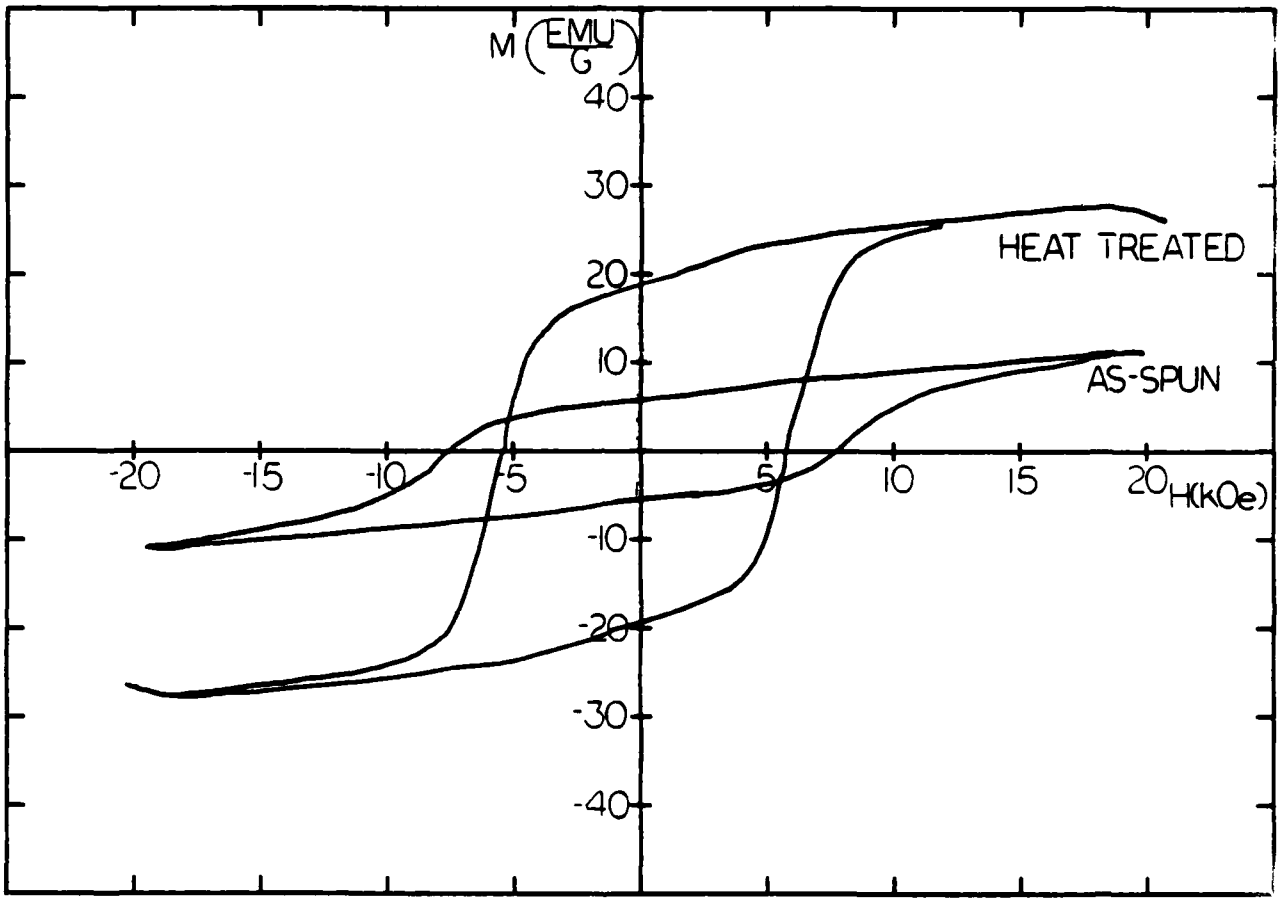

FIG. 4. Hysteresis loops of melt-spun Pr Tb Fe_2 before and after heat treatment at 450°C for 182 minutes.

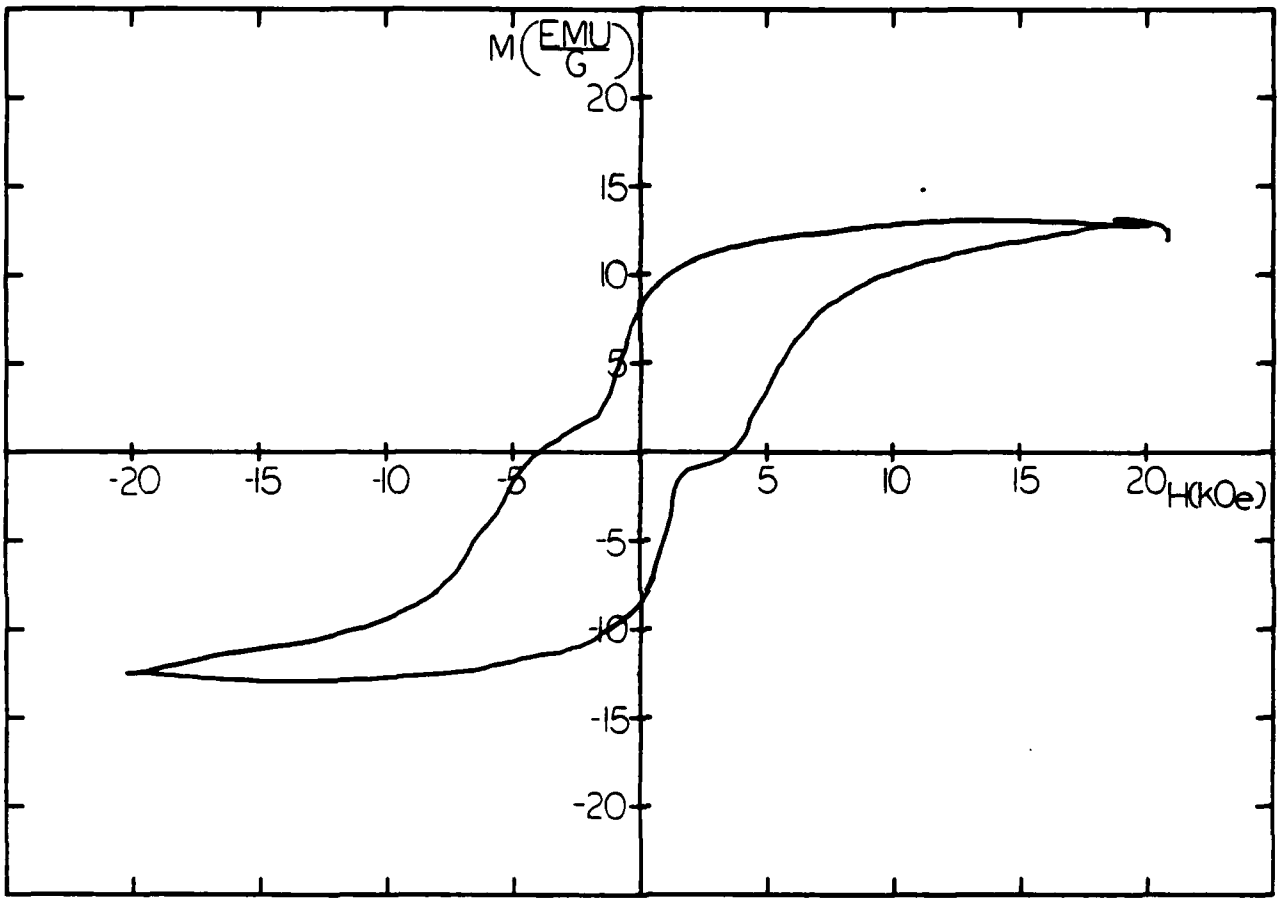

FIG. 5. Hysteresis loop of melt-spun $Pr_{0.5}Tb_{0.5}Fe_2$ after heat treatment at 520°C for two minutes.

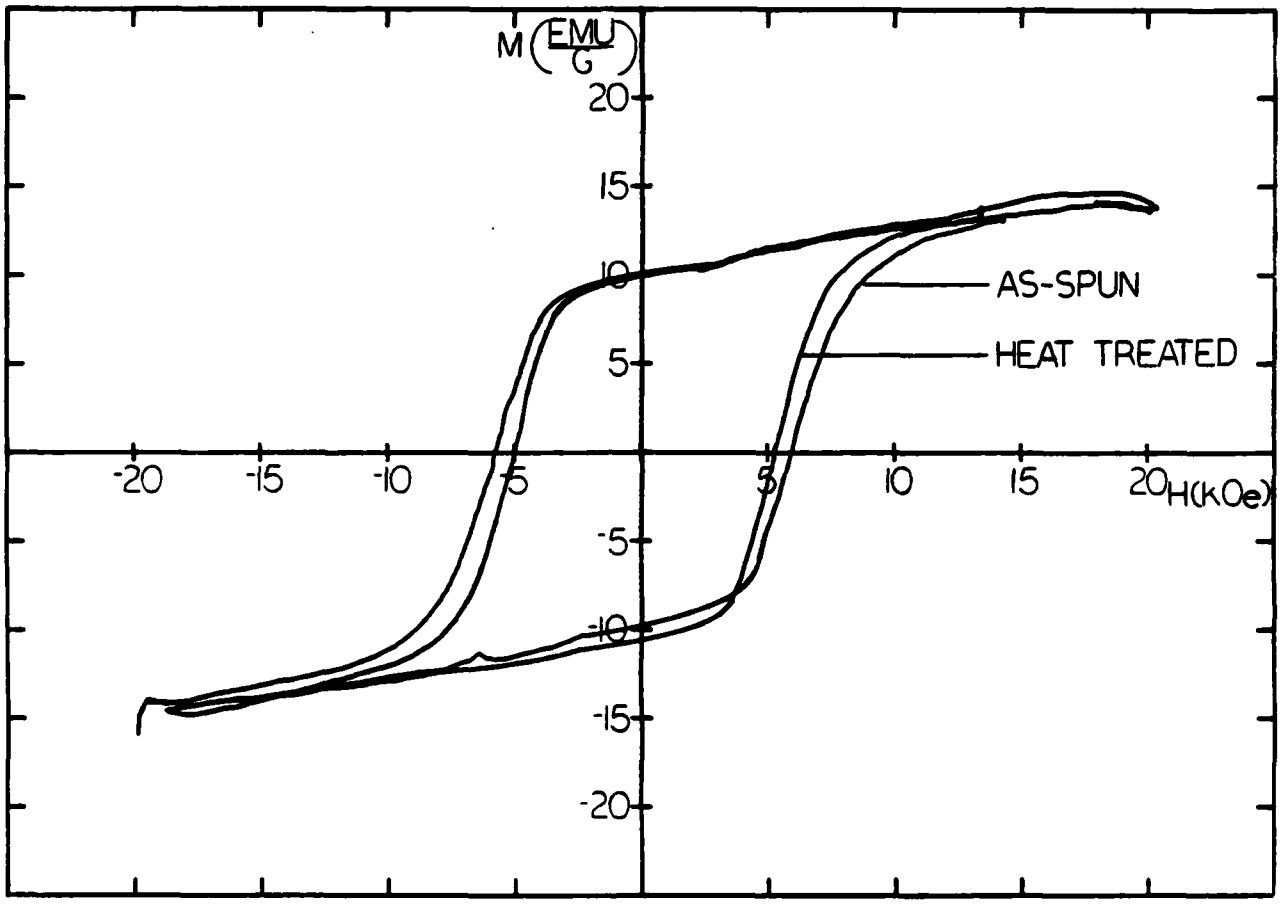

FIG. 6. Hysteresis loops of melt-spun $MM_{20}Tb_{20}Fe_{60}$ before and after heat treatment at 450°C for 15 minutes.

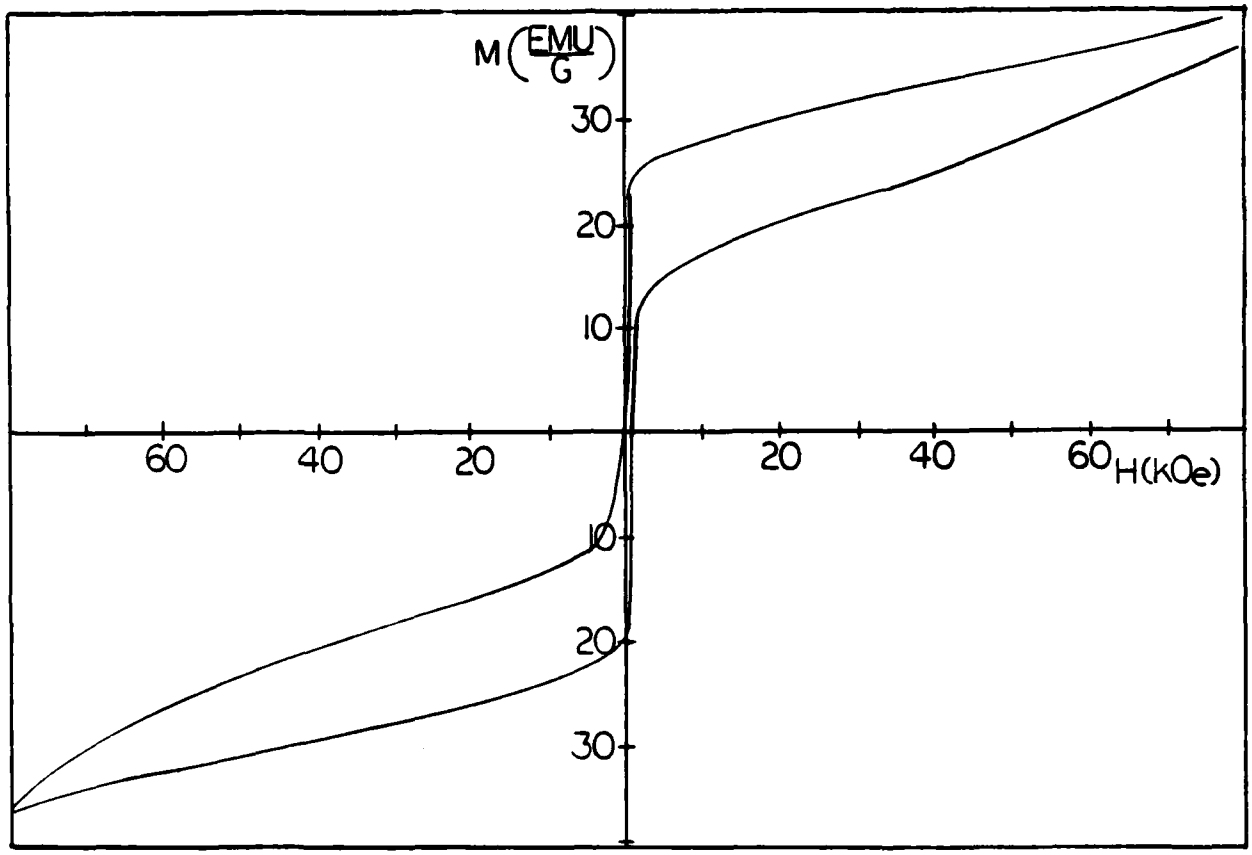

FIG. 7. Constricted hysteresis loop for as quenched $Pr_{11.1}Tb_{11.1}Fe_{66.8}Co_6B_{4.7}Si_{0.3}$.

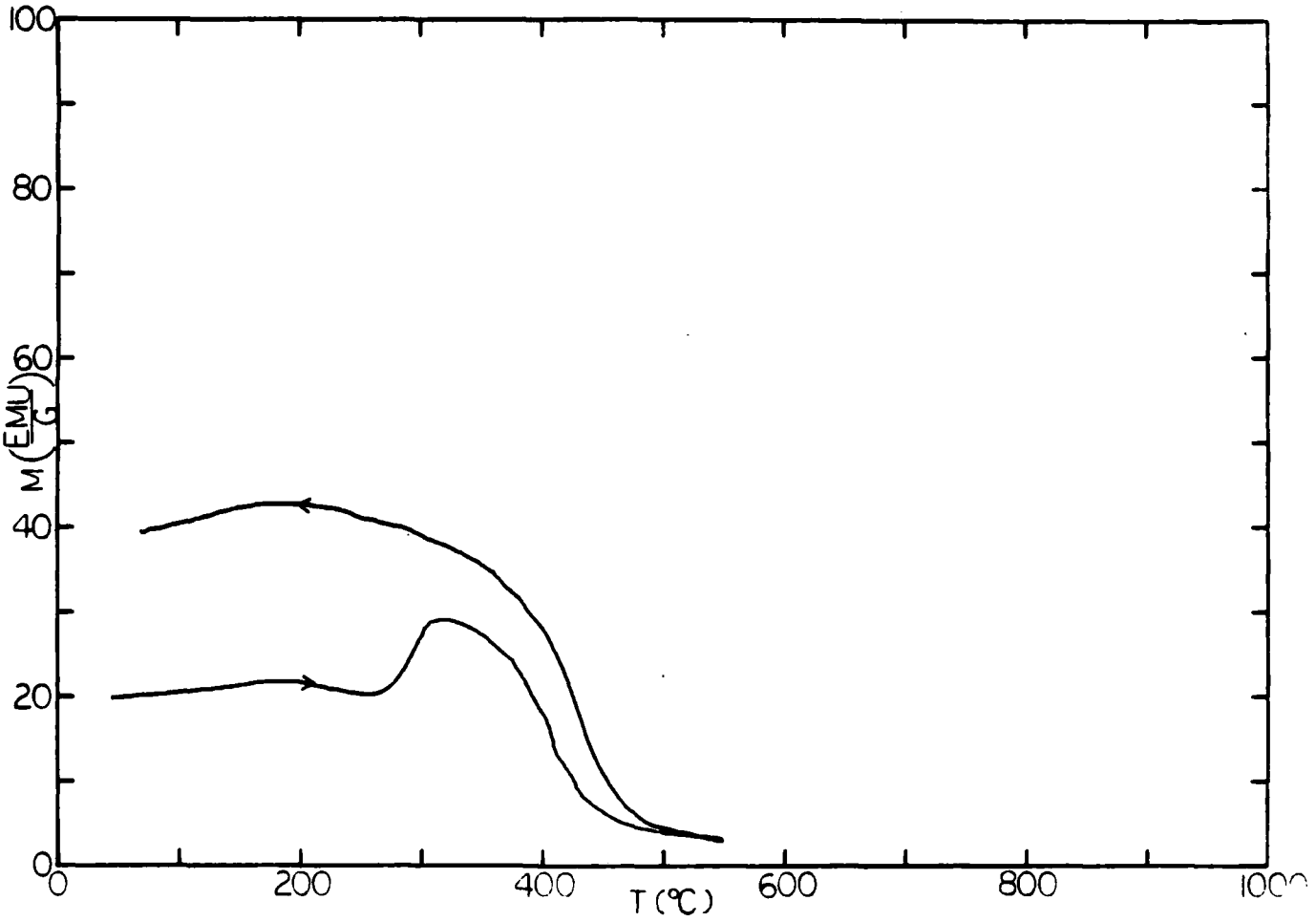

FIG. 8. Thermomagnetic data for melt-spun $Pr_{11.1}$ $Tb_{11.1}$ $Fe_{66.8}Co_6$ $B_{4.7}$ $Si_{0.3}$.

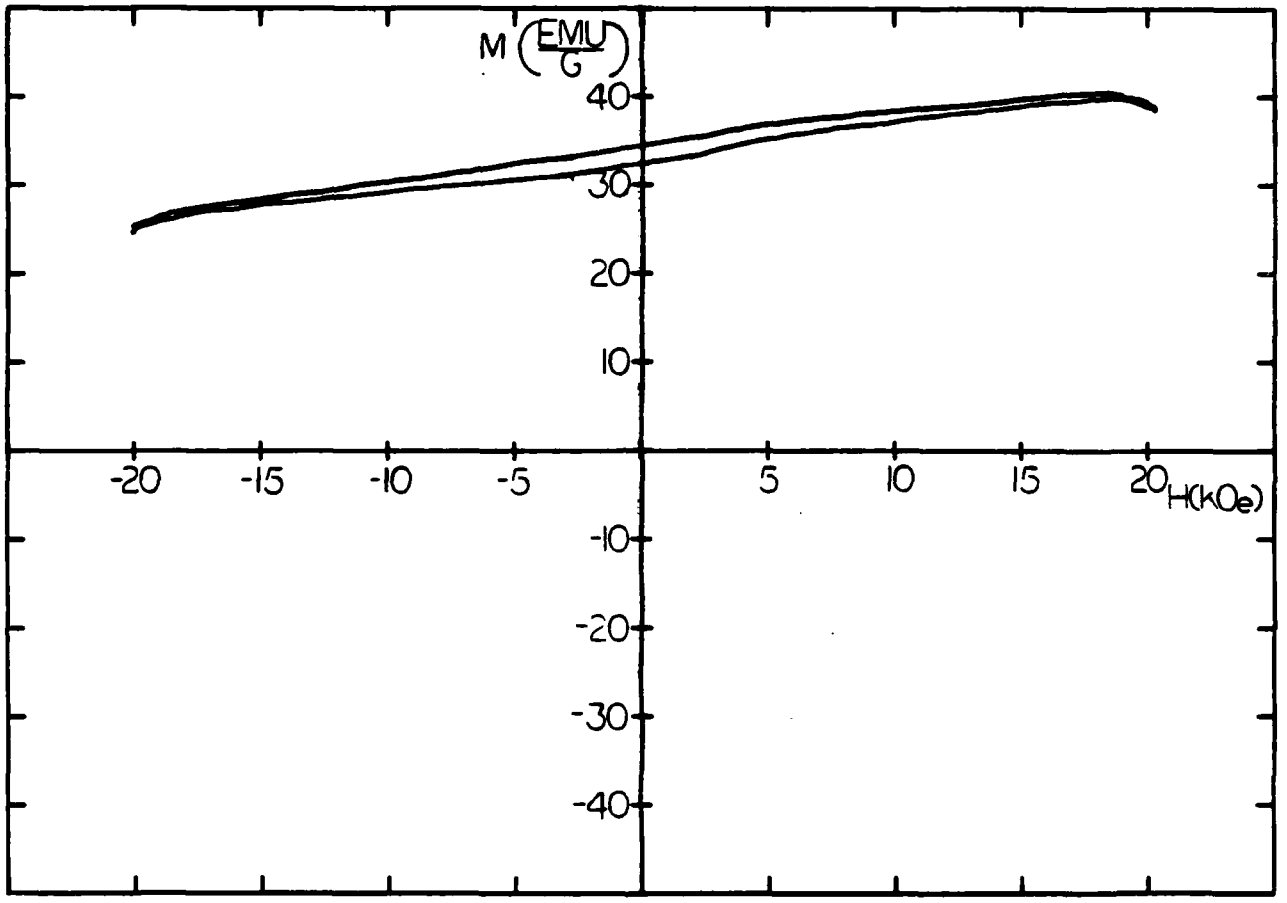

FIG. 9. Irreversible hysteresis loop for melt-spun $Pr_{11.1}Tb_{11.1}Fe_{66.8}Co_6 B_{4.7} Si_{0.3}$ after heat treatment shown in Fig. 8.

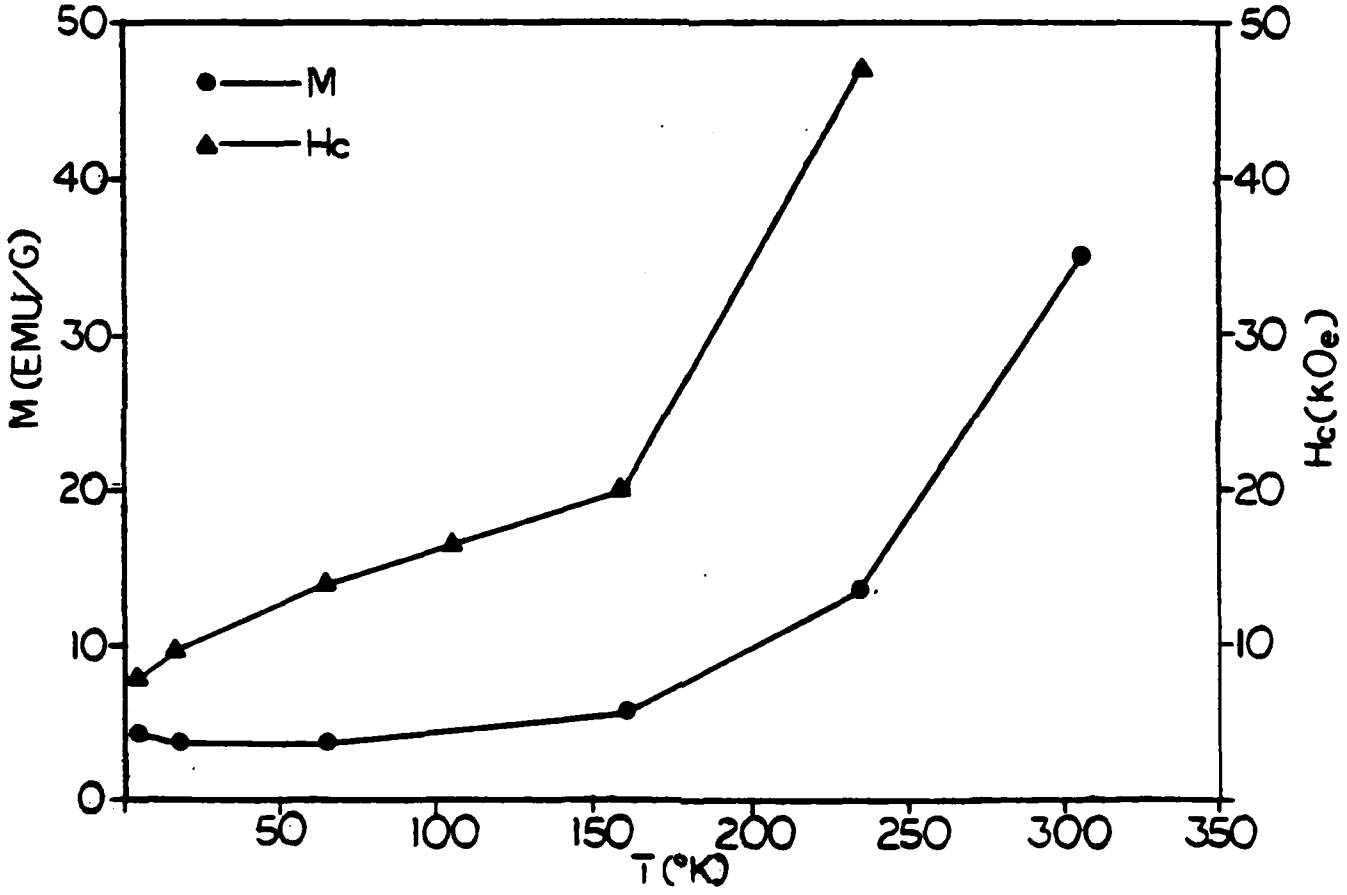

FIG. 10. Low temperature magnetic properties of $Pr_{11.1}Tb_{11.1}Fe_{66.8}Co_{6.}B_{4.7}Si_{0.3}$.

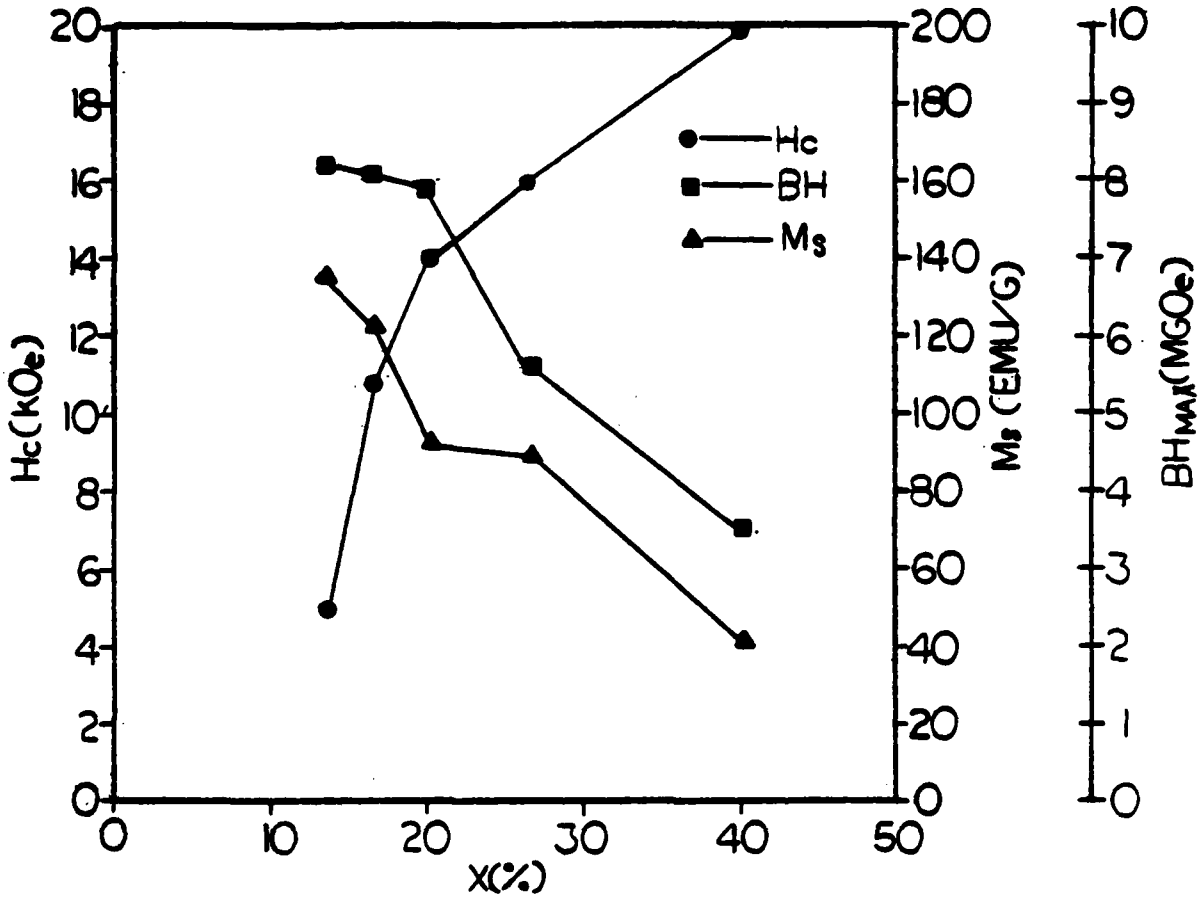

FIG. 11. Effect of Pr concentration on the magnetic properties of $Fe_{89-x}Pr_xCo_6(BSi)_5$.

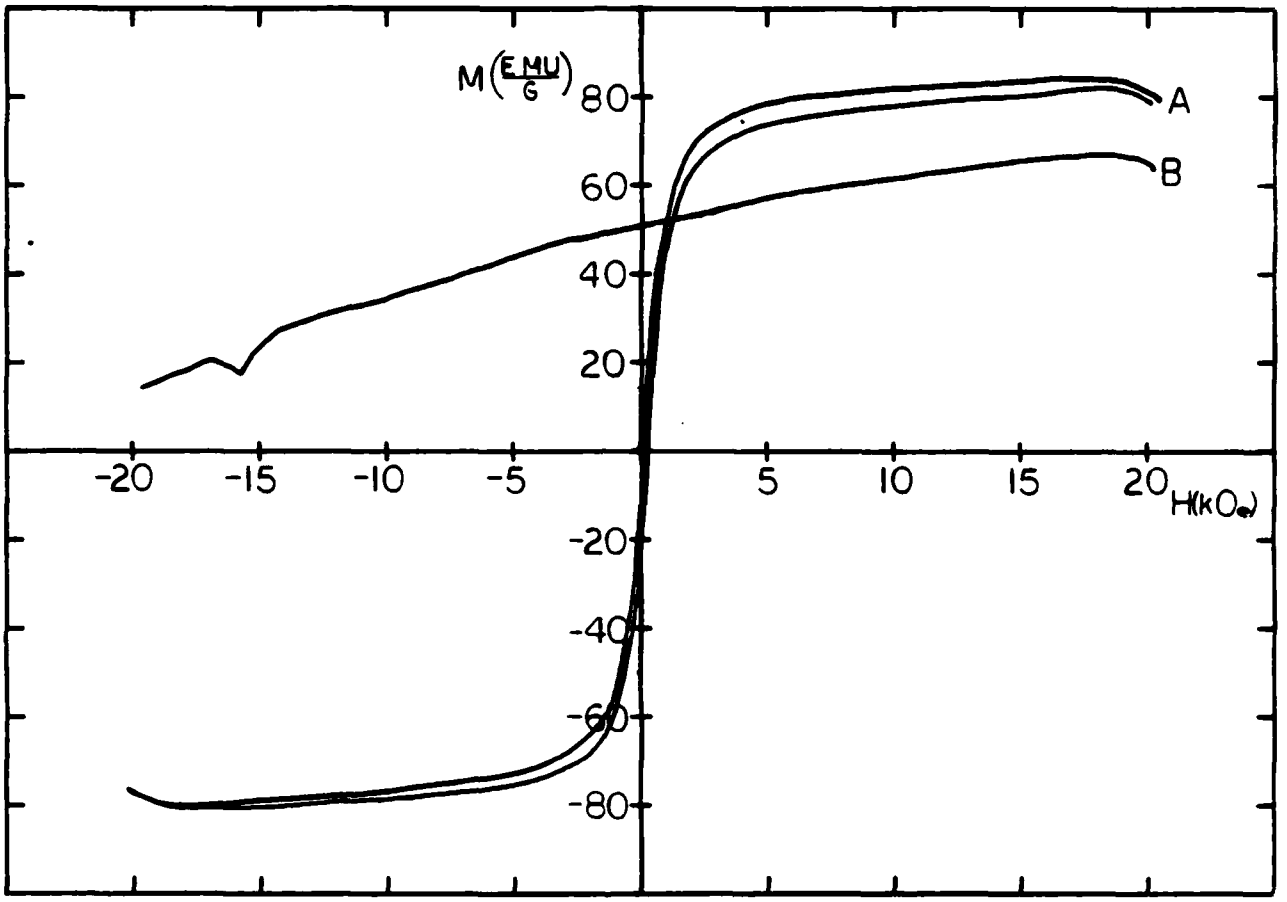

FIG. 12. Hysteresis loop for melt-spun $Pr_{26.8}$ $Fe_{62.3}$ C_{06} $B_{4.6}$ $Si_{0.3}$ before and after heat treatment at 550°C for 30 minutes.

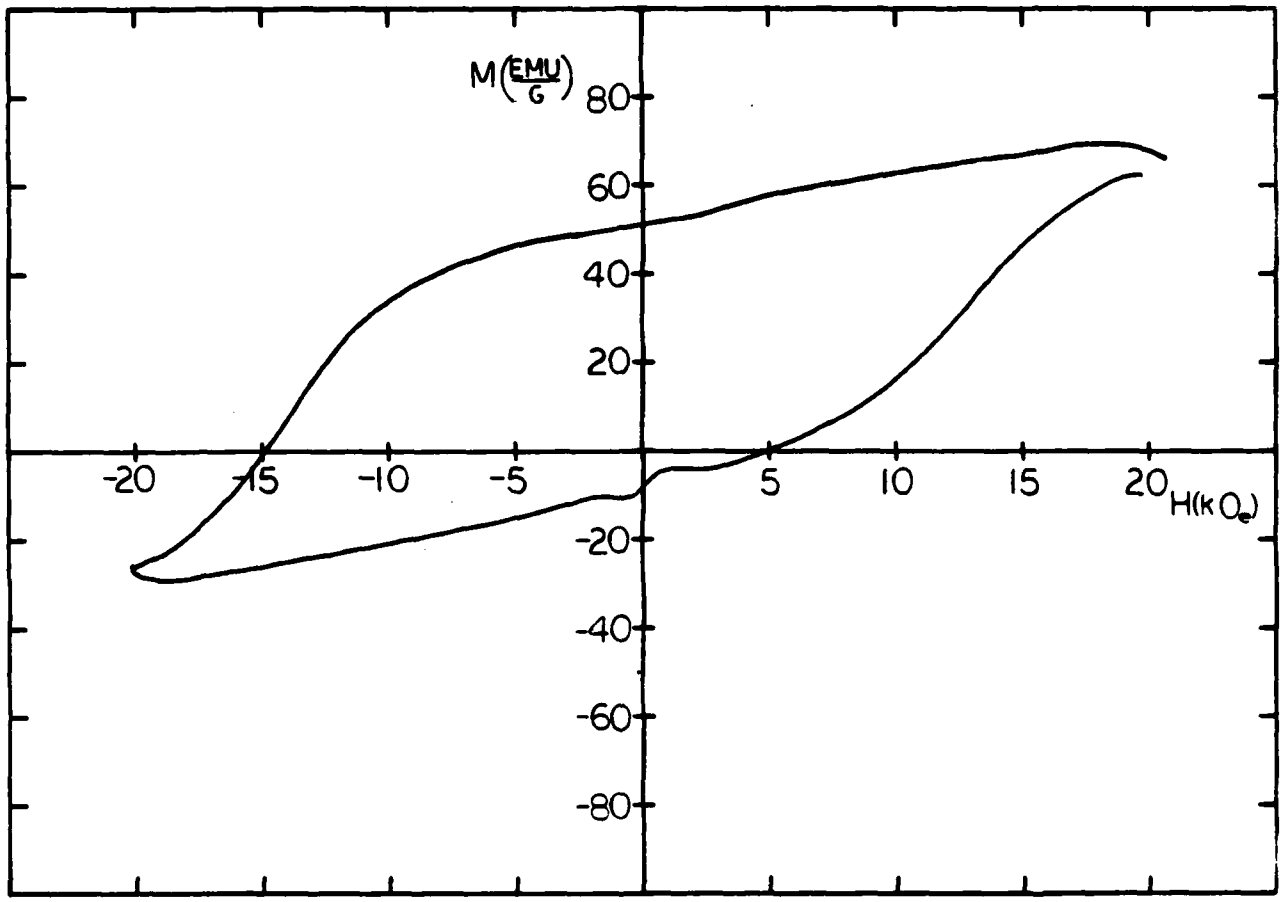

FIG. 13. Hysteresis loop for melt-spun $Pr_{26.8}Fe_{62.3}Co_6B_{4.6}Si_{0.3}$ after heat treatment for an additional 60 minutes at 650°C. (See Fig. 12 for previous heat treatment.)

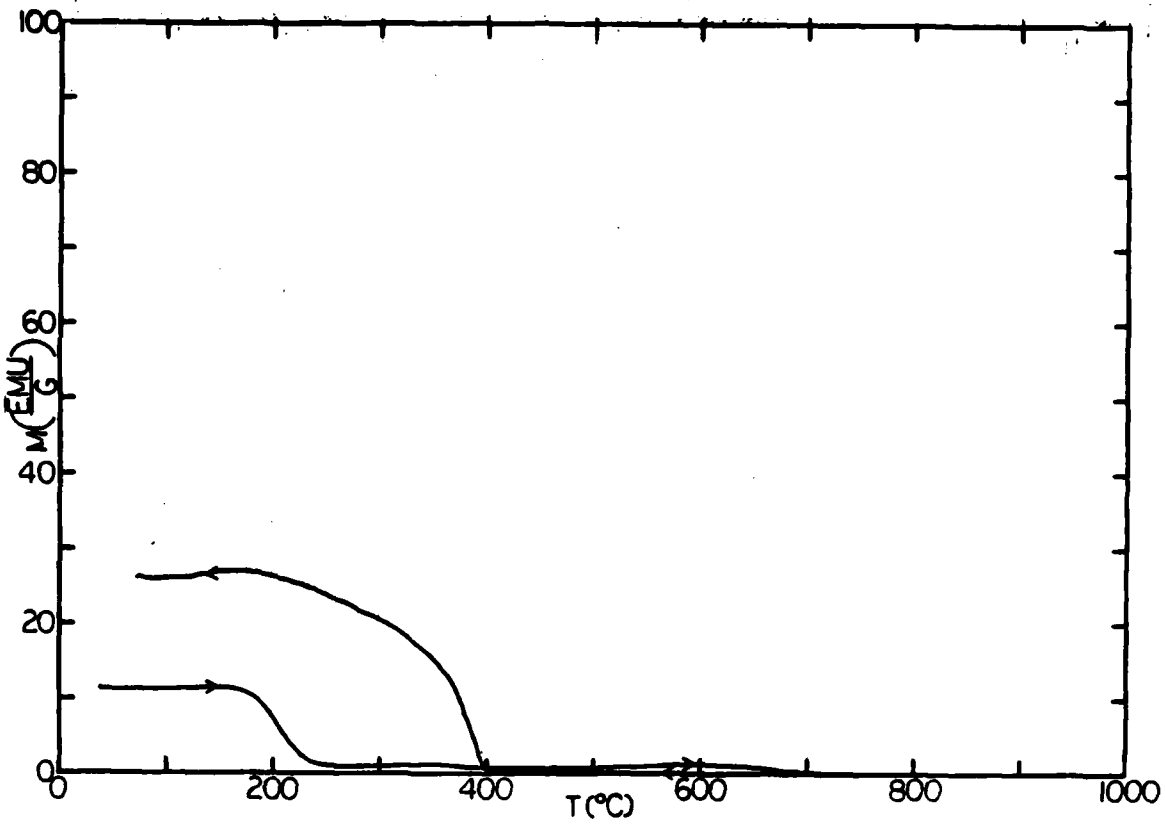

14 (a)

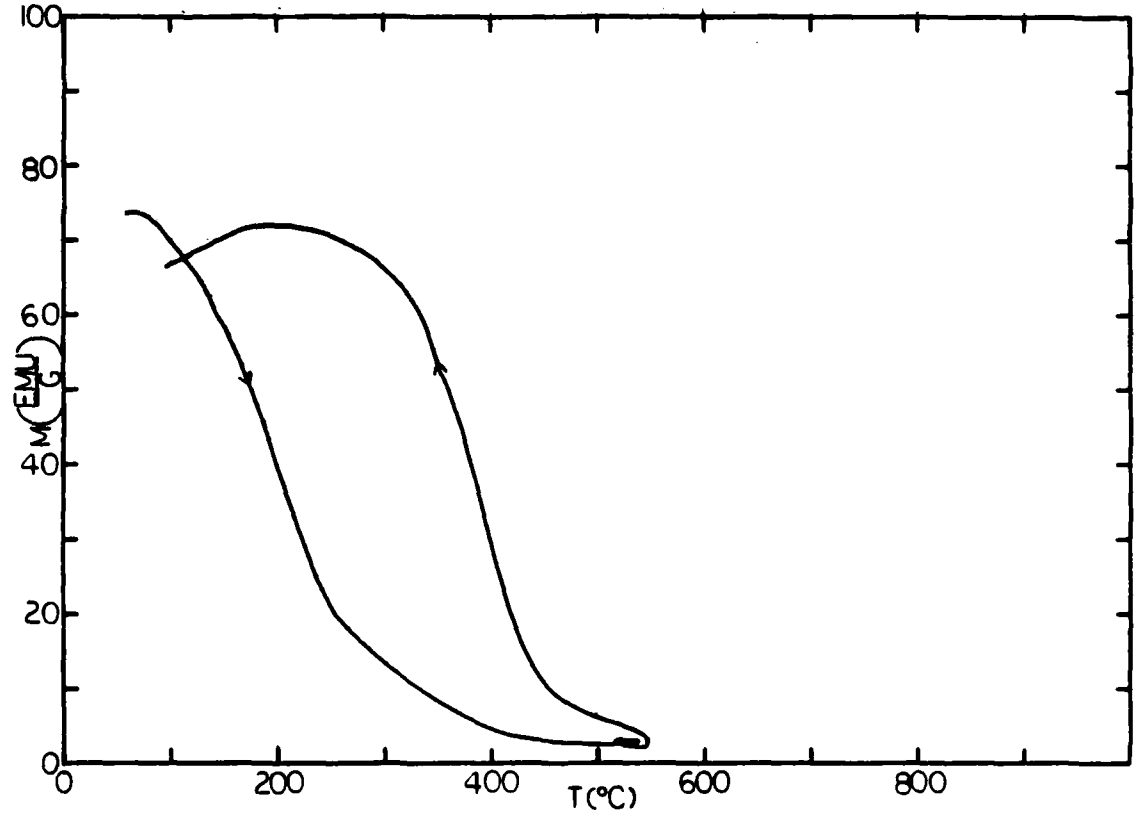

14 (b)

FIG. 14. Thermomagnetic data for (a) melt-spun $Pr_{20.1}Fe_{69}Co_6B_{4.6}Si_{0.3}$ and (b) melt-spun $Pr_{26.8}Fe_{62.3}Co_6B_{4.6}Si_{0.3}$

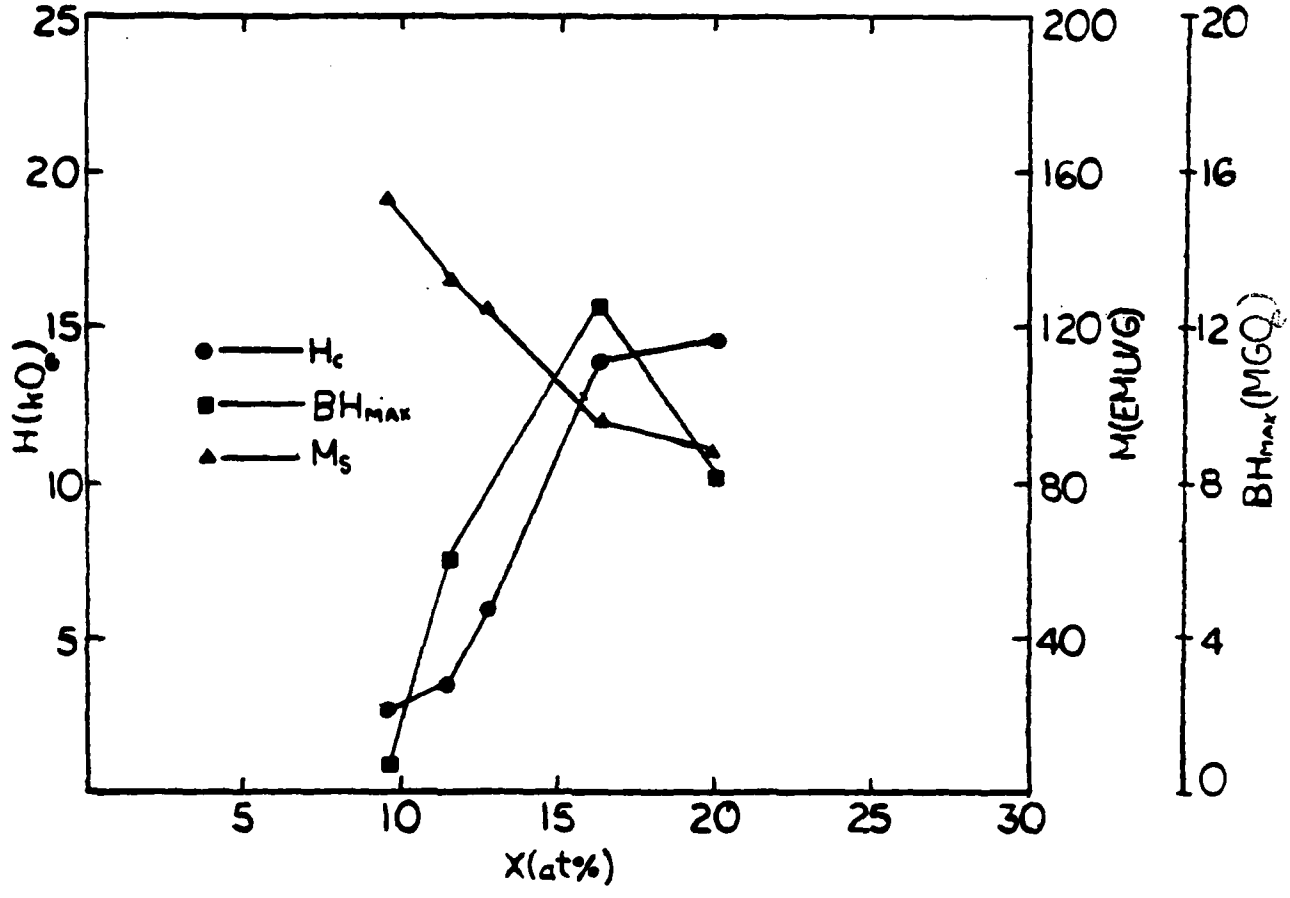

FIG. 15. Effect of Pr concentration on the magnetic properties of $Fe_{92-x}\ Pr_x(BSi)_8$.

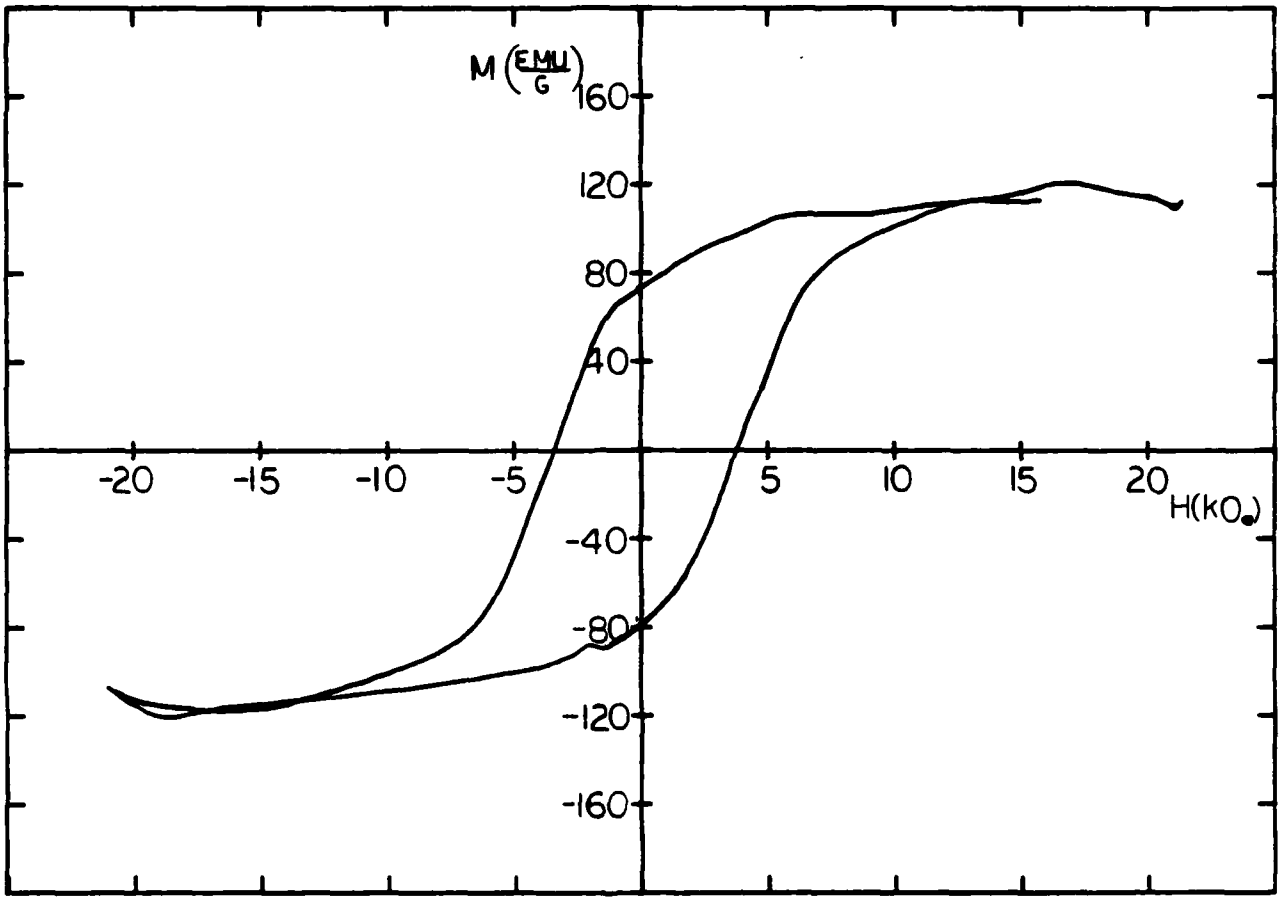

FIG. 16. Hysteresis loop for melt-spun $Pr_{11.4}Fe_{79.1}B_{5.6}Si_{3.9}$ after heat treatment at 780°C for 15 minutes.

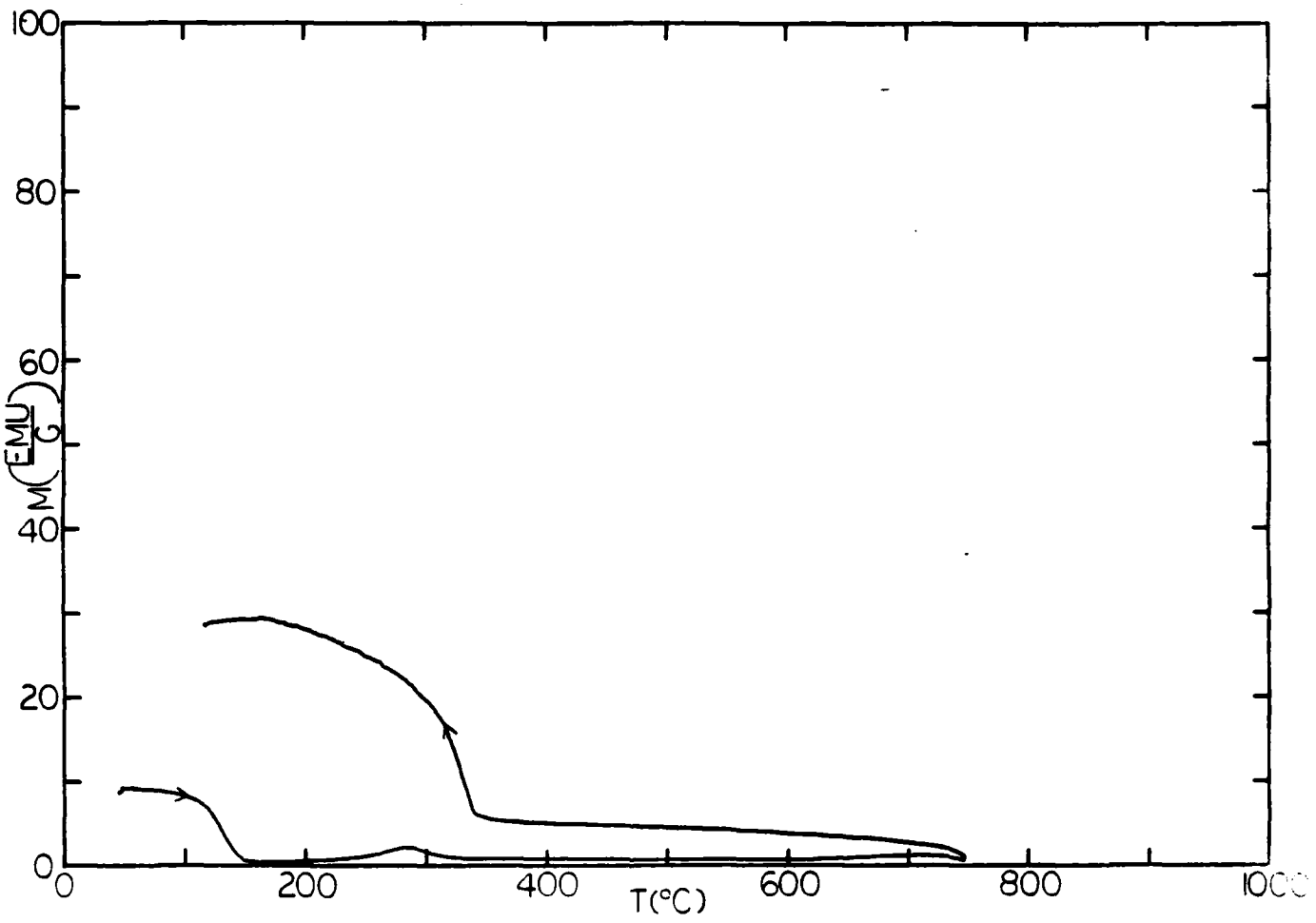

FIG. 17. Thermomagnetic data for melt-spun $Pr_{12.9}Fe_{79.2}B_{4.7}Si_{3.2}$.

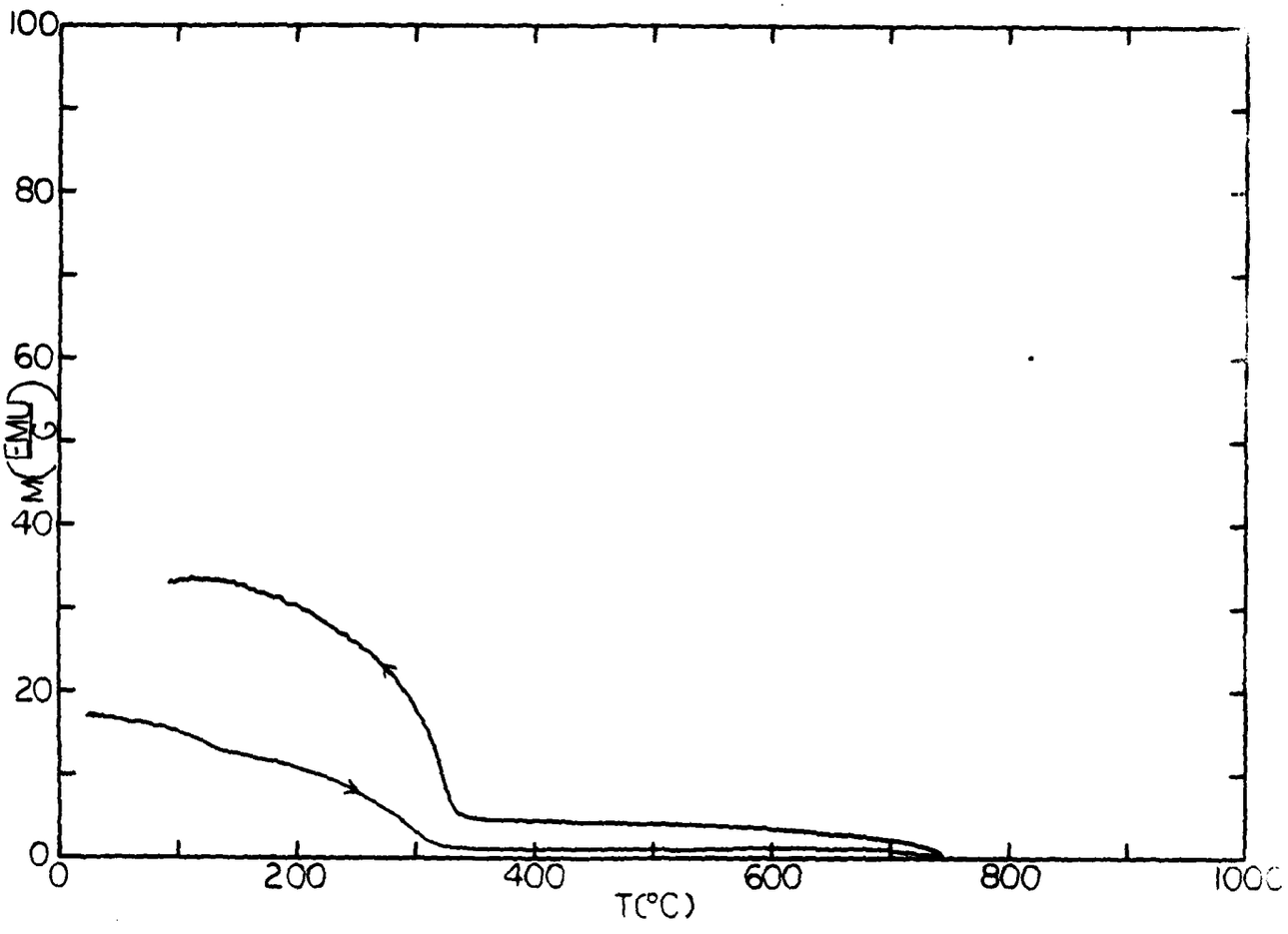

FIG. 18. Thermomagnetic data for melt-spun $Pr_{20.5}Fe_{71.6}B_{4.7}Si_{3.2}$.

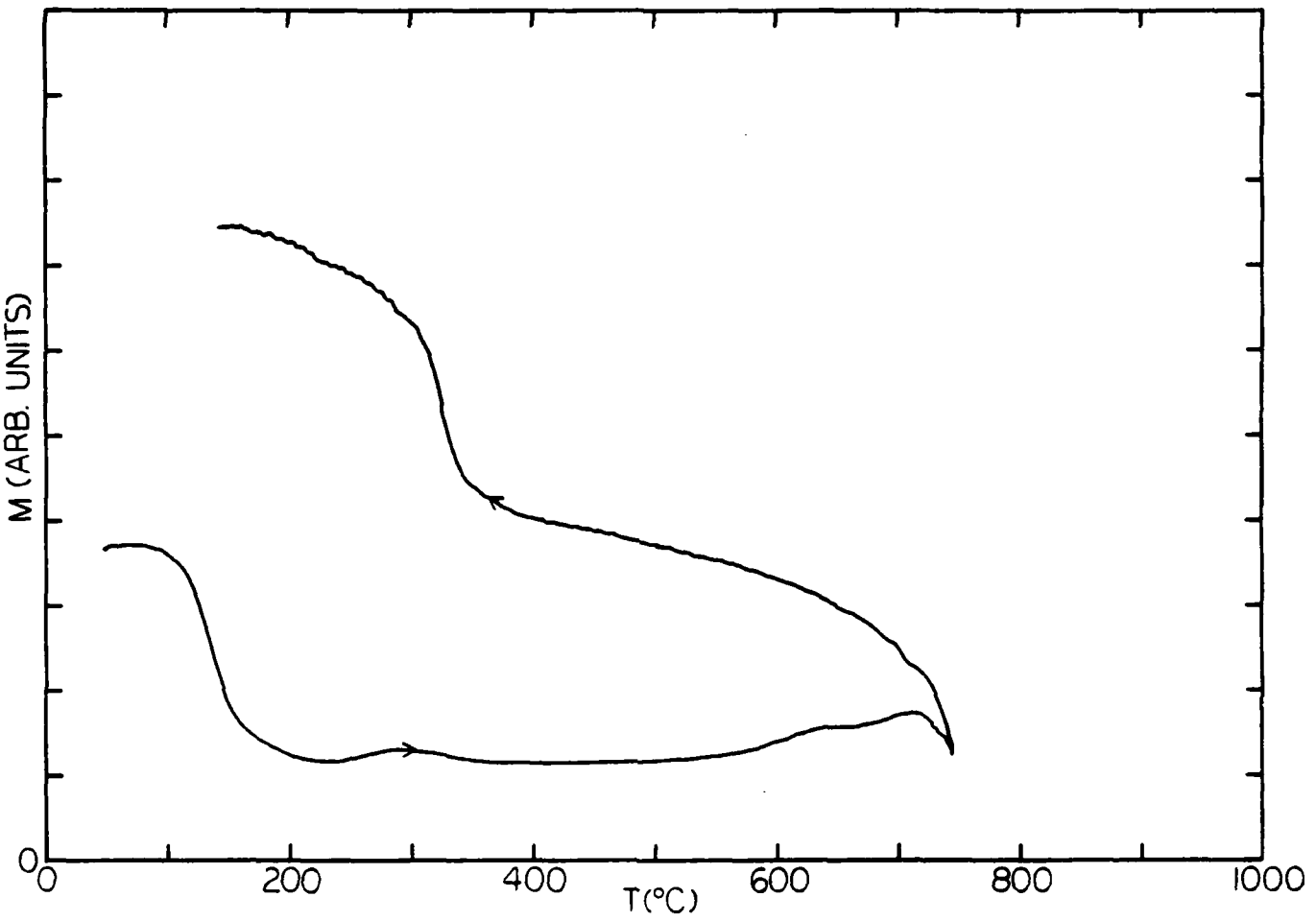

FIG. 19. Thermomagnetic data for melt-spun $Pr_{9.6}Fe_{82.5}B_{4.7}Si_{3.2}$.

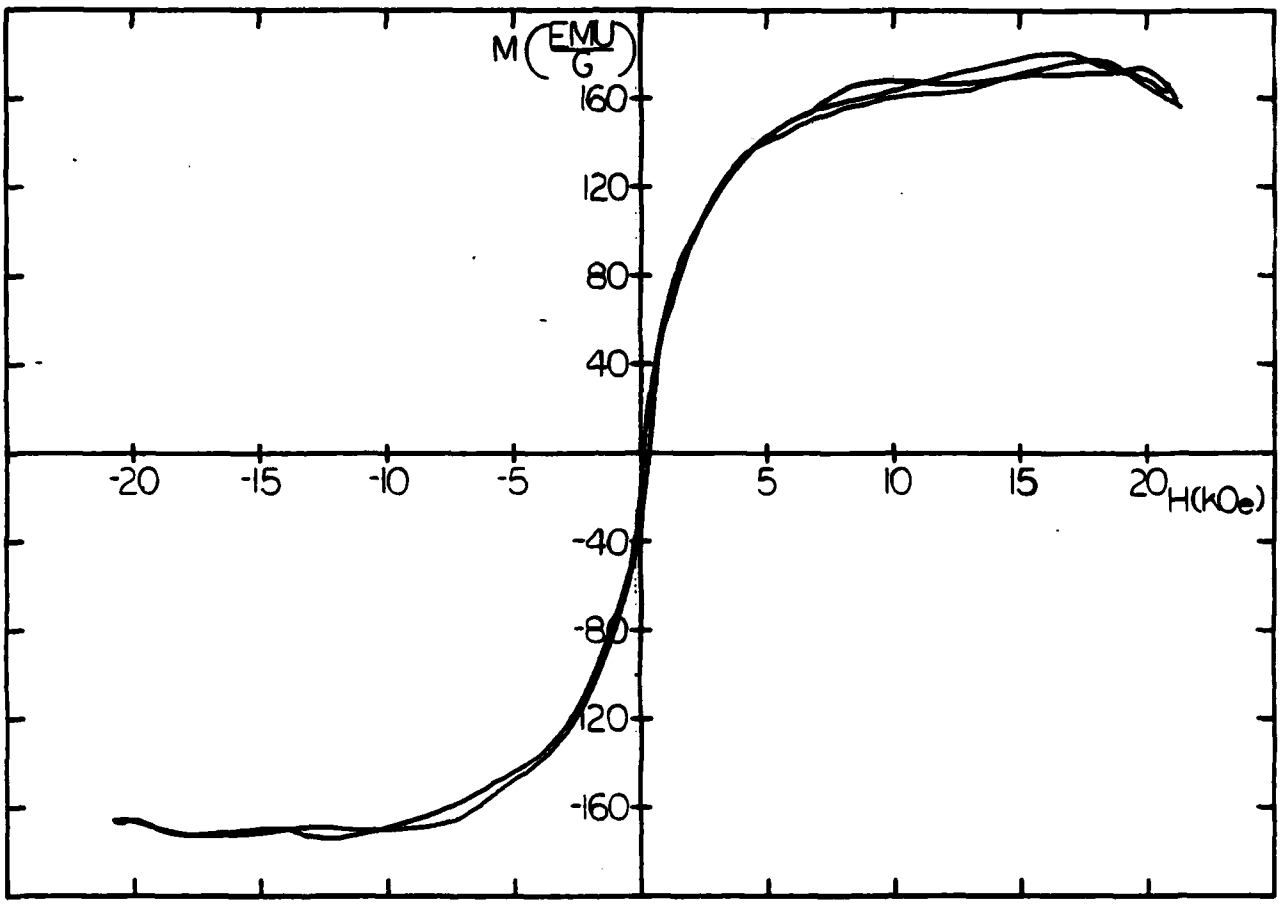

FIG. 20. Hysteresis loop for melt-spun $Pr_{24.7}Fe_{70.3}Si_5$ after heat treatment to 750°C.

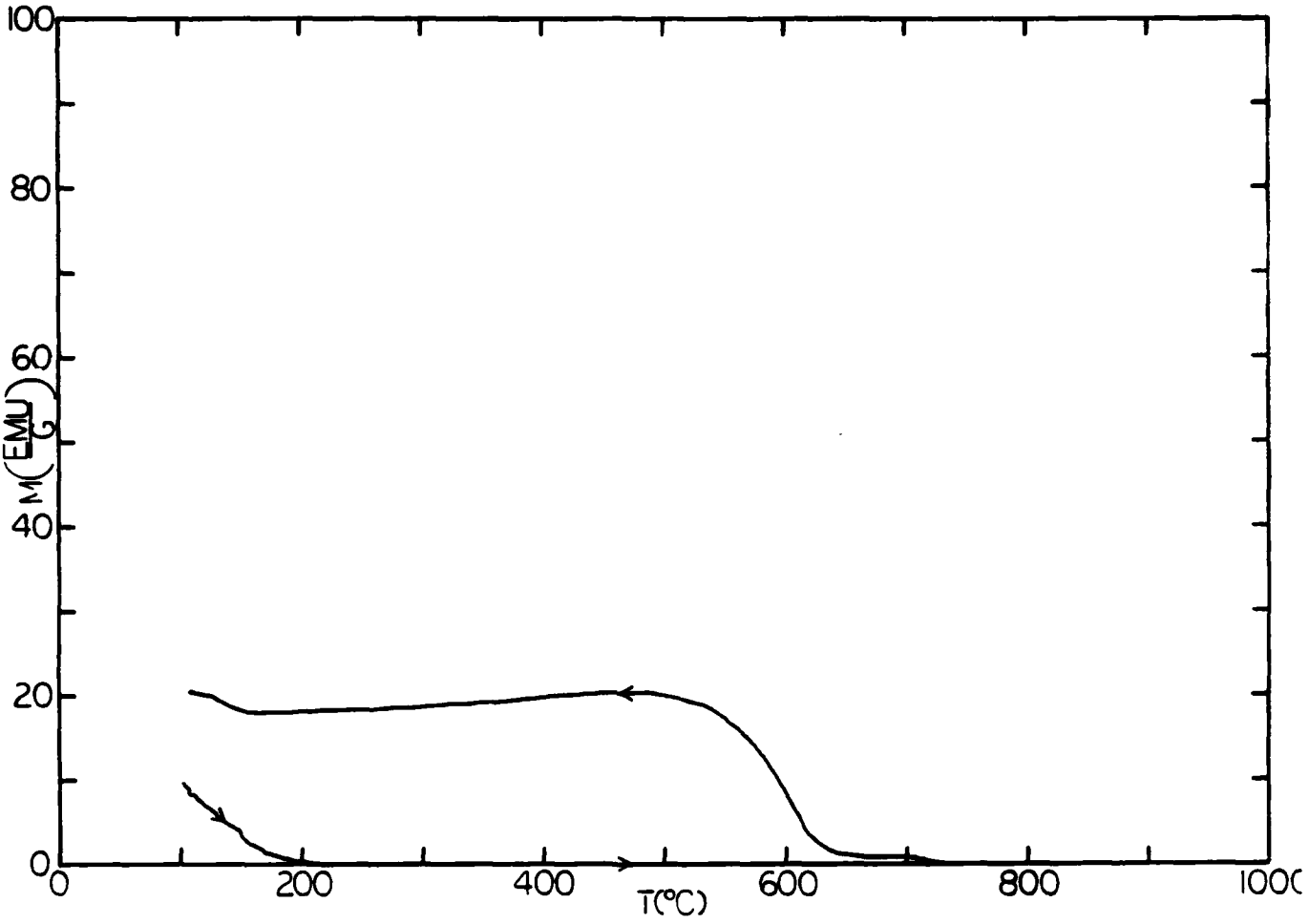

FIG. 21. Thermomagnetic data for melt-spun $Pr_{24.7}Fe_{70.3}Si_5$.

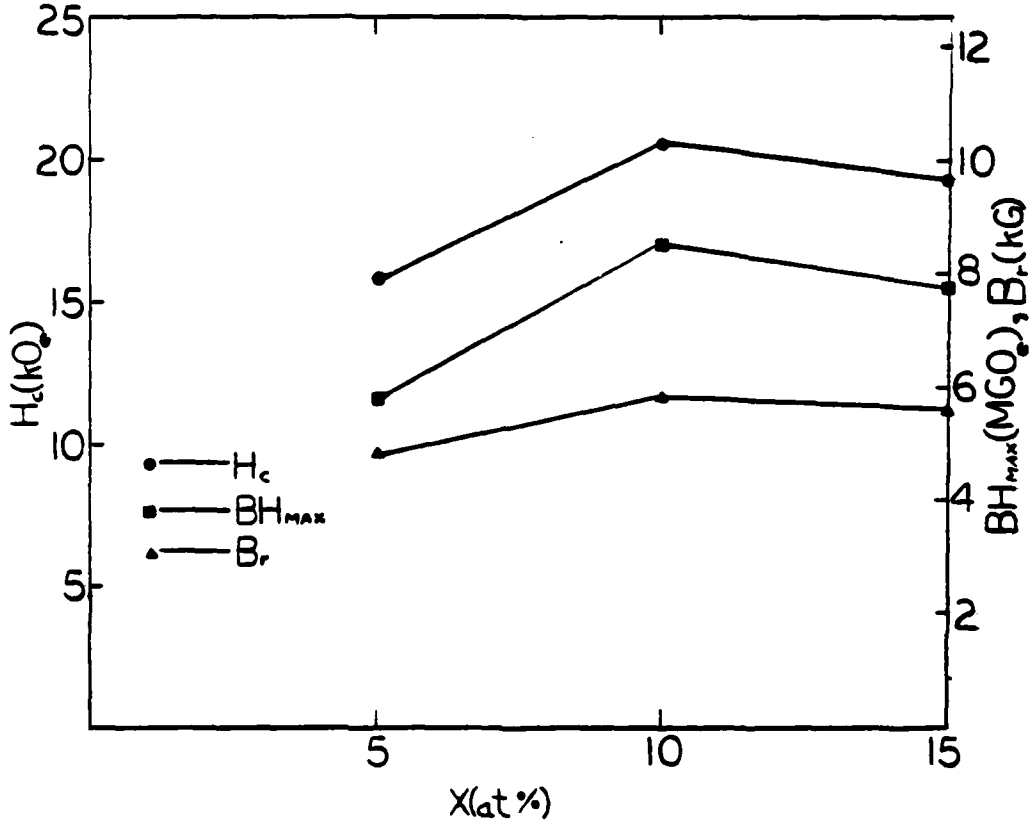

FIG. 22. Effect of boron concentration on the magnetic properties of $(Pr_6Fe_{23})_{100-x}B_x$.

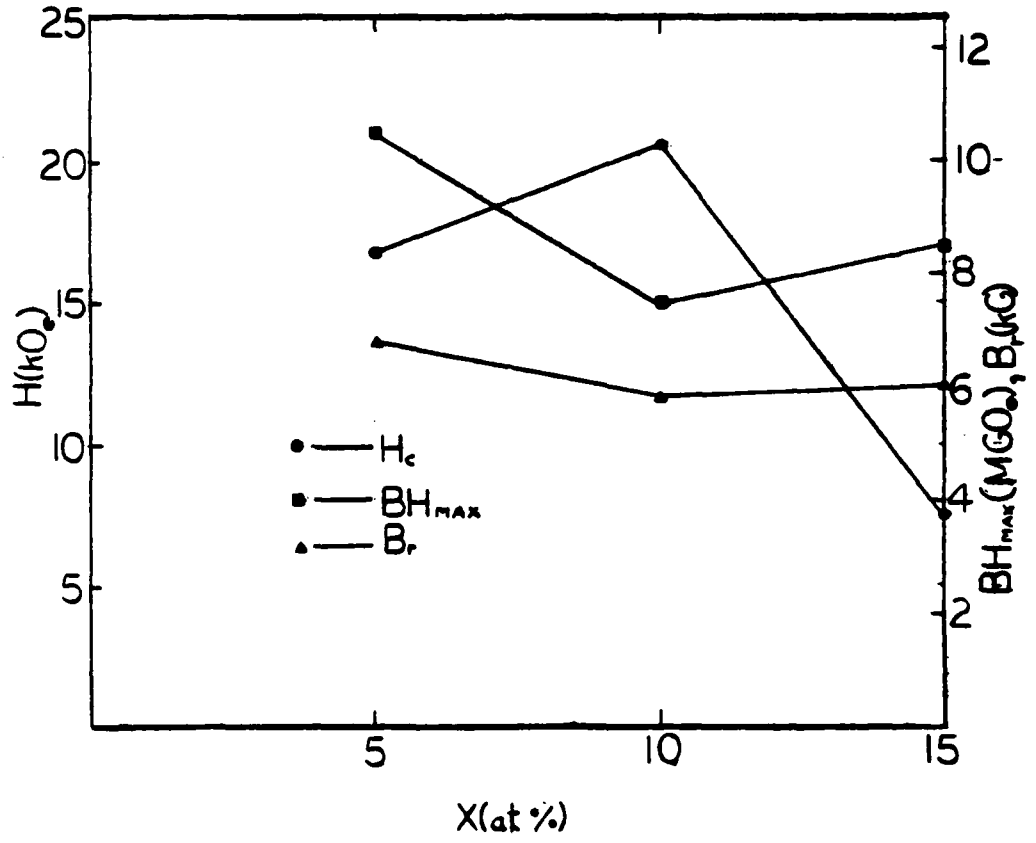

FIG. 23. Effect of boron concentration on the magnetic properties of $(Pr\ Fe_5)_{100-x}B_x$.

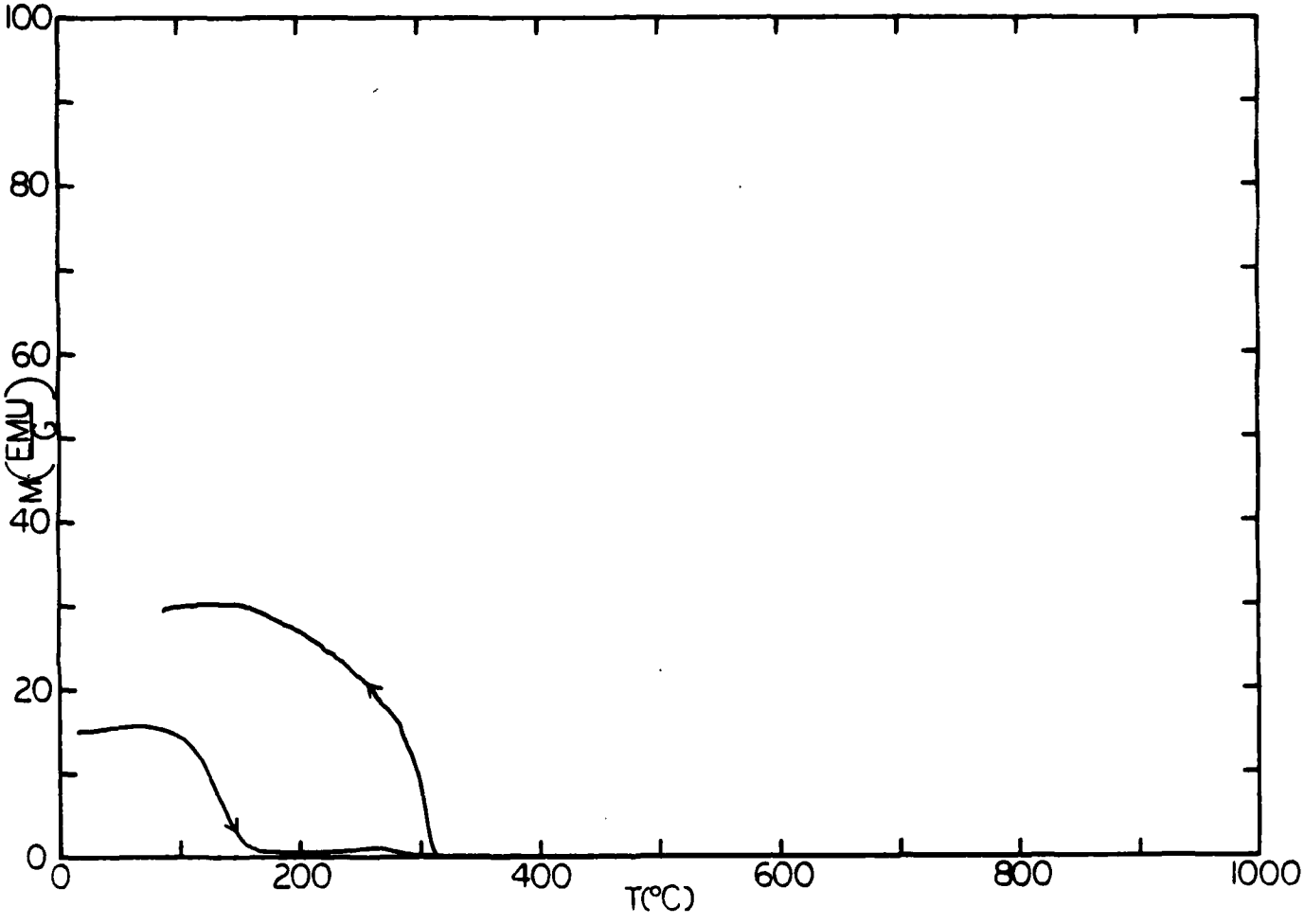

FIG. 24. Thermomagnetic data for melt-spun $Pr_{18.6}Fe_{71.4}B_{10}$.

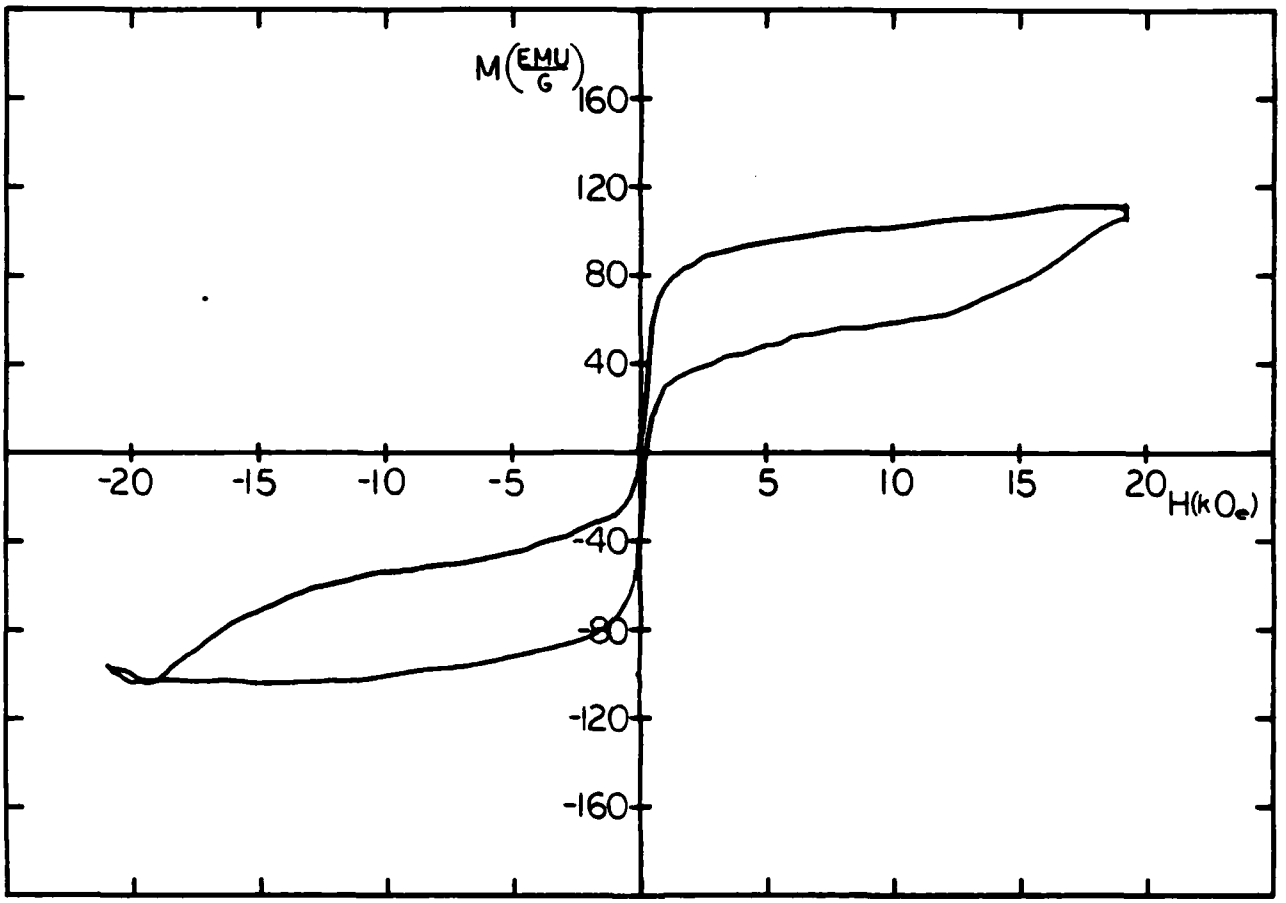

FIG. 25. Hysteresis loop for melt-spun $Pr_{16.4}Fe_{75.5}B_{4.8}Si_{3.3}$ in the as-quenched state.

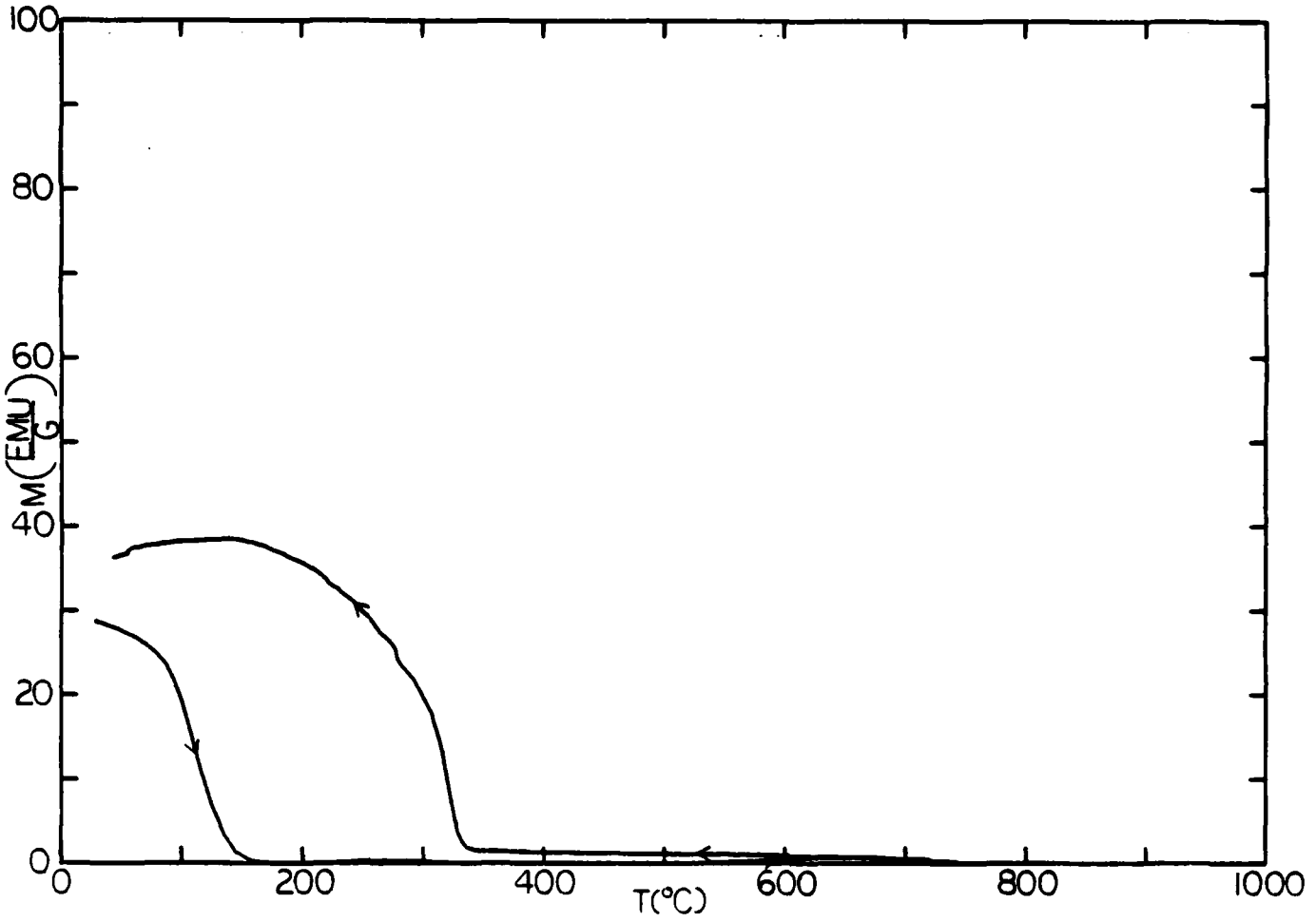

FIG. 26. Thermomagnetic data for melt-spun $Pr_{16.4}Fe_{75.5}B_{4.8}Si_{3.3}$.

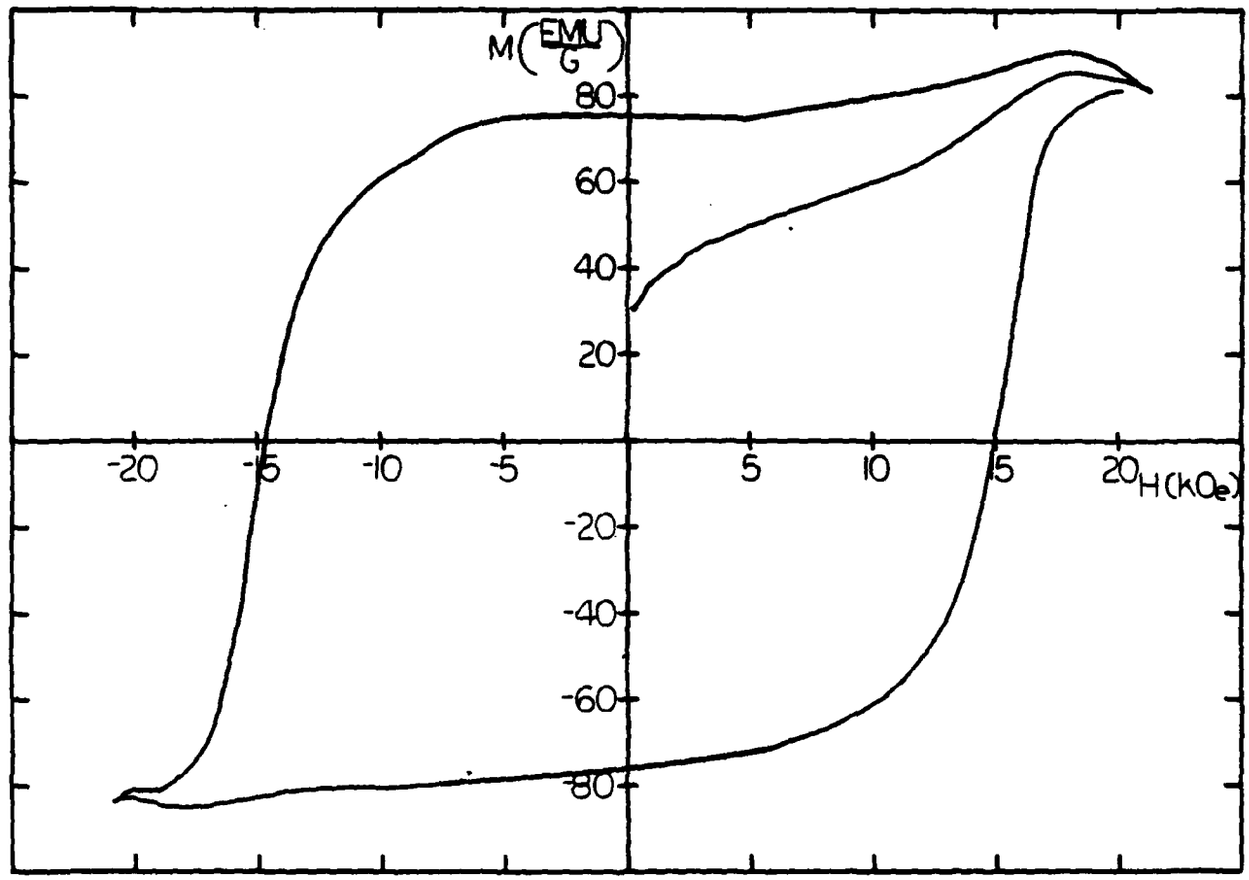

FIG. 27. Hysteresis loop for melt-spun $Pr_{16.4}Fe_{75.5}B_{4.8}Si_{3.3}$ after heat treatment at 750°C for 15 minutes.

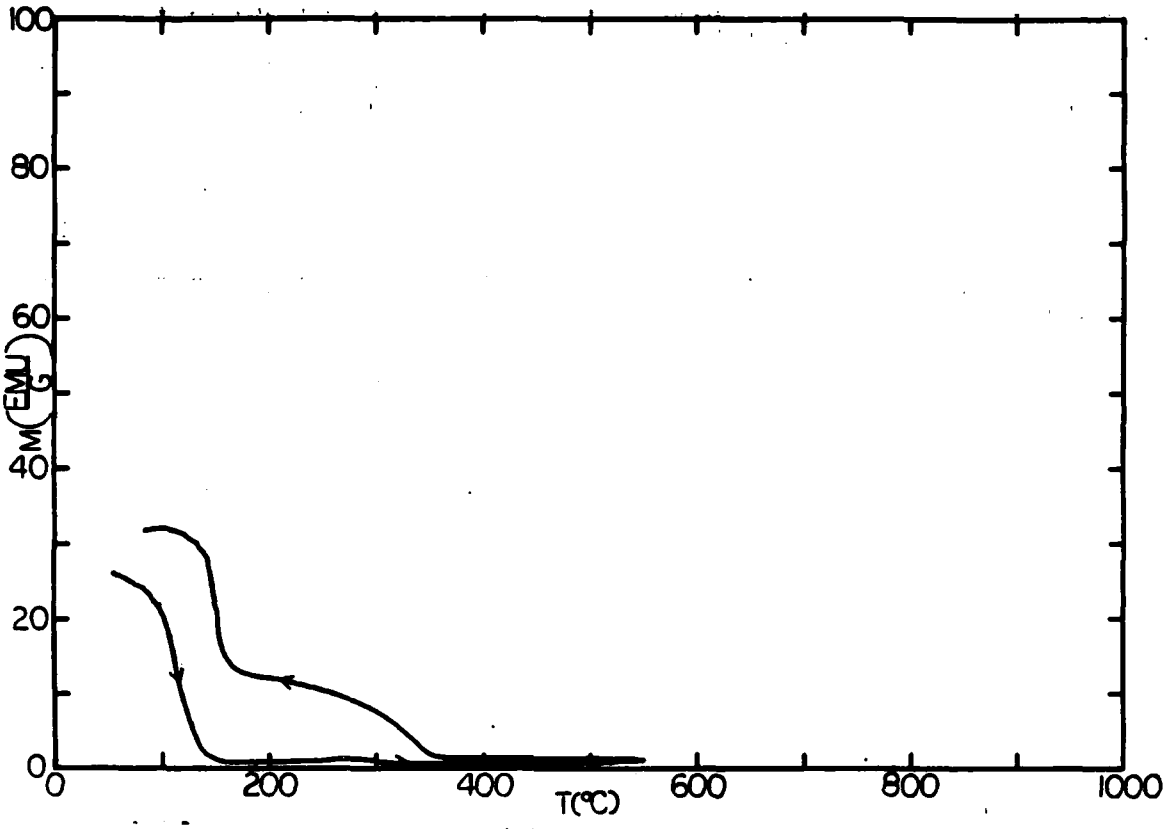

28(a)

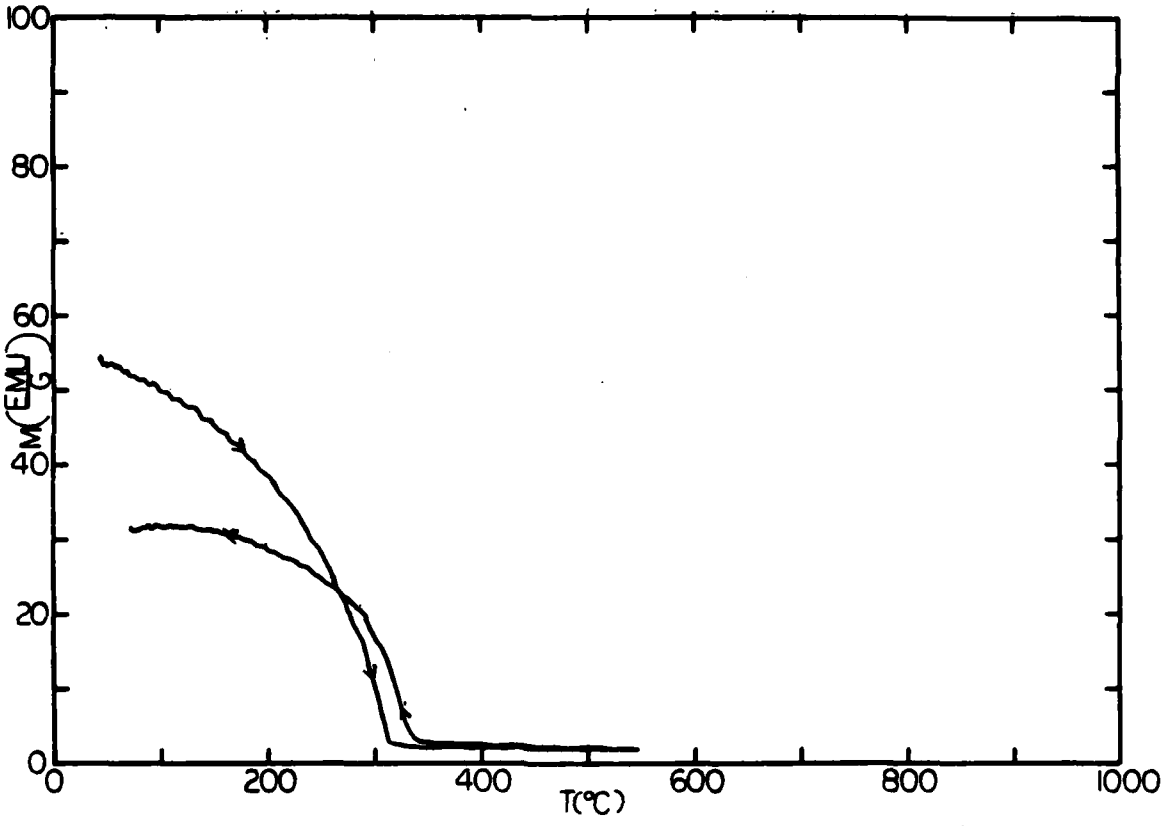

28(b)

FIG. 28. Thermomagnetic data for melt-spun $Pr_{16.4}Fe_{75.5}B_{4.8}Si_{3.3}$ for
(a) an as-quenched sample and
(b) a sample which was magnetically annealed for 7 hours at an applied field of 15 kOe.

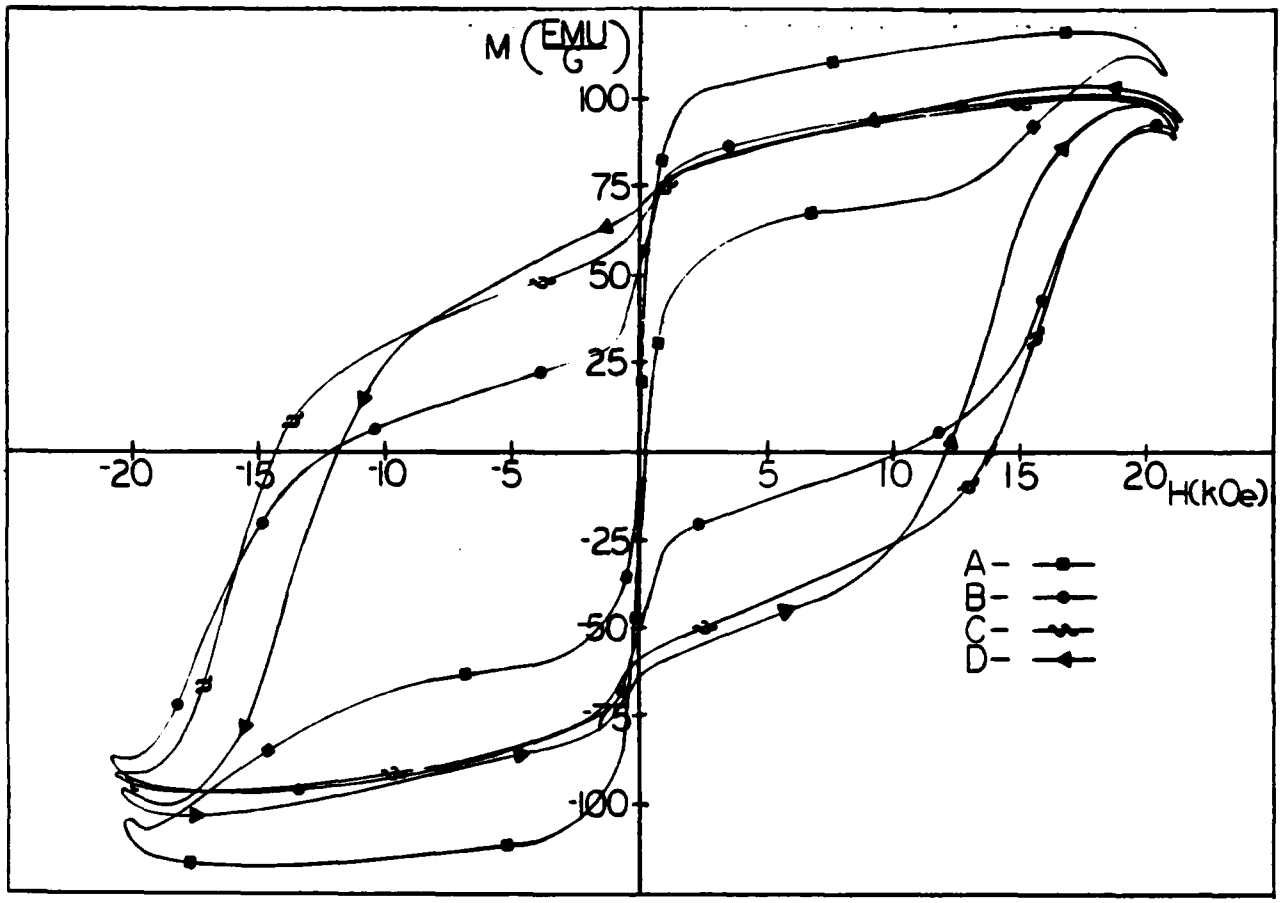

FIG. 29. Hysteresis loops of melt-spun $Pr_{16.4}Fe_{75.5}B_{4.8}Si_{3.3}$ showing the development of magnetic properties at various stages of a 550°C heat treatment. A. After thermomagnetic data taken; B. 1 hour; C. 2 hours; D. 5 hours; E. Additional 30 minutes at 750°C.

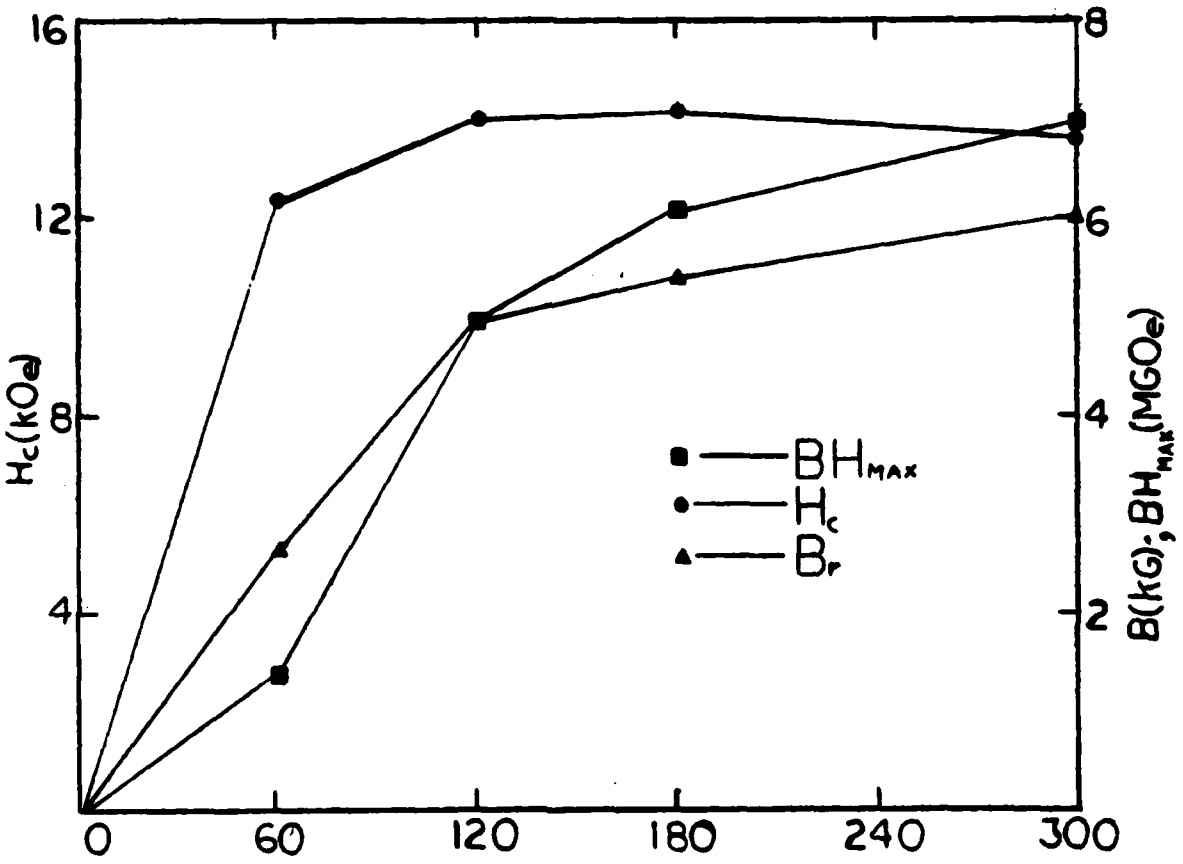

FIG. 30. Effect of annealing time at 550°C on the magnetic properties of $Pr_{16.4}Fe_{75.5}B_{4.8}Si_{3.3}$.

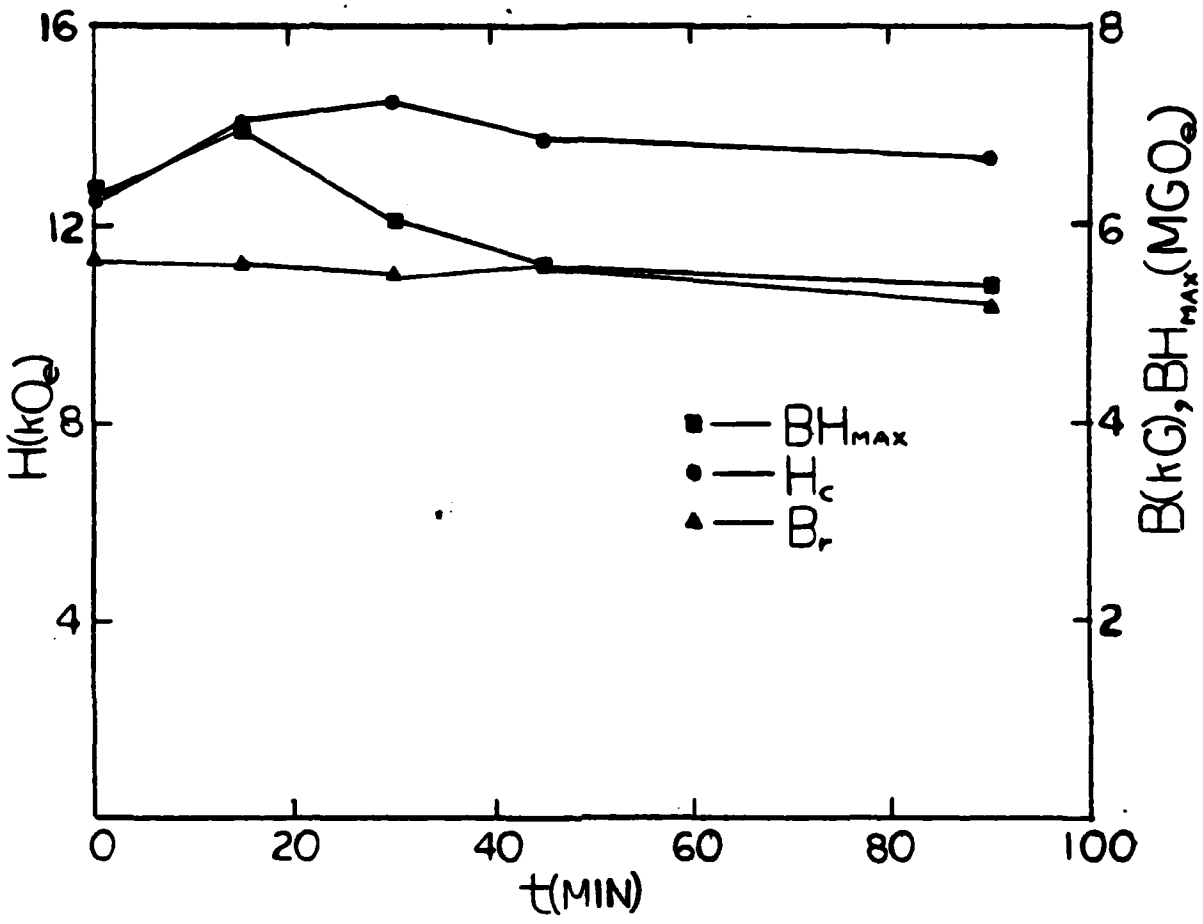

FIG. 31. Effect of annealing time at 650°C on the magnetic properties of $Pr_{16.4}Fe_{75.5}B_{4.8}Si_{3.3}$.

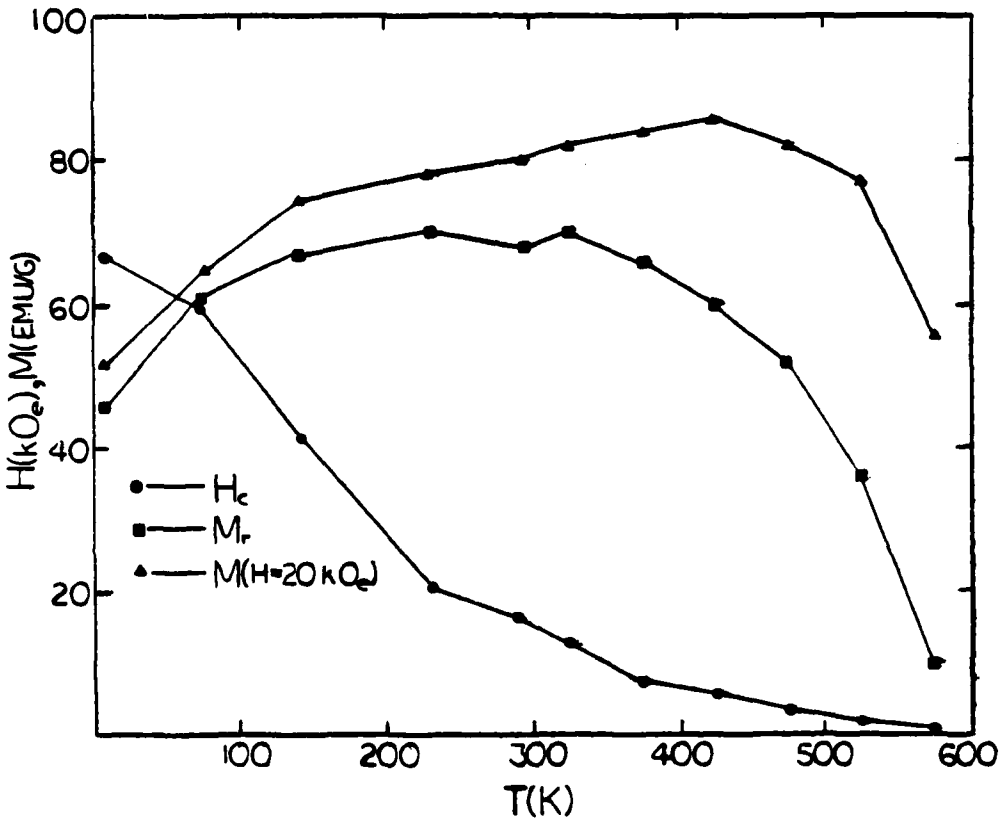

FIG. 32. Temperature dependence of the magnetic properties of $Pr_{16.4}Fe_{75.5}B_{4.8}Si_{3.3}$.

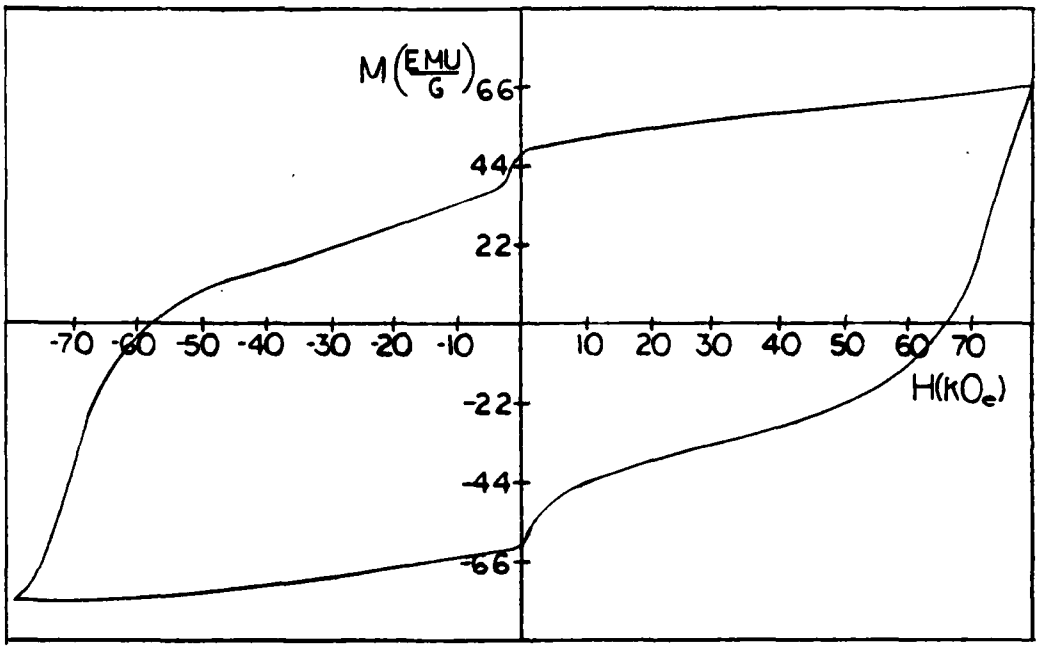

FIG. 33. Hysteresis loop of melt-spun $Pr_{16.4}Fe_{75.5}B_{4.8}Si_{3.3}$ taken at 4.2 K after a 15 minute heat treatment at 750°C.

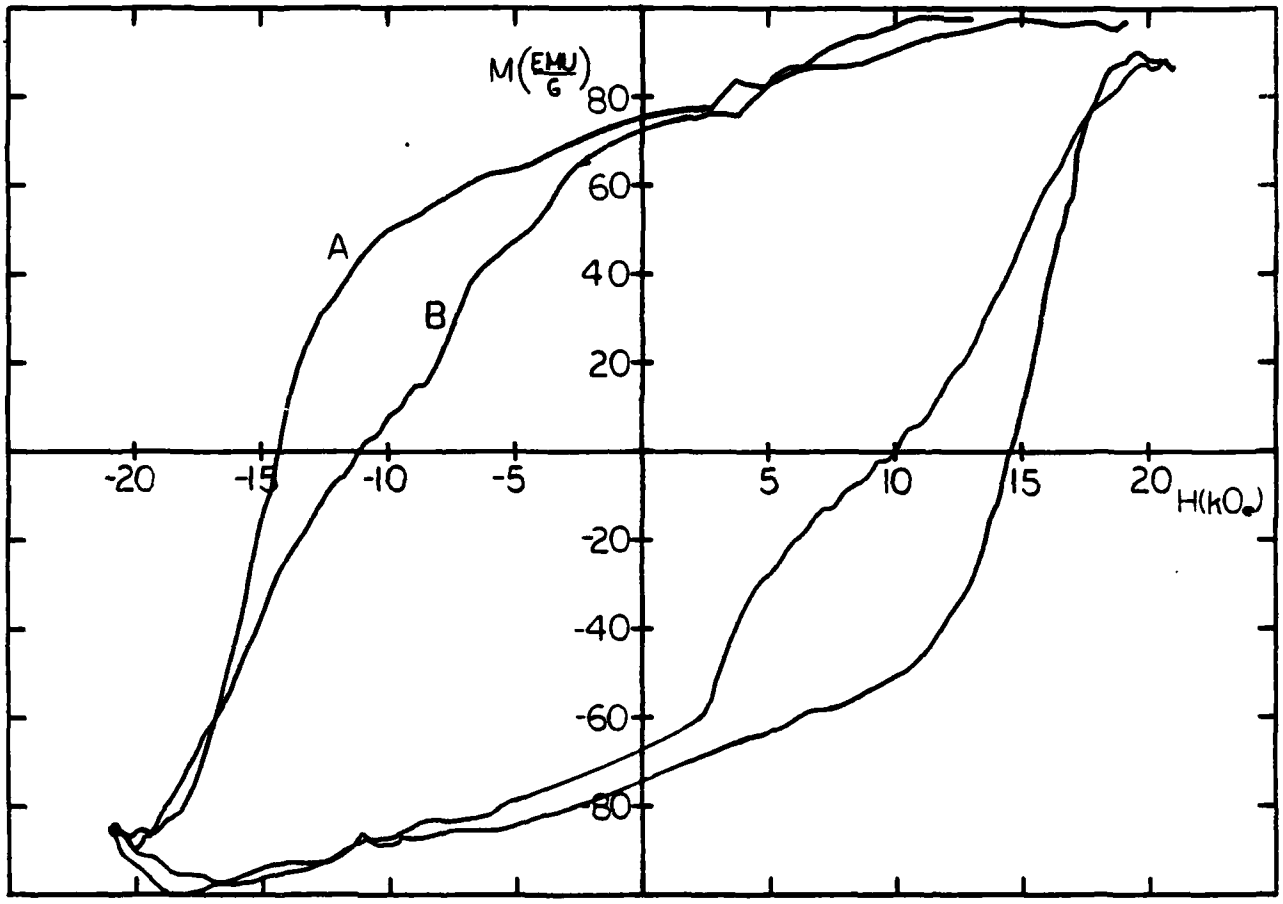

FIG. 34. Hysteresis loops of melt-spun $Pr_{16.4}Fe_{75.5}B_{4.8}Si_{3.3}$ taken (A) parallel and (B) perpendicular to the plane of the ribbon.

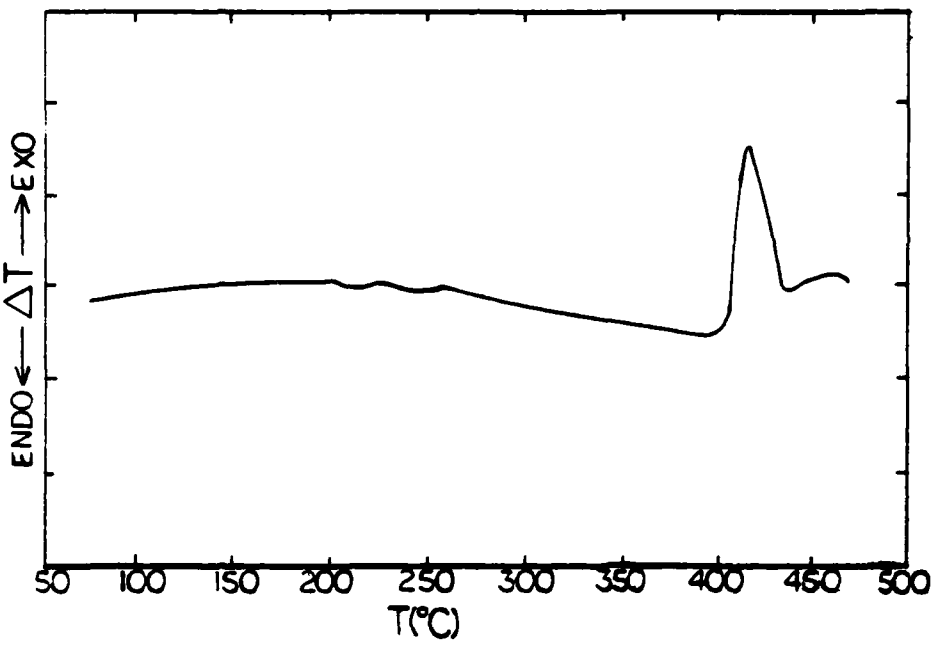

FIG. 35. Differential scanning calorimetry data for melt-spun $Pr_{18.6}Fe_{71.4}B_{10}$.

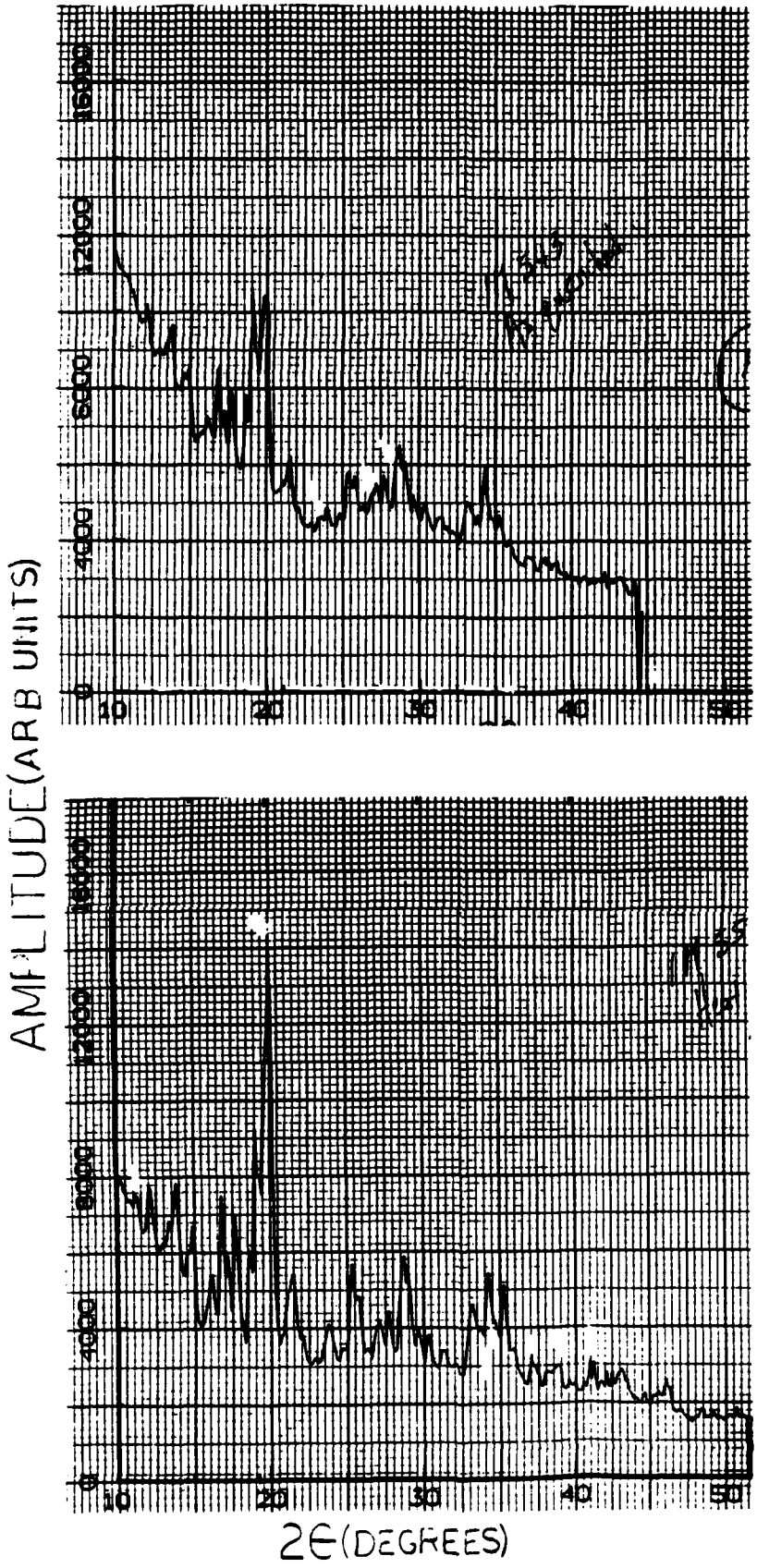

36 (a)

36 (b)

FIG. 36. X-ray diffraction data for melt-spun $Pr_{16.4}Fe_{75.5}B_{4.8}Si_{3.3}$ sampled in the (a) as-quenched state and (b) heat treated state.

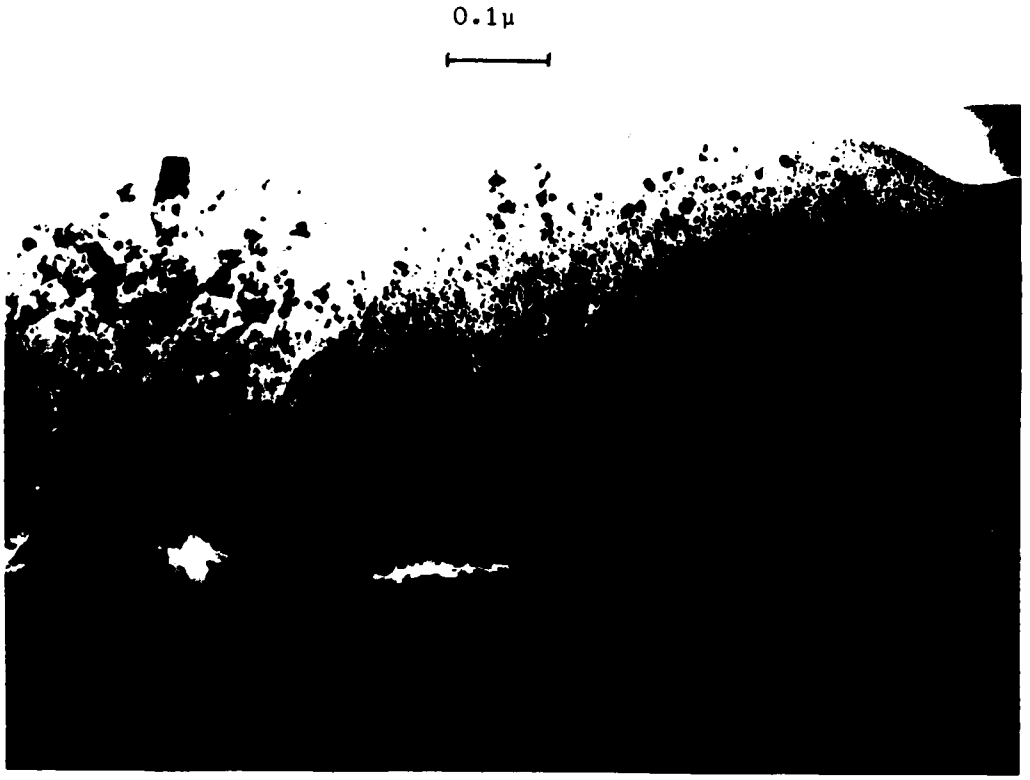

FIG. 37. Microstructure of heat-treated $Pr_{16.4}Fe_{75.5}B_{4.8}Si_{3.3}$.

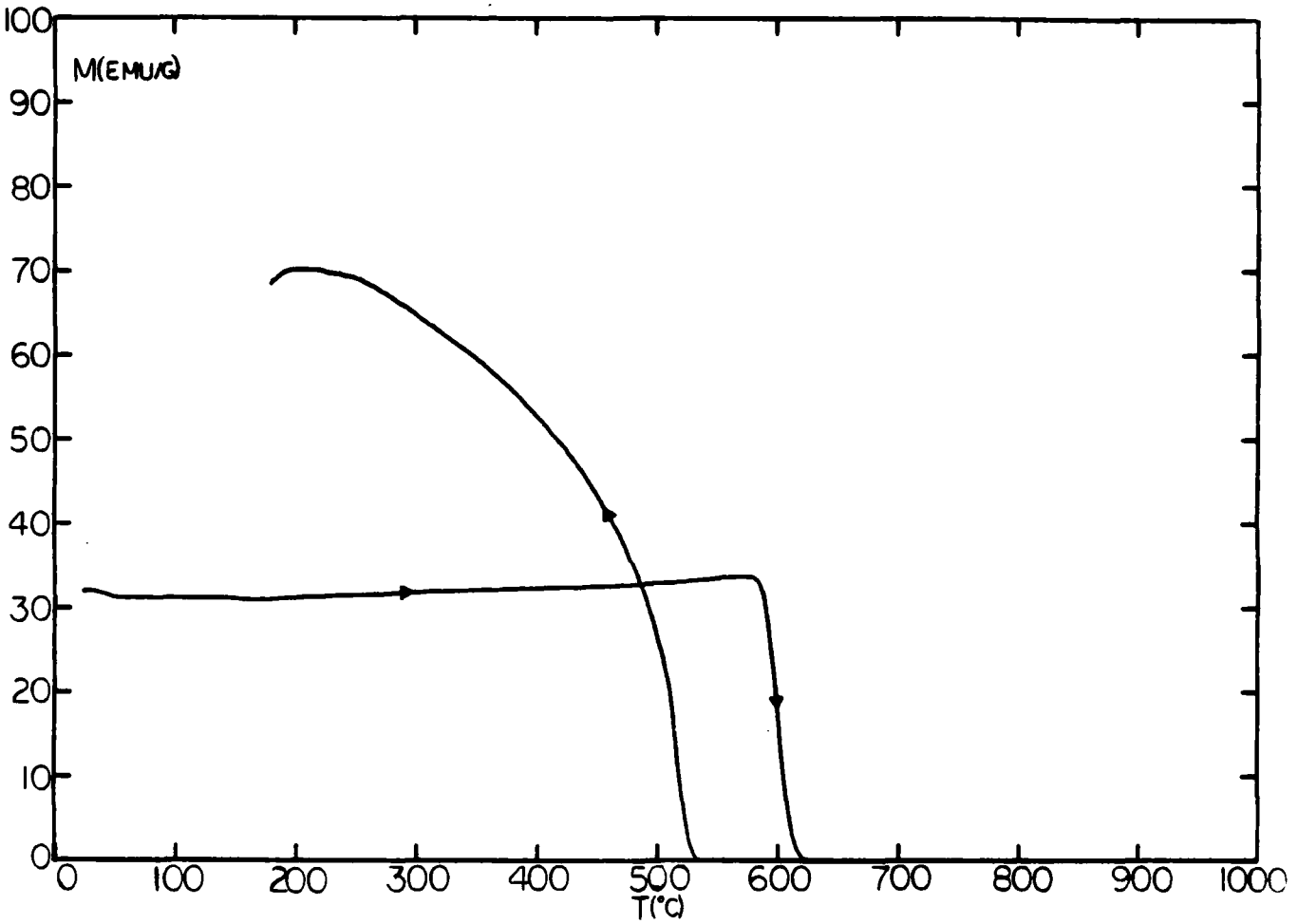

FIG. 38. Thermomagnetic data for $Co_{52}Pt_{48}$.

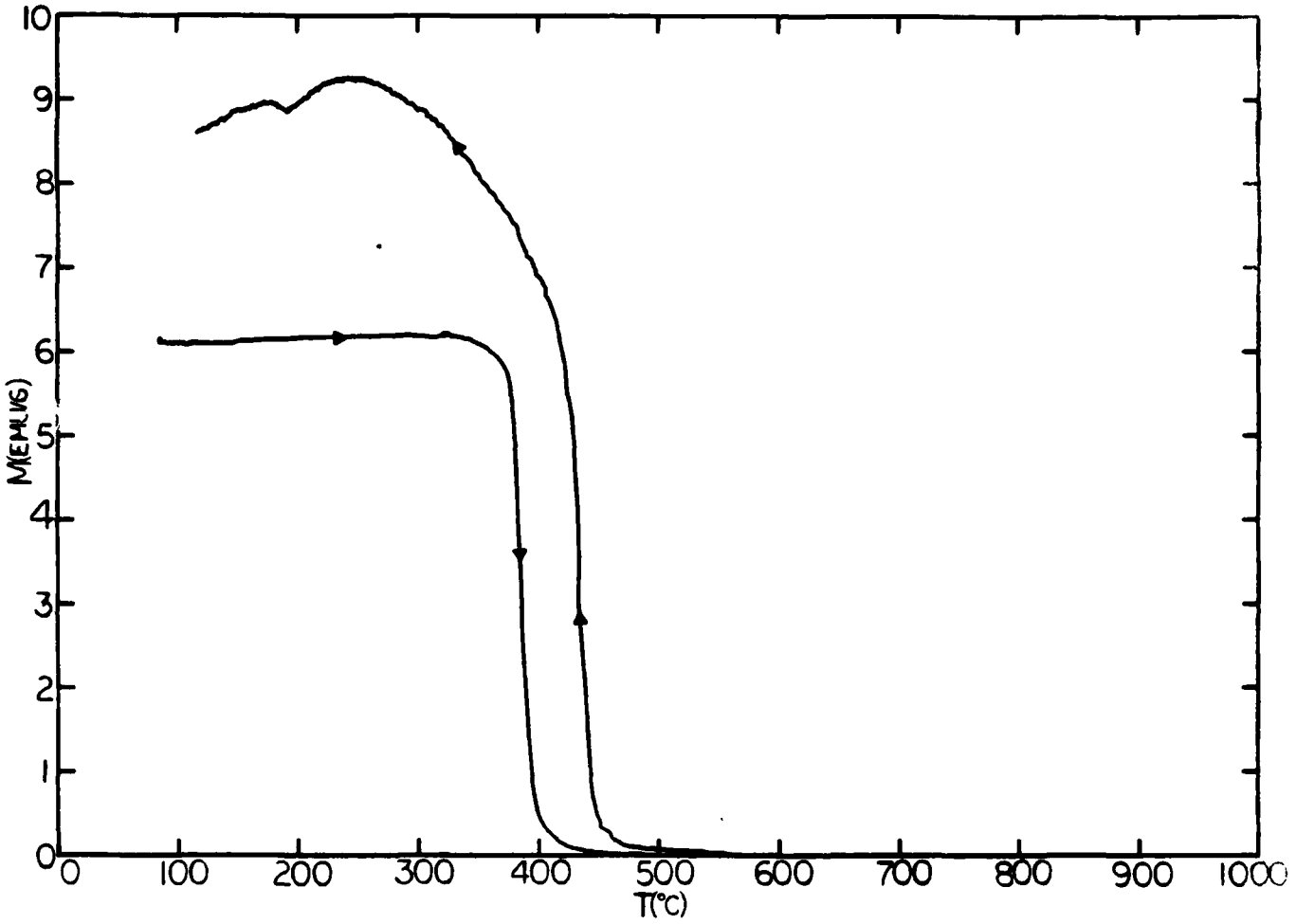

FIG. 39. Thermomagnetic data for $Fe_{10}Pt_7Ni_3$.

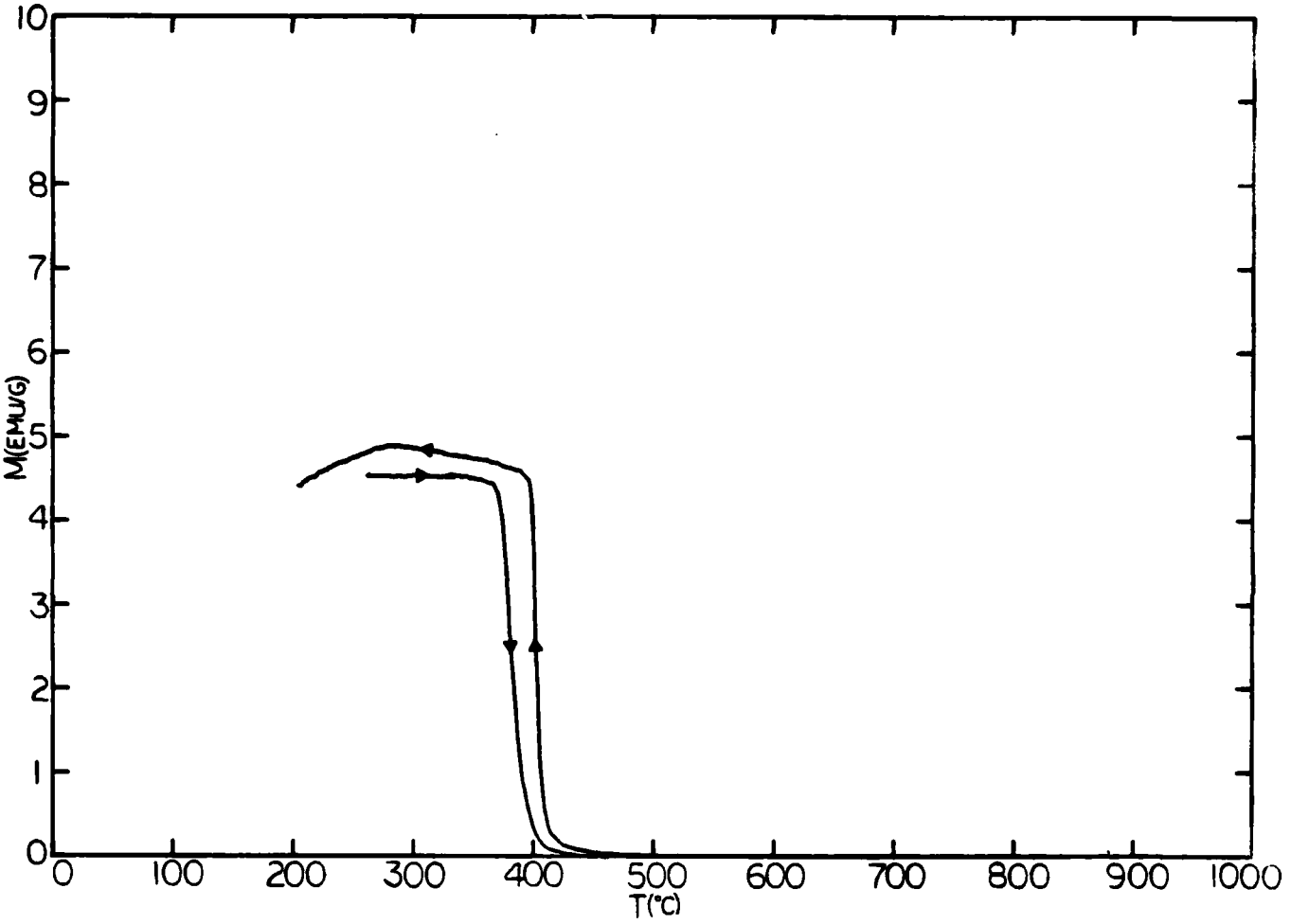

FIG. 40. Thermomagnetic data for $Fe_9Pt_6Ni_4Cu_1$.

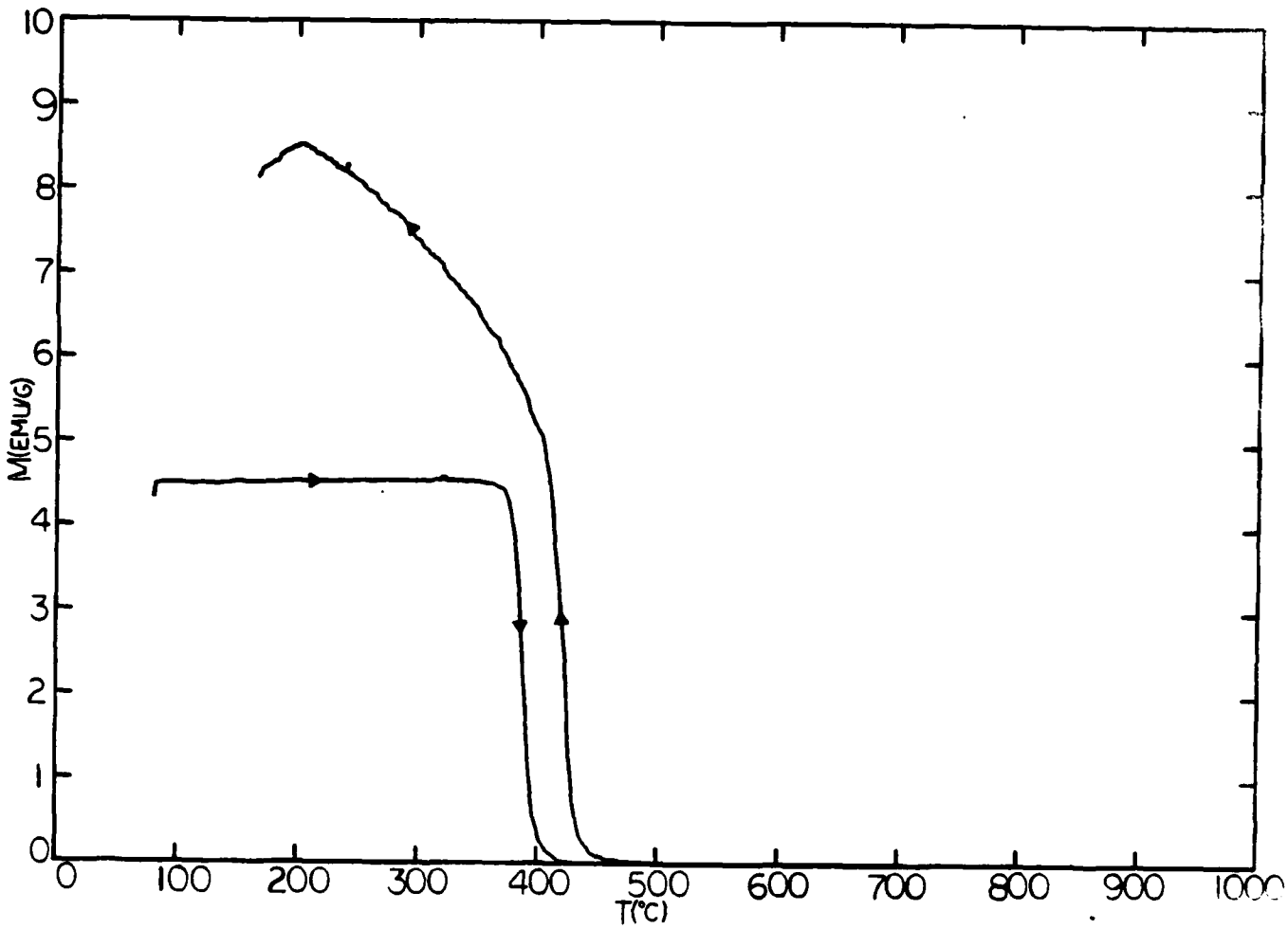

FIG. 41. Thermomagnetic data for $Fe_9Pt_6Ni_4Sn_1$.

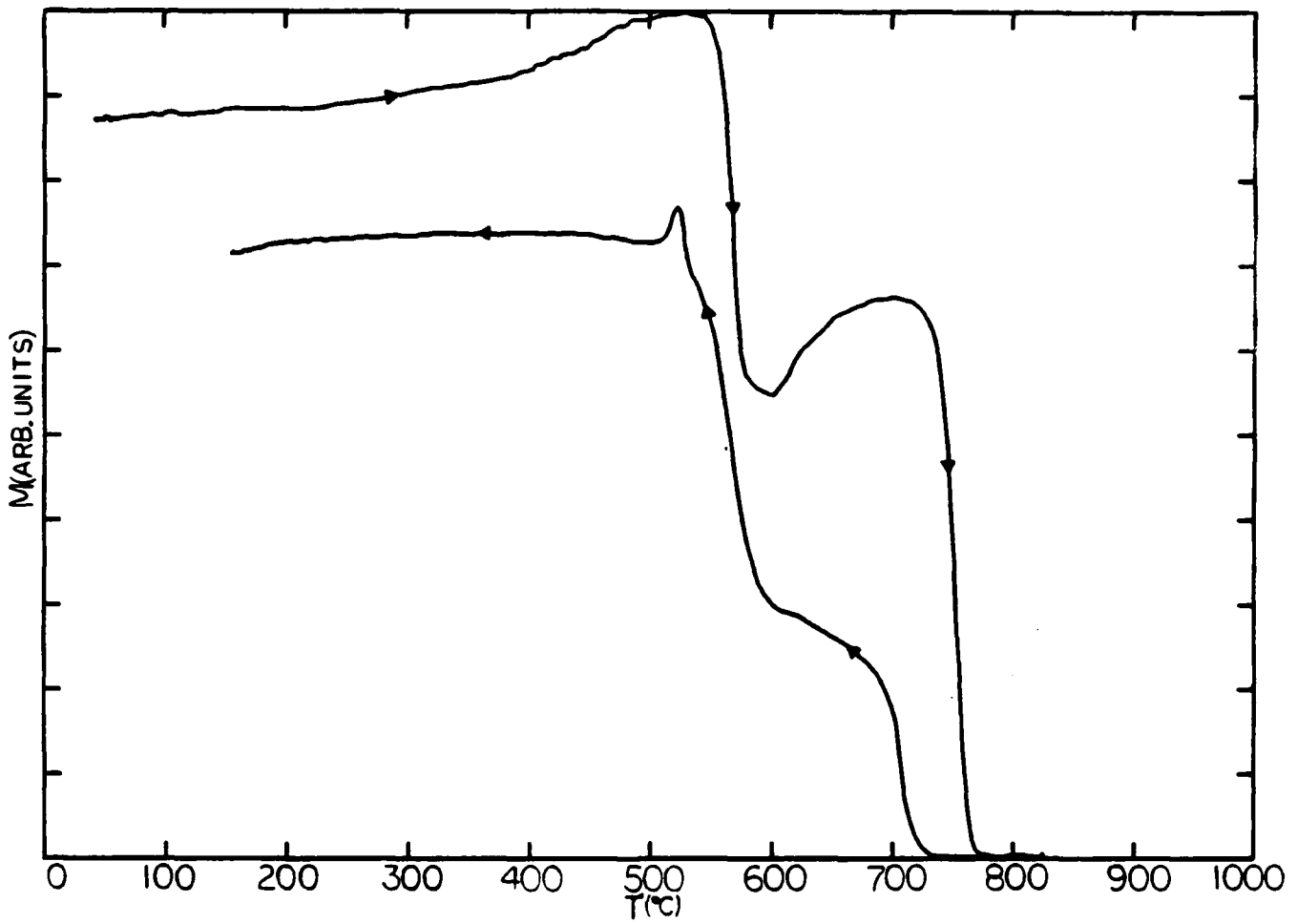

FIG. 42. Thermomagnetic data for $Fe_{10}Ni_5In_5$.

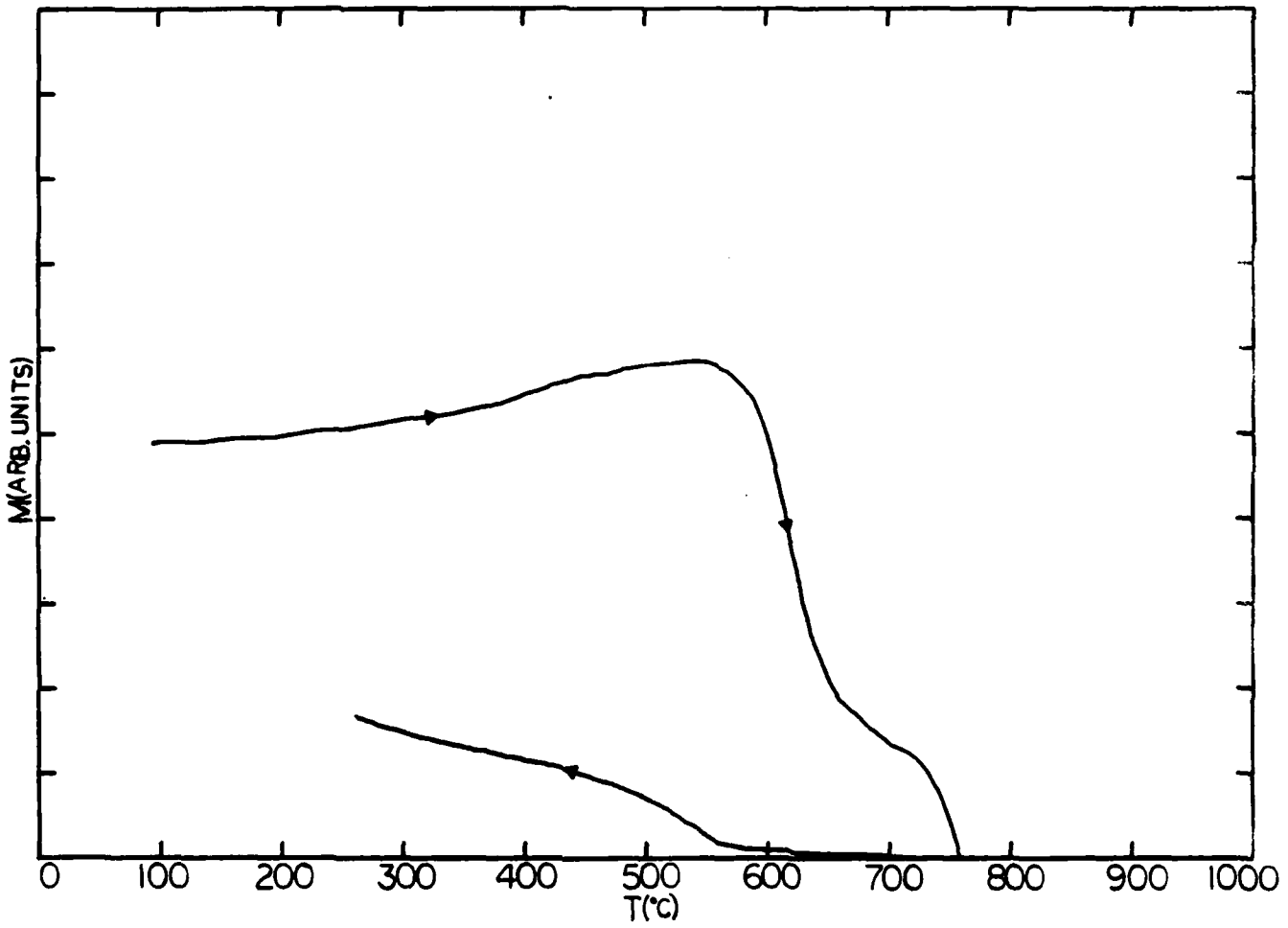

FIG. 43. Thermomagnetic data for unhomogenized $Fe_{10}Ni_5In_5$.

TABLE I

Magnetic Properties of $(Pr_{80}Ga_{20})_{100-x}Fe_x$ Alloys

Sample (x)	H_c (Oe)	M(20 kOe) (emu/g)	M_r (emu/g)	T_c (K)	T_{cr} (K)
30	2400*	22.5	0.9	475	753
40	1300	22.7	8.8	460	625
60	220	75.15	5.4	455	725
80	300	153.22	-	783; 1053	780

*Displaced hysteresis loops (600 Oe).

TABLE II

Effect of heat treatment on magnetic properties of melt-spun $SmTbFe_2$.

Surface Speed[cm/sec]	Hci[kOe]	Ms[$\frac{emu}{g}$]	Heat Treatment
900	3.1/2.7	24/29	30 min @ 550°C
1900	3.2/3.5	16/23	47 min @ 450°C
3900	2.5/2.8	20/27	30 min @ 450°C
	As Spun/Heat Treated		30 min @ 550°C

TABLE III

Effect of heat treatment on magnetic properties of melt-spun $PrTbFe_2$

Surface Speed[cm/sec]	Hci[kOe]	Ms[$\frac{emu}{g}$]	Heat Treatment
1900	7.2/6.6	9/14	1 min @ 450°C
2900	7.1/4.8	11/28	182 min @ 450°C
3900	5.7/5.0	17/22	15 min @ 450°C
	As Spun/Heat Treated		

TABLE IV

Thermomagnetic data of $Fe_{89-x}Pr_xCo_6(BSi)_5$ alloys

Composition x	T_{c1} (^oC)	T_{c2} (^oC)	T_m (^oC)
13.4	250	400	330 520
16.7	250	415	320 525
20	235	400	310 530
26.8	250		
40.2	180	380	

T_{c1} Curie temperature of as-quenched phase

T_{c2} Curie temperature of crystallized phase

T_m Temperature where local maxima have been observed in the M vs T curve.

TABLE V

Thermomagnetic data of $Fe_{92-x}Pr_x(BSi)_8$ alloys

Composition x(at %)	T_{c1} (^oC)	T_{c2} (^oC)
9.3	220	400
9.8	170	350
12.8	150	350
16.4	150	340
25	140	320

T_{c1} Curie temperature of as-quenched phase

T_{c2} Curie temperature of crystallized phase

TABLE VI

Effect of B-content on the thermomagnetic data of FePrB alloys

	$(Pr_6 Fe_{23})_{100-x} B_x$		$(Pr Fe_5)_{100-x} B_x$	
Boron at (at %)	$T_{c\ 1}$ (^oC)	$T_{c\ 2}$ (^oC)	$T_{c\ 1}$ (^oC)	$T_{c\ 2}$ (^oC)
5	140	300	150	320
10	170	310	150	320
15	170	320	200	320

$T_{c\ 1}$ Curie temperature of as-quenched phase

$T_{c\ 2}$ Curie temperature of crystallized phase

TABLE VII

$Fe_9Pt_6Ni_4In_1$		$Fe_{10}Pt_5Ni_4In_1$		$Fe_9Pt_6Ni_4In_1$		$Fe_9Pt_5Ni_4In_2$		$Fe_{10}Pt_6Ni_3Mo_1$		$Fe_{10}Pt_6Ni_3Mn_1$		$Fe_{10}Pt_6Ni_3Zr_1$		$Fe_9Pt_6Ni_4Sn_1$		$Fe_{10}Pd_6Ni_4$		$Fe_{10}Pd_7Ni_3In_1$	
M_s	H_{ci}	M_s	H_{ci}	M_s	H_{ci}	M_s	H_{ci}	M_s	H_{ci}	M_s	H_{ci}	M_s	H_{ci}	M_s	H_{ci}	M_s	H_{ci}	M_s	H_{ci}
emu/g	Oe	emu/g	Oe	emu/g	Oe	emu/g	Oe	emu/g	Oe	emu/g	Oe	emu/g	Oe	emu/g	Oe	emu/g	Oe	emu/g	Oe
			1050°C for 15 minutes															1050°C for 15 minutes	
73	25	73	25	77	0	76	0	63	30	72	45	70	75	72	290	120	0	100	0
			650°C for 2 hours															700°C for 15 minutes	
-	70	-	30	-	115	-	0	-	75	72	240	-	60	-	-	-	0	-	0
			650°C for 4 hours total															700°C for 30 minutes	
-	25	-	35	-	150	-	30	-	95	72	260	-	65	-	-	-	0	-	25
			650°C for 8 hours total																
-	85	-	40			-	-	-	65	71	225	-	65	-	-	-	-	-	-
			1000°C for 15 minutes + 700°C for 20 minutes																
-	25	-	40			-	-	-	30	71	90	-	90	-	-	-	-	-	-
			700°C for 40 minutes total																
-	60	-	30			-	-	-	20	69	30	-	60	-	-	-	-	-	-
			600°C for 4 hours																
-	90	-	0			-	-	-	30	86	35	-	110	-	-	-	-	-	-

M_s - magnetization ergs/Oe-g - emu/g (±5%)

H_{ci} - intrinsic coercivity (±10/Oe)

APPENDIX

Characterization Studies of Rare Earth-Iron Magnetic Materials

Final Report

Charlottesville, Virginia

Prepared by:

Kenneth Lawless

Roseanne Prestipino

January 14, 1983

Characterization Studies of Rare Earth-Iron Magnetic Materials

For ease in their presentation, this report divides the results into 4 sections according to specimen type.

I. PrGaFe

The initial work was directed toward microstructural studies of $(Pr_{80}Ga_{20})_{70}Fe_{30}$. Transmission electron microscope (TEM) results show an amorphous structure with a few isolated crystalline regions in the as-quenched state. After heat treatment, the crystalline regions form an Fe-rich grid structure while the amorphous regions are Ga-rich. More detailed results are not available as studies were discontinued due to poor magnetic properties. (See micrographs of amorphous region in as-quenched and diffraction patterns of amorphous as-quenched and amorphous/crystalline heat treated. Spectrum is of a crystalline region in heat treated specimen.)

II. Pre-metglas alloys

This group of 8 samples consists of 5 specimens of $Pr_1Tb_1Fe_2$; 4 as-quenched ones which were melt spun at different rpm's and 1 heat treated sample. The 3 remaining specimens are $Pr_{.5}Tb_{.5}Fe_2$, $Pr_{.25}Tb_{.75}Fe_2$, and $MM_{20}Tb_{20}Fe_{60}$.

Of the 4 $Pr_1Tb_1Fe_2$ as-quenched samples, only 1 yielded an electron transparent specimen suitable for TEM work. This sample was prepared by electropolishing in a methanol-perchloric acid solution and then ion milled to clean off any surface contamination. The electron diffraction patterns show both amorphous and unidentified crystalline regions (see diffraction pattern and spectrum). In conjunction with the TEM, energy dispersive x-ray analysis (EDAX) was used and shows both Pr-rich and Fe-rich regions.

Unidentified crystalline electron diffraction patterns were obtained from the heat treated $Pr_1Tb_1Fe_2$ specimens. EDAX data indicates the crystal-

line regions are Fe-rich (see micrograph, diffraction patterns, and spectrum).

The as-quenched $Pr_{.5}Tb_{.5}Fe_2$ sample was prepared for TEM work by ion milling. Electron diffraction data and EDAX data show unidentified Fe-rich crystalline regions (see diffraction pattern). An x-ray diffractometer run shows weak crystalline peaks that may be Fe_2Pr.

The as-received $MM_{20}Tb_{20}Fe_{60}$ where MM represents mischmetal, was prepared for TEM analysis using the same procedure as the as-quenched $Pr_1Tb_1Fe_2$ sample. Electron diffraction and EDAX reveal Fe-rich amorphous regions. No crystalline material is apparent.

The last sample, as-quenched $Pr_{.25}Tb_{.75}Fe_2$, shows only amorphous material.

As better magnetic properties were seen in the following group, work in this category was discontinued.

III. This group consists of MM Tb Fe metglas alloy, 1 each as-quenched and heat treated. The metglas also contains B, Co and Si. Both samples were prepared by electropolishing in methanol-perchloric acid mixture and then ion milling to remove any surface contamination. This group of specimens contain the largest number of elements - Ce, La, Nd, Pr, Tb, Fe, B, Co, Si. Both samples contain amorphous and unidentified Fe-rich crystalline regions (see diffraction patterns). The electron diffraction patterns show at least two different crystalline phases, neither corresponding to any known compounds. X-ray diffractometer data on the as-quenched sample shows some very weak crystalline peaks.

Due to the complexity of this alloy (9-component system) efforts through the remainder of the project were aimed towards reducing the number of elements and creating better magnetic properties.

IV. This final group of alloys is a set of 6 different samples that have good magnetic properties. The first 4 contain Pr, Fe, B, Si, and the last 2 Pr, Fe, B in various amounts. All 6 specimens were prepared for TEM work

by ion milling. In general the samples consisted of very small and large (smallest less than 100 Å, largest several microns) α-Fe crystals, an amorphous phase, and other unknown crystalline phases.

Possible compounds considered are various combinations of Pr and Fe, and combinations of these elements with B and Si. There are 5 possibilities for PrFe, 1:2, 1:3, 1:5, 2:17, and 6:23. Diffraction information is directly available only for $PrFe_2$ and $PrFe_7$. $PrFe_2$ data was obtained at high pressure and temperature (32-35 kbar and 1000°C). Data for 1:3, 1:5, and 2:17 is available for PrCo, not PrFe. And finally no data is available for 6:23. None of the electron diffraction patterns match any of these. Further work will investigate the possbility of iron borides.

Looking at each of the 6 separately, the first consists of as-quenched and heat treated $Pr_{16.4}Fe_{73.5}B_{4.8}Si_{3.3}$. The as-quenched specimen electron diffraction data shows an amorphous matrix, with a large amount of small α-Fe crystallites, and unidentified crystalline material (see diffraction patterns and micrograph). The heat treated sample shows unidentified crystalline material (see diffraction pattern). X-ray diffractometer data also show crystalline peaks.

With the second specimen, IM 558, no composition data was included. Semiquantitative analysis using EDAX gave concentrations of 81% Fe and 19% Pr (weight %). The amount of metglas present was not determined. All the crystalline areas viewed using TEM were α-Fe, in an amorphous matrix (see diffraction pattern and micrograph).

The third sample, $Pr_{17}Fe_{75}B_5Si_3$ was heat treated. TEM data shows both large and small α-Fe precipitates as well as some unidentified crystallites in an amorphous matrix (see micrographs and diffraction patterns). X-ray diffractometer data also show crystalline peaks. The largest grains, on the order of microns, were seen in this sample.

Sample four, $(Pr_{26}Fe_{74})_{2/3}$(B,Si metglas)$_{1/3}$, is also a heat treated specimen. The grains are much smaller (on the order of 100 Å) than those in the sample just discussed. A small amount of amorphous material is visible but the specimen is basically composed of very small crystallites with some larger precipitates. Most of the crystalline material is α-Fe, some remains unidentified (see diffraction patterns and micrographs). The x-ray diffractometer data show 2 strong crystalline peaks, both α-Fe.

The fifth sample, $Pr_{18.6}Fe_{71.4}B_{10}$ represents a further simplification of the chemical composition, from 4 elements to 3. This set consists of as-quenched and heat treated specimens. The as-quenched sample contains unidentified fine crystalline material in an amorphous matrix (see micrographs and diffraction patterns). No good TEM samples were obtained from the heat treated material.

The final specimen consists of as-quenched and heat treated $Pr_{16}Fe_{79}B_5$. The as-quenched shows various sizes of α-Fe crystallites in an amorphous matrix (see micrographs and diffraction patterns). The heat treated sample shows an amorphous matrix with α-Fe and unidentified crystalline regions (see micrographs and diffraction patterns).

In the time available it has not been possible to make specific identification of some of the crystalline phases present. These are not known materials, and therefore JCPDS powder diffraction data is not available. Considerable additional study will clearly be necessary to identify the structure and composition of these intermetallic phases in more detail.

PrGaFe
As-quenched

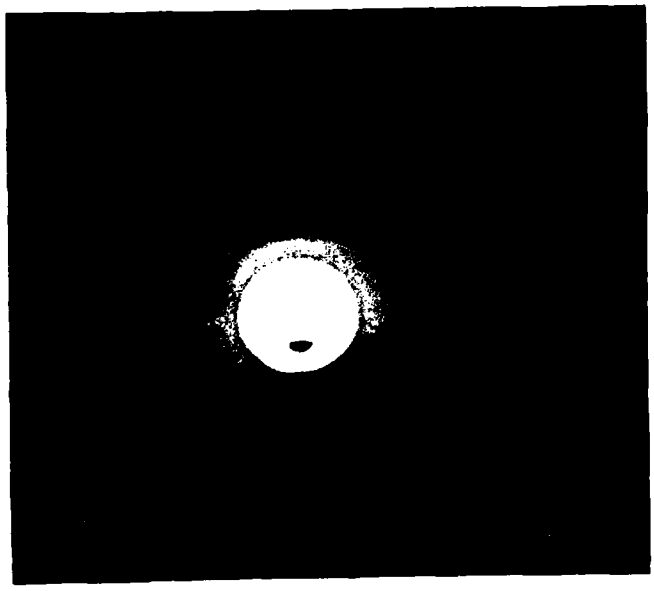

184,000 X

PrGaFe Heat Treated

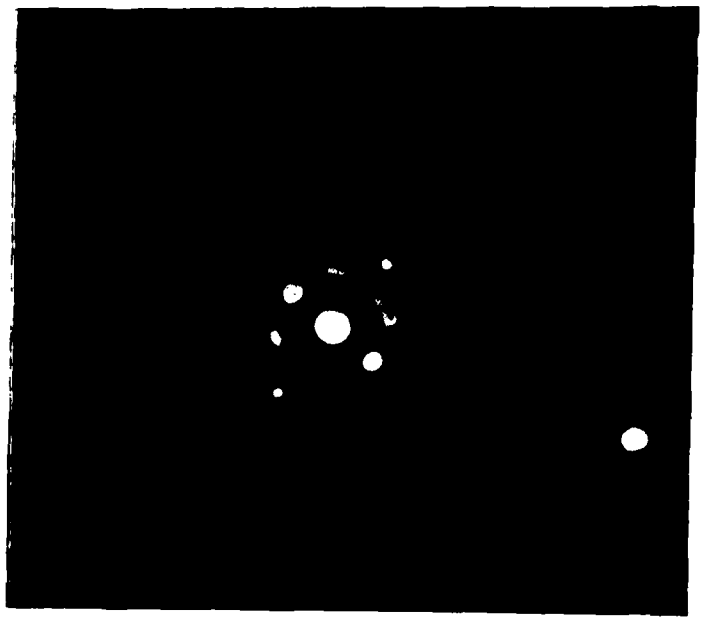

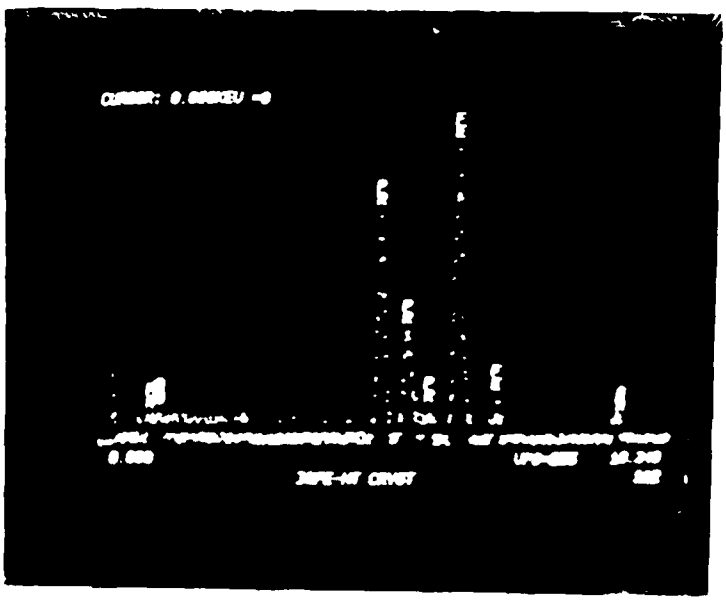

$Pr_1Tb_1Fe_2$ As-quenched

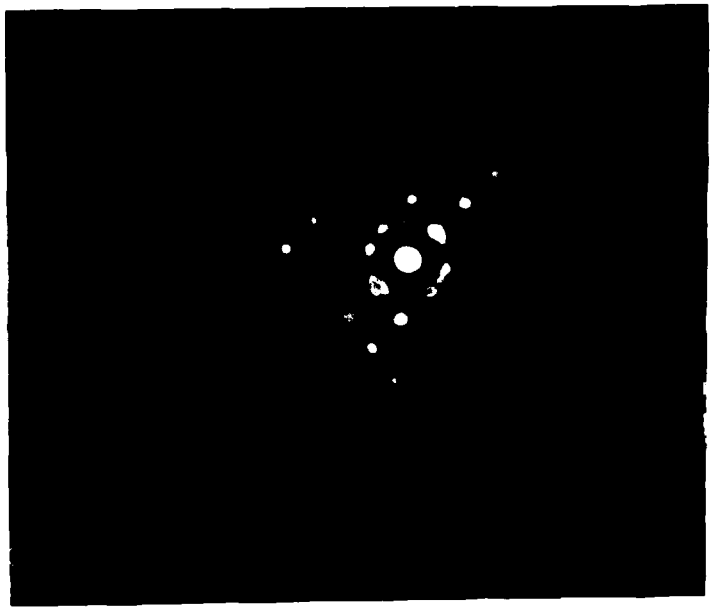

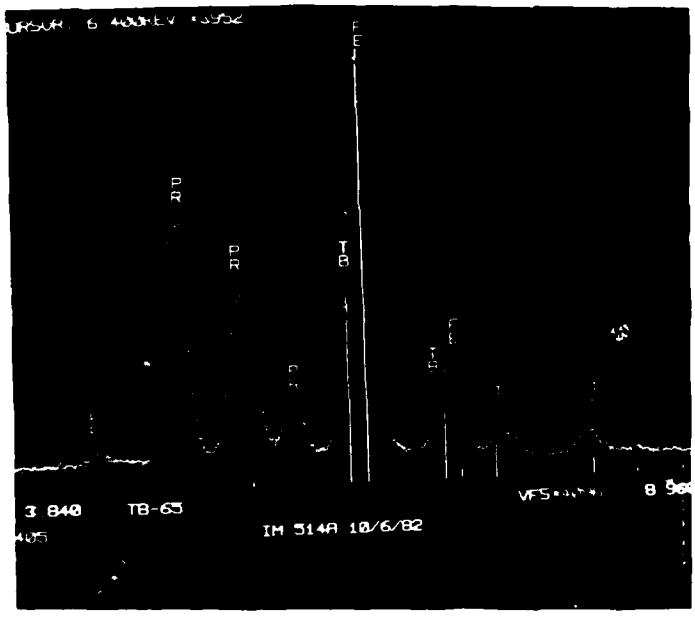

$Pr_1Tb_1Fe_2$ Heat Treated

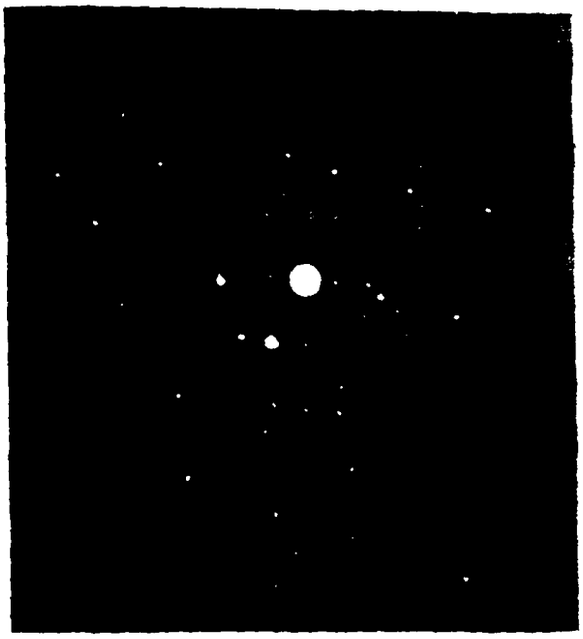

241,500X

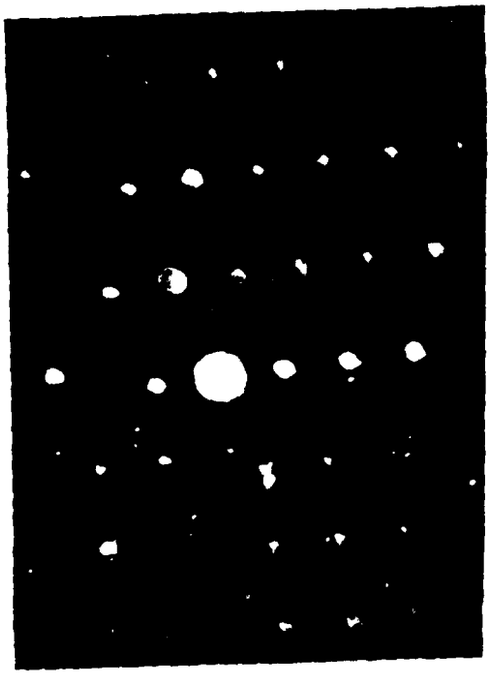

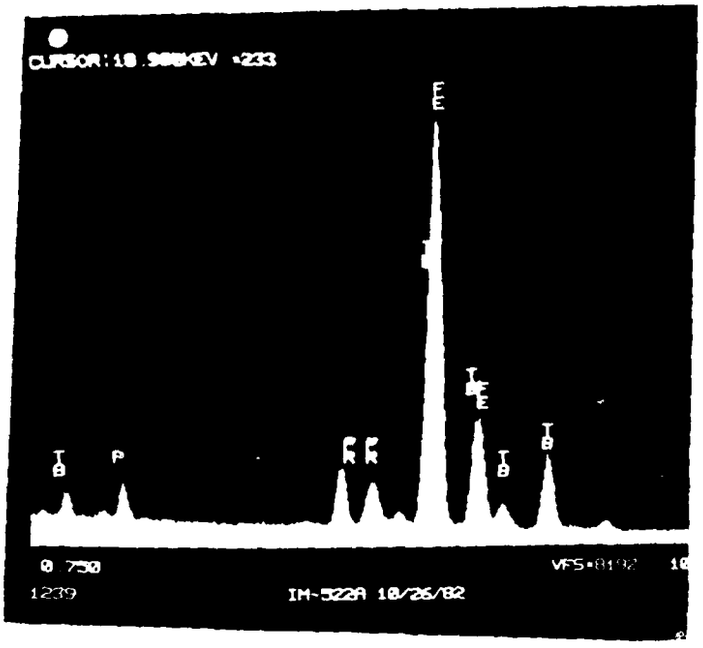

$Pr_{.5}Tb_{.5}Fe_2$ As-quenched

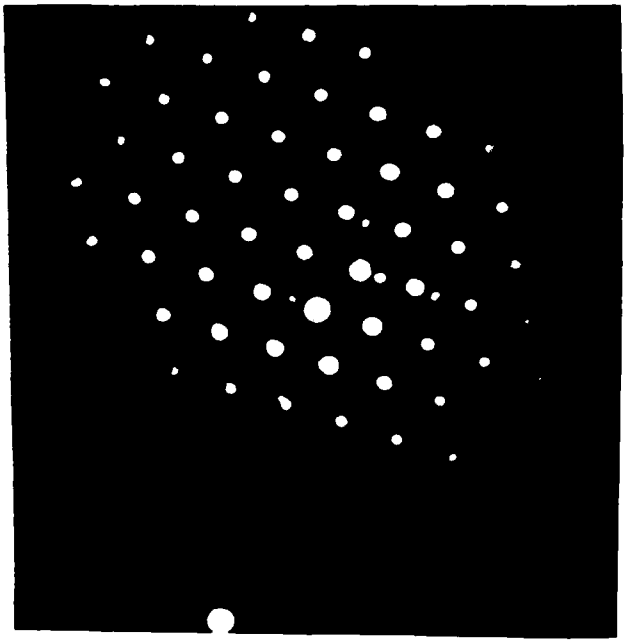

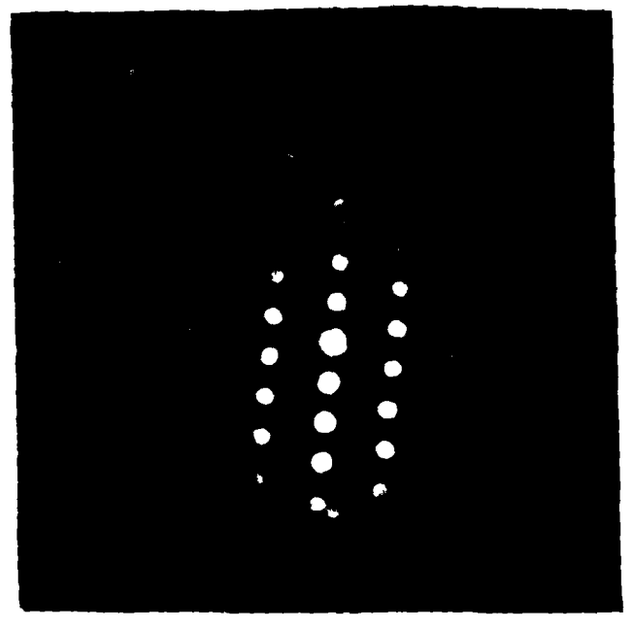

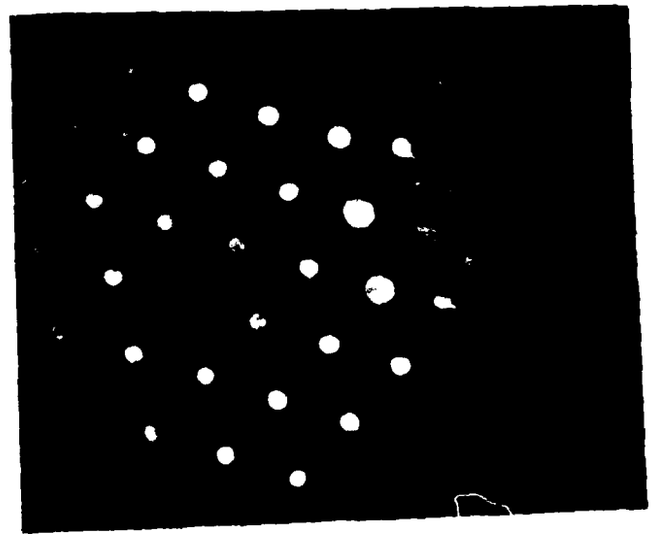

$Pr_{16.4}Fe_{73.5}B_{4.8}Si_{3.3}$ As-quenched

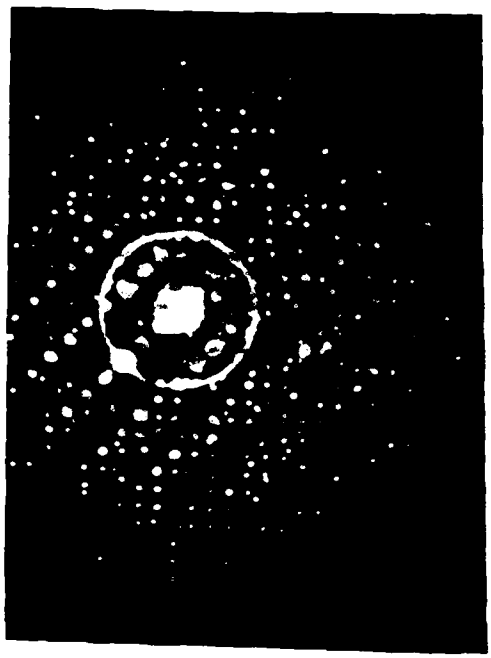

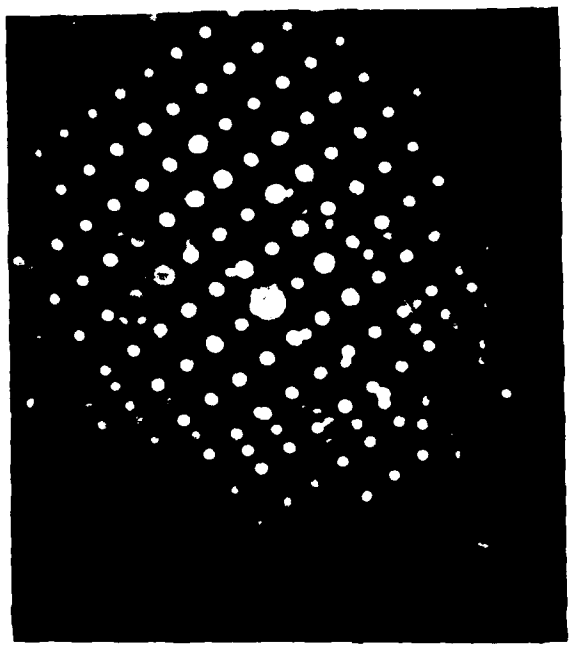

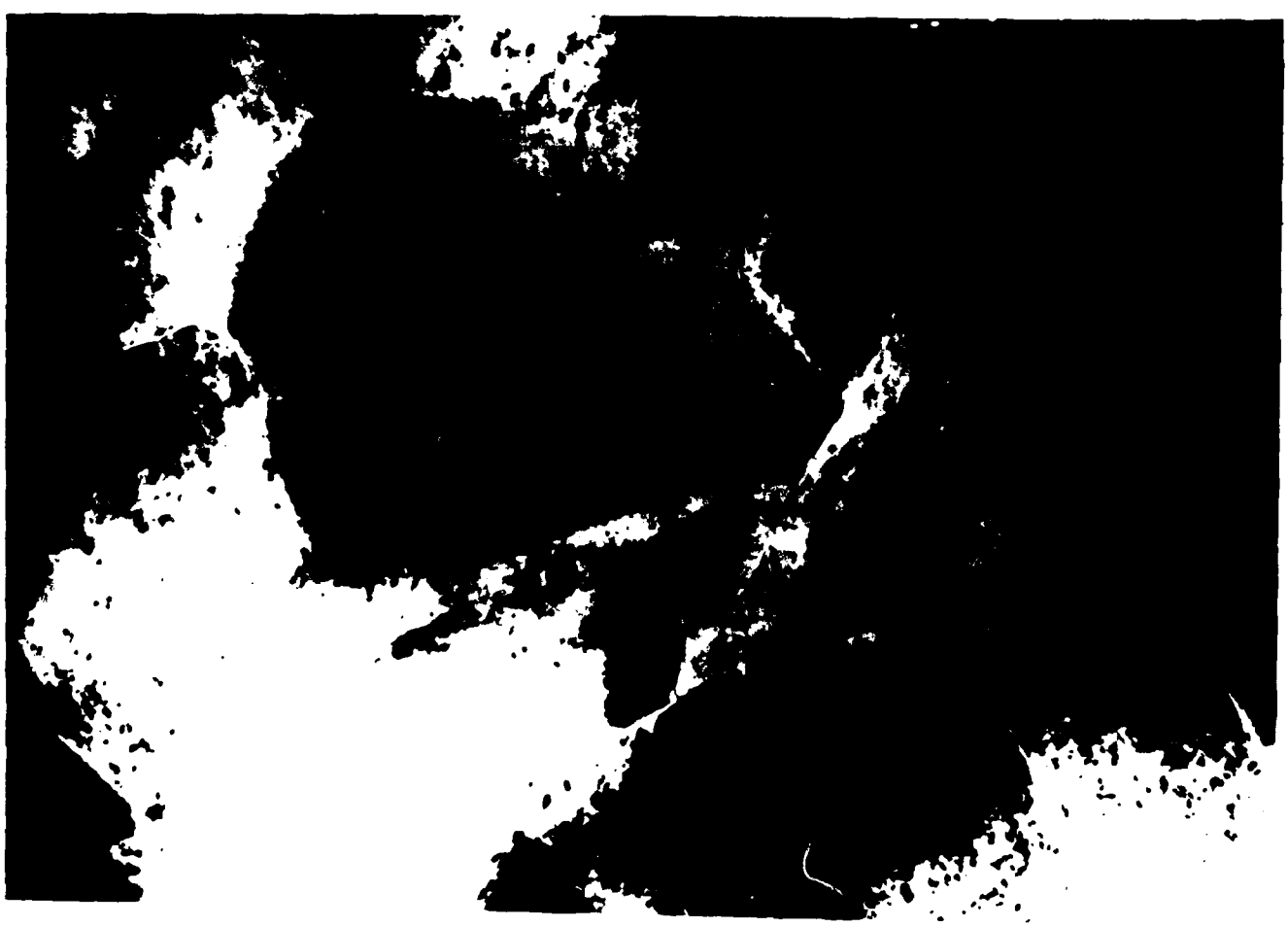

230,000X

$Pr_{16.4}Fe_{73.5}B_{4.8}Si_{3.3}$ As-quenched

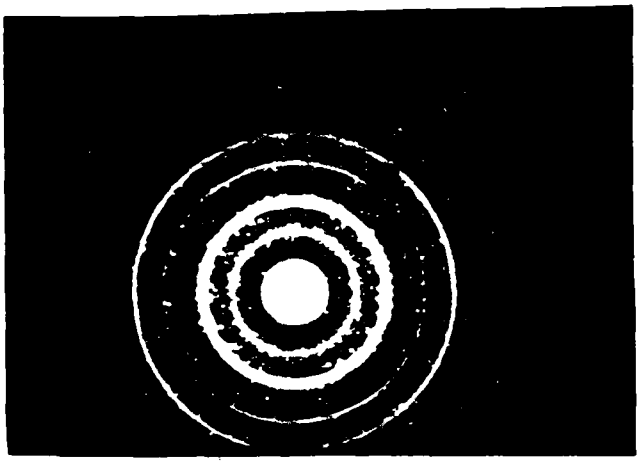

82,800 X

$Pr_{16.4}Fe_{73.5}B_{4.8}Si_{3.3}$ Heat Treated

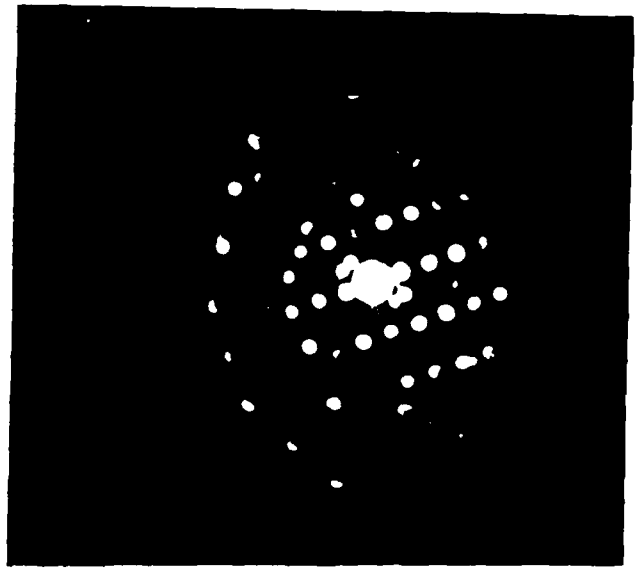

AD-A158 686 INVESTIGATION OF CRYSTALLINE IRON-PLATINUM NICKEL AND AMORPHOUS RARE EART..(U) KOLLMORGEN CORP RADFORD VA G C HADJIPANAYIS ET AL. 15 MAR 83 0001AE 2/2

UNCLASSIFIED N00014-81-C-0752 F/G 20/3 NL

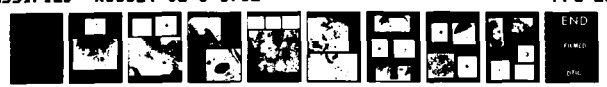

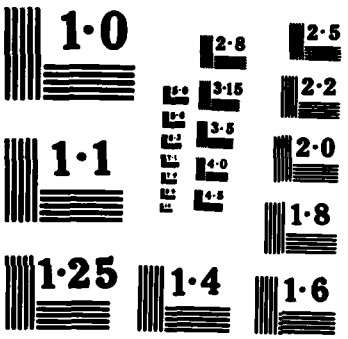

NATIONAL BUREAU OF STANDARDS
MICROCOPY RESOLUTION TEST CHART

391,000X

$Pr_{17}Fe_{75}B_5Si_3$ Heat Treated

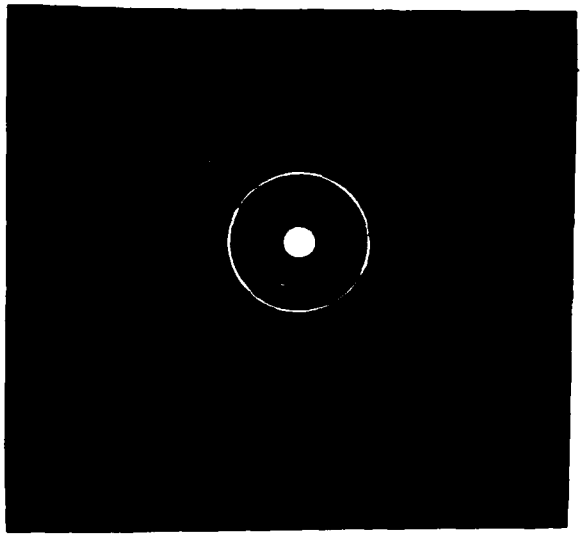

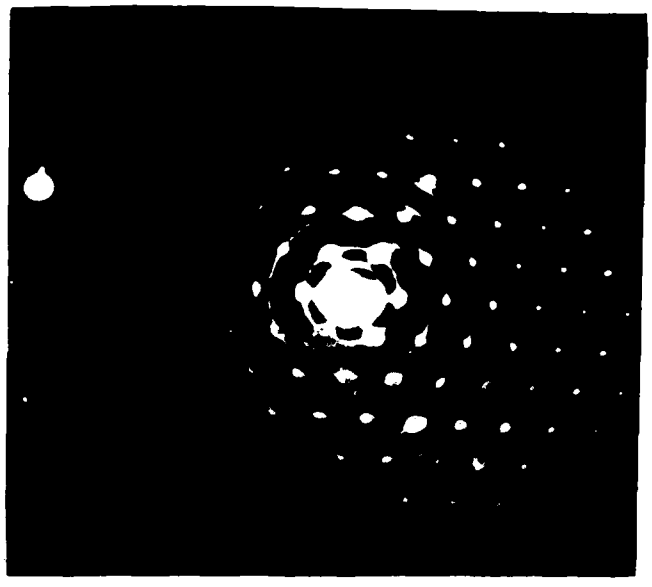

184,000 X

$Pr_{17} Fe_{75} B_5 Si_3$ Heat Treated

230,000 X

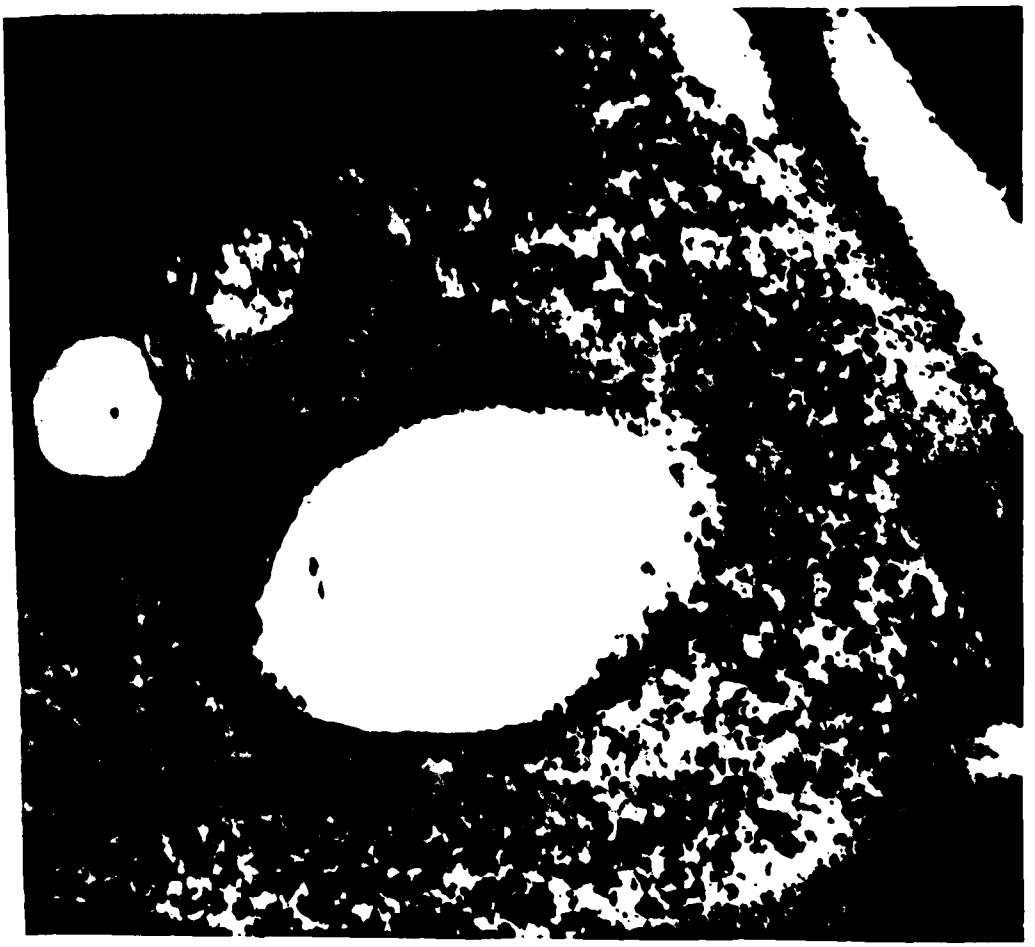

184,000 X

$(Pr_{26}Fe_{74})_{2/3}$metglas$_{1/3}$ Heat Treated

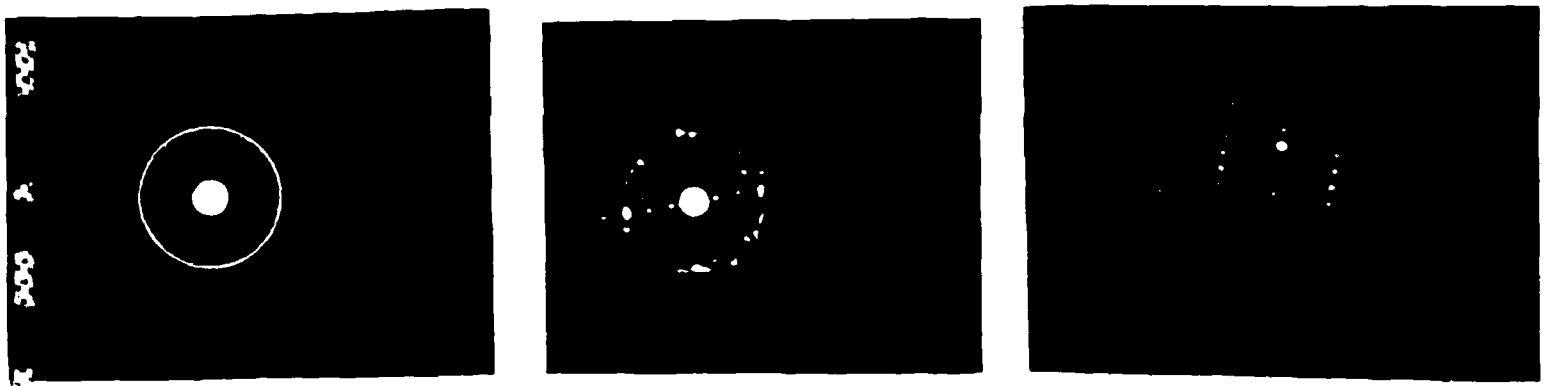

506,000X

$(Pr_{.26}Fe_{.74})_{.75}$ metglas $_{1/3}$ Heat Treated

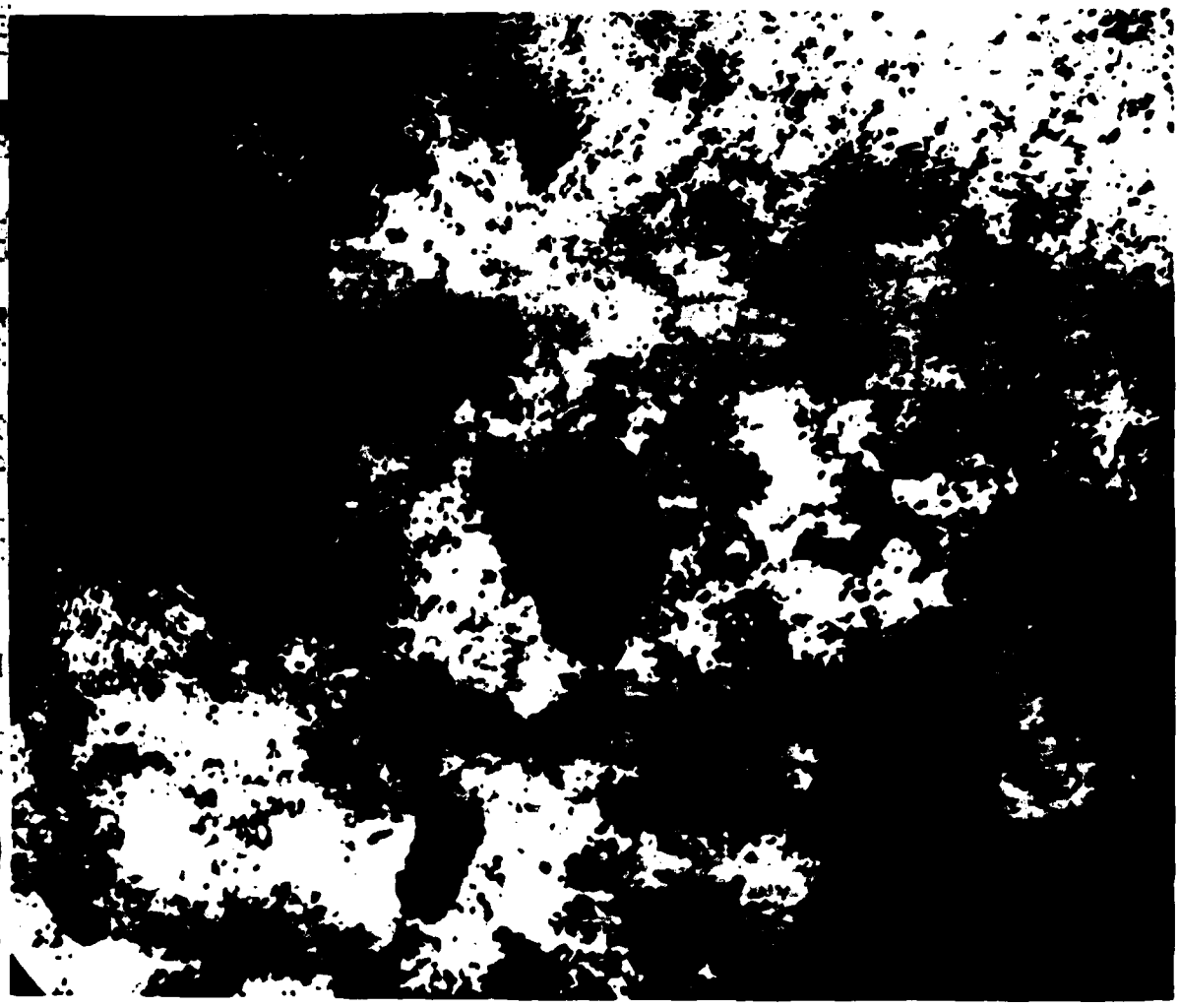

299,000X

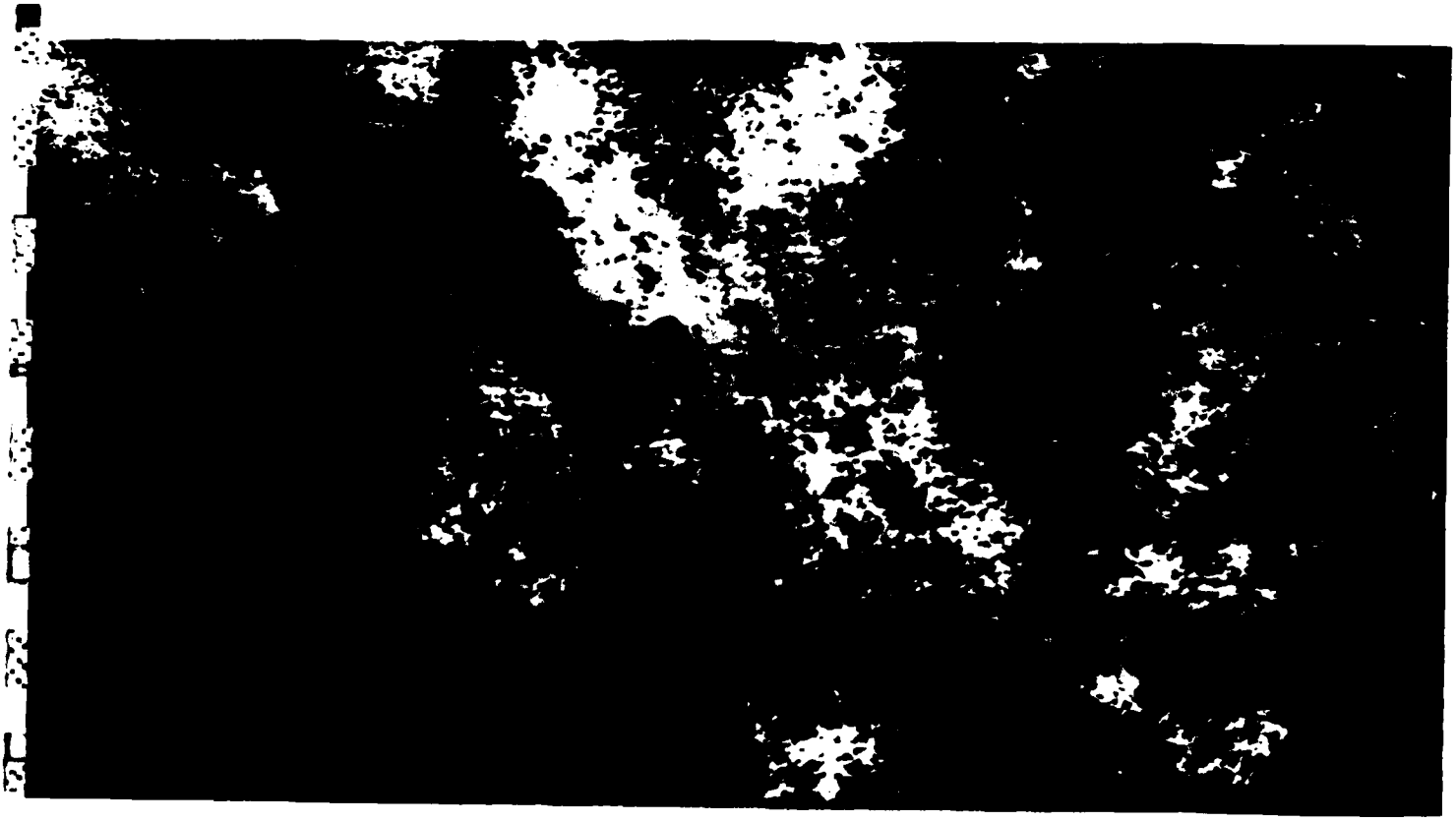

299,000X

$Pr_{18.6}Fe_{71.4}B_{10}$ As-quenched

299,000X

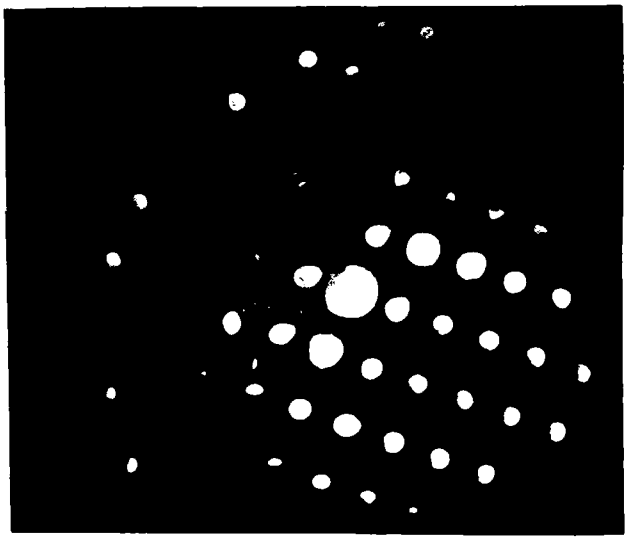

299,000X

$Pr_{16}Fe_{79}B_5$ As-quenched

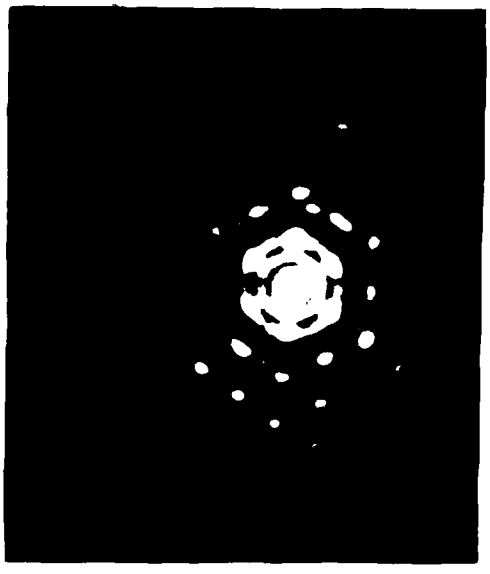

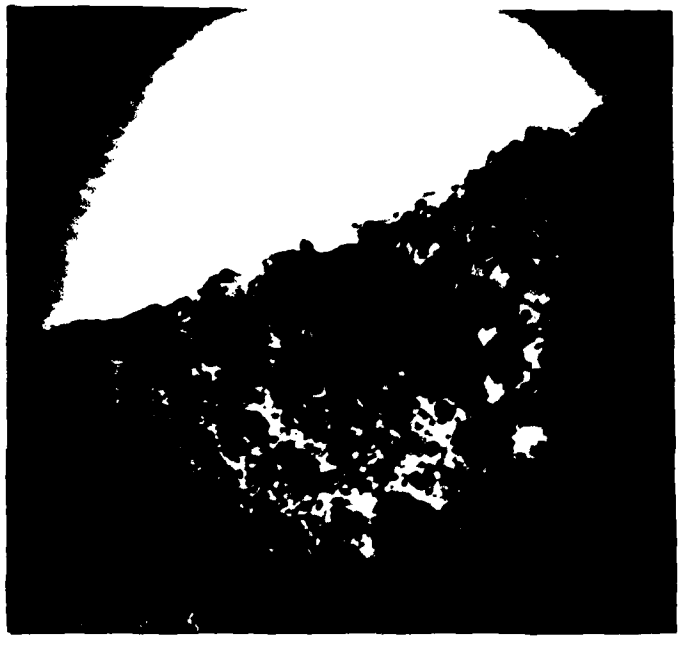

506,000X

506,000X

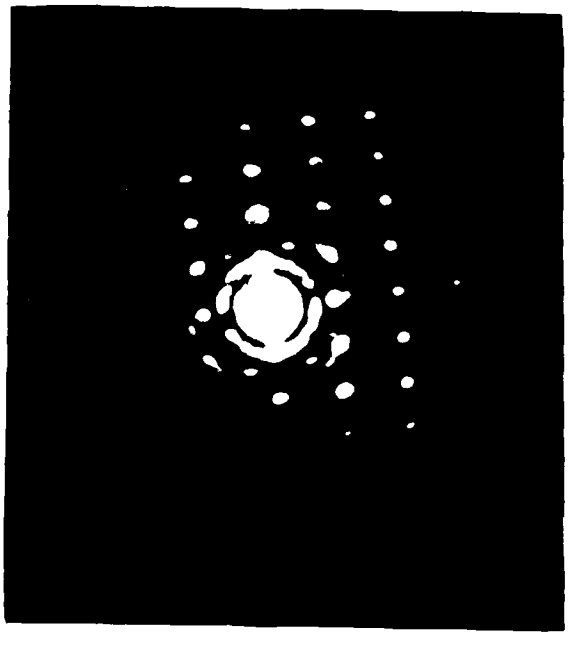

$Pr_{16}Fe_{79}B_5$ Heat Treated

138,000X

184,000X

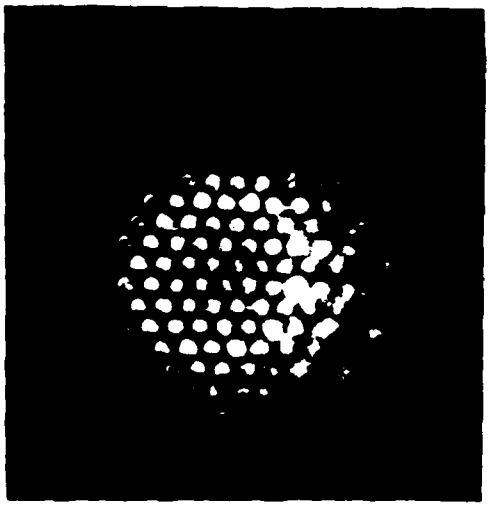

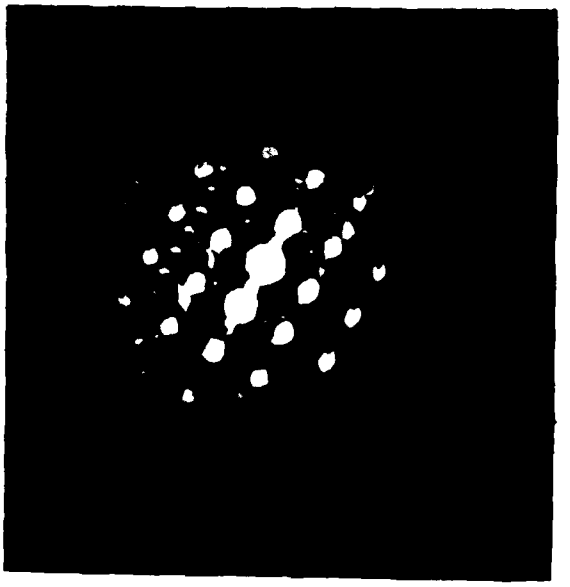

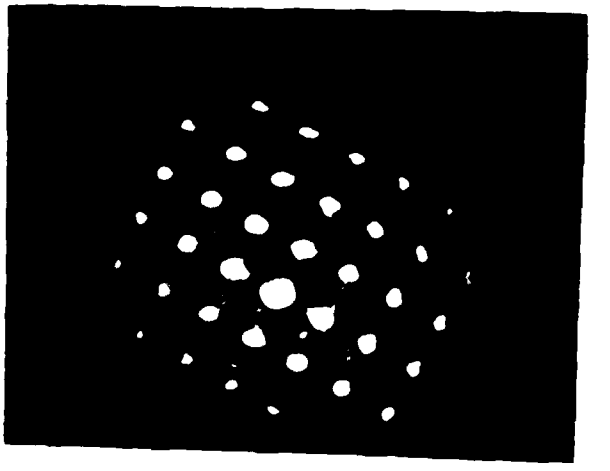

END

FILMED

10-85

DTIC